PROTEIN KINASE-MEDIATED IMMUNITY IN *ARABIDOPSIS* AND *NICOTIANA BENTHAMIANA*

A Dissertation

Presented to the Faculty of the Graduate School

of Cornell University

In Partial Fulfillment of the Requirements for the Degree of

Doctor of Philosophy

by

Elizabeth Kalinda Brauer

February 2016

PROTEIN KINASE-MEDIATED IMMUNITY IN *ARABIDOPSIS* AND *NICOTIANA BENTHAMIANA*

Elizabeth Kalinda Brauer, Ph.D.

Cornell University 2016

Protein kinases constitute a major component of the plant cellular signaling machinery, allowing plants to survive in diverse environments. However protein kinases are functionally redundant and are predominantly regulated by post-translational mechanisms, making them difficult to study using reverse genetics or transcriptomics. While the mechanisms by which some kinases perceive and respond to pathogens have been described, several important steps in signal transduction remain unstudied and an understanding of cross-talk between signaling pathways is lacking. By expanding our knowledge of protein kinases and their role in immunity, we can identify novel signaling components to target the pathways which are most likely to enhance stress tolerance.

Here, we present studies outlining the role of select protein kinases in plant immunity using a proteomics approach. We first present a large-scale method for elucidating kinase interactions and target phosphorylation using protein microarrays. Next, we outline a functional study of pathogen effector-interacting kinases in *Nicotiana benthamiana* and demonstrate a role for the majority of these kinases in multiple immune pathways. This provides a novel view of the plant immune system where that different stimuli induce both shared and unique stress response pathways. We also observed a novel effector-specific immune response which is partially dependent on kinases. Finally, we describe the kinase activity and physiological role of the *integrin-linked kinase 1* (*ILK1*) in ion transport, osmotic stress tolerance and immunity in

Arabidopsis thaliana. Together with its interactor, the K^+ transporter *HAK5*, *ILK1* regulates plasma membrane depolarization, ion homeostasis and signaling in response to bacterial flagellin.

Taken together, the findings presented here provide insights into the plant immune response. In particular, we demonstrated that disruption of select kinases can induce resistance to bacterial pathogens carrying specific effectors, indicating an undescribed form of immunity. We also identified the first molecular components involved in flagellin-induced membrane depolarization in mesophyll cells, indicating the potential importance of nutrient homeostasis in immune responses.

BIOGRAPHICAL SKETCH

Elizabeth K. Brauer was raised in Guelph, Ontario where she developed an early interest in plants through vegetable gardening. This interest was strengthened at the University of Guelph where Liz received exceptional training in plant biology during her undergraduate degree and through her work with Dr. Barry Shelp. Liz completed an MSc with Dr. Shelp on the contribution of nitrogen assimilation pathways to yield responses in rice in 2009. She went on to contribute to viral research at the International Potato Center in Peru prior to beginning her PhD in Plant Pathology and Plant-Microbe Biology at Cornell University in 2010. In 2011, Liz joined the lab of Dr. Sorina Popescu at the Boyce Thompson Institute where she studied protein kinases involved in stress response and immunity.

Dr. Brauer has been an active member of her department throughout her time at Cornell. She served as the vice-president of the departmental graduate student committee, and as the departmental representative on the graduate professional student association. Dr. Brauer also helped to establish the Innovation Workshop Exchange program between Cornell and the Tokyo University of Agriculture and Technology which is currently in its fifth year. Dr. Brauer has been honored with several academic awards including the Canada Postgraduate Scholarship and the Barbara McClintock Award. Outside of the lab, Dr. Brauer enjoys long distance swimming and swimming in Ithaca's many beautiful gorges.

Upon completion of her PhD, Dr. Brauer will continue her research in plant immunity and plant stress responses through post-doctoral training. She hopes to examine the relationship between immunity and environmental responses and to contribute to translating basic research findings to improve crop stress resistance.

To Francis M.C. Prescott,

My partner in crime, my constant companion and my biggest supporter

ACKNOWLEDGEMENTS

I am grateful for the time and dedication that many people have contributed in order to bring this thesis to fruition. I would first like to thank my advisor, Dr. Sorina Popescu for taking me on as her first graduate student. Sorina's constant support, expertise and passion for science has allowed me to develop as a researcher and as a person and I am grateful to have had the opportunity to learn from her. I would like to thank my committee members Drs. Leon Kochian, Alan Collmer and Gregory Martin for their valuable insights and support throughout my degree. I have also benefitted immensely from the experience of Dr. Stewart Gray, and Dr. Gillian Turgeon who generously helped me navigate degree requirements and fellowship applications. I'm also grateful to the teaching faculty including Drs. Alan Collmer, Michael Milgroom and Keith Perry, who provided me with an understanding of plant pathology through many interesting discussions. I would like to thank the people who have contributed directly to this work including Mauricio Calvino, Austin Lee, Meeta Srivastava, Alison Coluccio, Renee Dale and Drs. Kamala Gupta, Bhaskar Gupta, Miguel Pineros, Naohiro Kato, Suma Chakravarthy, Jay Thelen, Nagib Ahsan, George Popescu and Patrick Boyle. Monetary support for my training was provided by the Natural Sciences & Engineering Research Council of Canada, the Boyce Thompson Institute, and the Cornell Graduate School. Finally, I appreciate I could not have accomplished this research without the support staff at the Boyce Thompson Institute and in the Plant Pathology & Plant-Microbe Biology section.

On a more personal note, I would like to thank my friends and family for their support and laughter throughout the years. To my friends, you are a constant inspiration to me and you have shaped the person I am today. Thank you to my father and mother, for imparting their love of biology and for teaching me to challenge my own assumptions. To my father and mother-in-law who have raised a wonderful son and have taught me so much. Finally, to my husband Francis, thank you for everything.

TABLE OF CONTENTS

LIST OF FIGURES

LIST OF TABLES

LIST OF ABBREVIATIONS

ROS	reactive oxygen species
RLK	receptor-like kinase
RLCK	receptor-like cytosolic kinase
MAPK	mitogen-activated protein kinase
CDPK	calcium-dependent protein kinase
PAMP	pathogen-associated molecular pattern
PTI	pattern-triggered immunity
ETI	effector-triggered immunity
PRR	pattern-recognition receptor
PM	plasma membrane
ER	endoplasmic reticulum
NB-LRR	nucleotide binding leucine rich repeat
PMA	protein microarray
BSA	bovine serum albumin
MS	Murashige & Skoog
KEI	effector-interacting kinase
PCD	programmed cell death
Pst	*Pseudomonas syringae* pv. *tomato*
SLCA	split luciferase complementation assay
Luc	luciferase
WT	wild type
BiFC	bimolecular fluorescence complementation

CHAPTER 1

Intersecting signal transduction pathways in biotic and abiotic stress

ABSTRACT

Like all organisms, plants use protein kinase-based cellular signal transduction pathways to detect and respond to fluctuations in their environment. Molecular dissection of these pathways has expanded our understanding of immunity and abiotic stress responses which can be initiated across most plant cell types. Recent advancements in proteomic methods to monitor the activation and interaction status of protein kinases provides a platform for genetic intervention to improve stress tolerance in cultivated plants. Here, we present a brief review of the role of protein kinases in mediating responses to biotic and abiotic stress and highlight the signaling processes which are activated in response to multiple independent stresses.

Overview of cellular responses to environmental stress

In order to procreate, plants must be able to sense dynamic changes in their environment and adjust their growth and metabolism accordingly. Plants achieve environmental surveillance across almost all cell types, unlike mammals, which rely on specific sensory organs to perceive particular stimuli. As a result, plant cells can respond to multiple types of signals, including living and abiotic stresses. For example, plant leaf mesophyll cells respond to pathogens, osmotic stress, ionic stress and extreme temperatures, which interestingly, induce a common set of cellular signaling responses. These early signaling responses include rapid calcium influx,

followed by activation of kinase-dependent processes, including reactive oxygen species (ROS) production, ion fluxes, signal transduction, hormone production and ultimately, changes in gene expression. The amplitude and localization of these early signaling responses can differ dramatically depending on the initial stress input (Tsuda *et al.*, 2013). However, the mechanisms underlying conversion of a generalized cellular stress response such as calcium flux, to a specific response, are not well understood. An increasing number of studies provide evidence that the activation or interaction specificity of protein kinases help to determine the type and extent of stress response (Ubersax and Ferrell Jr, 2007). The study of protein kinases is thus essential for not only understanding the initial steps in plant stress response but also to clarify how plants differentiate between stresses to produce a specific response. This information is critical in developing pathogen-resistant crops, since altering disease resistance pathways can affect abiotic stress response and vice versa (Fujita *et al.*, 2006).

Kinase activity and regulation

Protein kinases modulate a wide range of processes in the cell including metabolism, cell division and environmental sensing. A majority of protein kinases are thought to use phosphorylation as a mechanism to modulate substrate activity, localization, or binding properties (Adams, 2003). Kinases phosphorylate substrates by facilitating the transfer of the gamma phosphate from ATP to a serine, threonine or tyrosine residue using a highly conserved kinase domain (Hrabak *et al.*, 2003). In turn, kinase activity is regulated by transcriptional and post-transcriptional mechanisms including phosphorylation or dephosphorylation of specific residues. In particular, most kinases undergo autophosphorylation in the activation loop, which enhances kinase activity by either exposing the active site or increasing efficiency of

phosphotransfer (Adams, 2003). Almost 13% of the Arabidopsis kinome are categorized as catalytically inactive pseudokinases, due to the presence of substitutions in conserved kinase motifs of the active site (Castells and Casacuberta, 2007). While some pseudokinases phosphorylate substrates through an alternative kinase mechanism (Mukherjee *et al.*, 2010), other pseudokinases such as ZED1 and ZRK1 cannot facilitate phosphotranfer but instead may function as scaffold proteins, allosteric switches, or traps for pathogen kinase-binding effectors (Lewis *et al.*, 2014). Thus, kinases are highly regulated proteins that modulate cellular responses through both enzymatic and non-enzymatic mechanisms.

The Arabidopsis and tomato kinomes contain 1352 and 1436 predicted kinases, which comprise 4% and 5% of their respective genomes (Singh *et al.*, 2014). Plant kinomes have been classified according to primary structure into five classes including the (I) transmembrane receptor kinases and related non-transmembrane kinases including receptor-like kinases (RLK) and receptor-like cytoplasmic kinases (RLCK), the (II) ATN1/CTR1/EDR1/GmPK6-like kinases, (III) the casein kinases, (IV) non-transmembrane protein kinases including mitogen activated protein kinases (MAPK) and calcium-dependent protein kinases (CDPK), and (V) other protein kinases (Gribskov *et al.*, 2001). Plant RLK families have undergone a dramatic expansion during establishment of the first land plants, making them the largest gene family in Arabidopsis (Lehti-Shiu *et al.*, 2009). Together, the RLKs and the RLCK facilitate perception of pathogens and hormone signals, which are transmitted and amplified by MAPK and CDPK-based signal transduction cascades to induce the stress response.

Kinase signaling during plant immunity

Plant immunity is produced by a number of constitutive and inducible hurdles, including physical barriers and chemical defense, to limit the growth of diverse pathogens. Two levels of inducible immunity have been identified, and are categorized based on how plants perceive the presence of a pathogen. The first level is dependent on the recognition of conserved molecular signatures, called pathogen-associated molecular patterns (PAMPs), which are recognized at the cellular surface by pattern-recognition receptors (PRR). These PRRs are typically leucine-rich repeat or LysM RLKs and may require a kinase co-receptor to initiate pattern-triggered immunity (PTI). To overcome this ubiquitous plant defense system, biotrophic pathogens have acquired diverse repertoires of effector proteins which are transferred into the cell to disrupt PTI. Over time, plants have evolved to recognize the presence of specific effectors with resistance (R) proteins in the cytoplasm thereby activating the second level of immunity, effector-triggered immunity (ETI). While PTI is thought to confer immunity through the production of physical barriers like callose and defensive compounds, ETI is thought to limit pathogen growth by inducing programmed cell death (PCD) in infected cells. ETI can be extremely effective at limiting the spread of biotrophic pathogens and imposes a high selective pressure leading to rapid changes in effector repertoires. The dynamic interplay between effectors and R proteins is thought to underlie boom-and-bust disease cycles of biotrophic pathogens (Jones and Dangl, 2006; Lindeberg *et al.*, 2012).

Protein kinases are intricately involved in PTI for both PAMP perception and downstream signaling responses. For example, the flg22 peptide from bacterial flagellin is recognized by the FLS2 RLK which heterodimerizes with the BAK1 receptor kinase within 2 minutes to initiate transphosphoylation and downstream responses (Chinchilla *et al.*, 2007).

Activation of ion transport across the plasma membrane (PM) leads to depolarization (a shift towards more positive voltages) of the trans-plasma membrane voltage gradient. The activated ion transport is also associated with apoplastic alkalinization and Ca^{2+} spiking in the cytoplasm. Downstream signaling cascades are induced within 3-5 minutes and include MAPK and CDPK-dependent pathways. For example, the MKK4/MKK5-MPK3/MPK6 and MEKK1-MKK1/2-MPK4 signaling cascades have a significant influence on pathogen resistance through their regulation of transcription factors (Asai *et al.*, 2002; Gao *et al.*, 2008). The MAPK and CDPK signaling pathways induce expression of an overlapping set of genes starting at 30 minutes after flg22 treatment. The *NHL10* and *CYP81F2* genes are induced by both pathways while other genes such as *WRKY29, FRK1* and *PHI-1* are specifically induced by either MAPKs or CDPKs (Boudsocq *et al.*, 2010). This indicates that these pathways induce both overlapping and independent responses and suggests some level of cross-talk between them.

Unlike PTI, the role of protein kinases in promoting effector-induced signaling is less clear and may depend on the effector that is being perceived. Effector perception is mediated by *R* genes, which encode nucleotide-binding leucine-rich repeat (NB-LRR) proteins. NB-LRRs have variable localization and activation sites including the cytosol, PM, Golgi, tonoplast or the nucleus and require *NDR1* or *EDS1* and *PAD4* for nuclear reprogramming (Bernoux *et al.*, 2011). In tobacco, *SIPK* and *WIPK* and their upstream *MEK2* are required for ETI response to the *tobacco mosaic virus N*-gene (Meng & Zeng, 2013). The MEK2-SIPK/WIPK cascade is also activated downstream of MAPKKKα and MAPKKKε in response to the avrPto and avrPtoB effector detection by Pto and Prf (Meng & Zeng, 2013). Interestingly in Arabidopsis, no kinase signaling components have been identified which are required for ETI signaling, but mutation or

reduced expression of *MPK3/MPK6* and *MPK4* induces ETI expression through activation of the SNC1 and SUMM2 *R* proteins, respectively (Meng & Zeng, 2013).

PTI and ETI are hypothesized to rely on an overlapping set of signaling components and to represent two extremes on a continuum of immune responses (Thomma *et al.*, 2011). This hypothesis is based on a number of factors, the first being that PTI likely appeared before ETI in plant evolution (Block *et al.*, 2008). Indeed both PTI and ETI induce similar signaling responses including ROS production and MPK3/MPK6 activation. However during ETI, these responses are sustained for longer than PTI (Zhang *et al.*, 2007; Underwood *et al.*, 2007). The functional relevance of both ROS production and MPK3/MPK6 phosphorylation in ETI remains unclear (Tsuda and Katagiri, 2010). Nevertheless, transcriptomic studies have demonstrated approximately half of the genes induced during PTI are also induced during ETI-inducing treatments, suggesting signaling conservation (Navarro *et al.*, 2004). However in light of the fact that a significant overlap in gene induction also occurs between PTI and abiotic stresses (Ma and Bohnert, 2007), some have hypothesized that plants induce an initial generalized stress response which may explain some of the overlap in ETI and PTI expression (Walley *et al.*, 2007). Indeed abiotic stresses also activate similar signaling responses as PTI including ROS production, Ca^{2+} spiking, ion transport and kinase cascades where signaling kinases are thought to be a major player in cross-talk between biotic and abiotic stress pathways (Fujita *et al.*, 2006; Tena *et al.*, 2001). For example, MPK4 and MPK6 are activated in response to pathogens, cold, low humidity, touch, drought and wounding in Arabidopsis (Ichimura *et al.*, 2000; Tsugama *et al.*, 2012; Droillard *et al.*, 2004). Thus, while it is tempting to assume that the same signaling machineries are used for PTI and ETI based on transcriptomic data, a more thorough investigation of the signaling kinases involved in these processes is warranted.

Dissertation overview

In light of the importance and functional redundancy of protein kinases in plant immunity, we have taken a proteomic approach to identify novel immunity-associated kinases. In chapter 2, we describe the development of a functional protein microarray method to measure interactions and enzymatic activity of kinases on a large scale. Chapter 3 presents a study on 36 effector-interacting kinases, in which we compare their role in multiple signaling pathways and bacterial resistance in *Nicotiana benthamiana*. Chapter 4 outlines the characterization of the *Arabidopsis thaliana Integrin-linked kinase1*, a positive regulator of basal immunity and salt stress response. Finally, Chapter 5 describes the implications of these findings for our understanding of immunity, and recommendations for future study.

REFERENCES

Adams, J. a. (2003) Activation loop phosphorylation and catalysis in protein kinases: Is there functional evidence for the autoinhibitor model? *Biochemistry*, **42**, 601–607.

Asai, T., Tena, G., Plotnikova, J., Willmann, M.R., Chiu, W.-L., Gomez-Gomez, L., Boller, T., Ausubel, F.M. and Sheen, J. (2002) MAP kinase signalling cascade in Arabidopsis innate immunity. *Nature*, **415**, 977–983.

Axtell, M.J., Chisholm, S.T., Dahlbeck, D. and Staskawicz, B.J. (2003) Genetic and molecular evidence that the Pseudomonas syringae type III effector protein AvrRpt2 is a cysteine protease. *Mol. Microbiol.*, **49**, 1537–1546.

Bernoux, M., Ellis, J.G. and Dodds, P.N. (2011) New insights in plant immunity signaling activation. *Curr. Opin. Plant Biol.*, **14**, 512–518.

Block, A., Li, G., Fu, Z.Q. and Alfano, J.R. (2008) Phytopathogen type III effector weaponry and their plant targets. *Curr. Opin. Plant Biol.*, **11**, 396–403.

Boudsocq, M., Willmann, M.R., McCormack, M., Lee, H., Shan, L., He, P., Bush, J., Cheng, S.-H. and Sheen, J. (2010) Differential innate immune signalling via Ca(2+) sensor protein kinases. *Nature*, **464**, 418–422.

Castells, E. and Casacuberta, J.M. (2007) Signalling through kinase-defective domains: the prevalence of atypical receptor-like kinases in plants. *J. Exp. Bot.*, **58**, 3503–3511.

Chinchilla, D., Zipfel, C., Robatzek, S., Kemmerling, B., Nürnberger, T., Jones, J.D.G., Felix, G. and Boller, T. (2007) A flagellin-induced complex of the receptor FLS2 and BAK1 initiates plant defence. *Nature*, **448**, 497–500.

Droillard, M.-J., Boudsocq, M., Barbier-Brygoo, H. and Laurière, C. (2004) Involvement of MPK4 in osmotic stress response pathways in cell suspensions and plantlets of Arabidopsis thaliana: activation by hypoosmolarity and negative role in hyperosmolarity tolerance. *FEBS Lett.*, **574**, 42–48.

Fujita, M., Fujita, Y., Noutoshi, Y., Takahashi, F., Narusaka, Y., Yamaguchi-Shinozaki, K. and Shinozaki, K. (2006) Crosstalk between abiotic and biotic stress responses: a current view from the points of convergence in the stress signaling networks. *Curr. Opin. Plant Biol.*, **9**, 436–442.

Gao, M., Liu, J., Bi, D., Zhang, Z., Cheng, F., Chen, S. and Zhang, Y. (2008) MEKK1, MKK1/MKK2 and MPK4 function together in a mitogen-activated protein kinase cascade to regulate innate immunity in plants. *Cell Res.*, **18**, 1190–1198.

Gribskov, M., Fana, F., Harper, J., Hope, D.A., Harmon, A.C., Smith, D.W., Tax, F.E. and Zhang, G. (2001) PlantsP: a functional genomics database for plant phosphorylation. *Nucleic Acids Res.*, **29**, 111–113.

Hrabak, E.M., Chan, C.W.M., Gribskov, M., et al. (2003) The Arabidopsis CDPK-SnRK superfamily of protein kinases. *Plant Physiol.*, **132**, 666–680.

Ichimura, K., Mizoguchi, T., Yoshida, R., Yuasa, T. and Shinozaki, K. (2000) Various abiotic stresses rapidly activate Arabidopsis MAP kinases ATMPK4 and ATMPK6. *Plant J.*, **24**, 655–665.

Johnson, K.C.M., Dong, O.X., Huang, Y. and Li, X. (2012) A rolling stone gathers no moss, but resistant plants must gather their mOSes. In *Cold Spring Harbor symposia on quantitative biology*. Cold Spring Harbor Laboratory Press, pp. 259–268.

Jones, J.D.G. and Dangl, J.L. (2006) The plant immune system. *Nature*, **444**, 323–329.

Lehti-Shiu, M.D., Zou, C., Hanada, K. and Shiu, S.-H. (2009) Evolutionary history and stress regulation of plant receptor-like kinase/pelle genes. *Plant Physiol.*, **150**, 12–26.

Lewis, J.D., Lo, T., Bastedo, P., Guttman, D.S. and Desveaux, D. (2014) The rise of the undead: pseudokinases as mediators of effector-triggered immunity. *Plant Signal. Behav.*, **9**, 18722–18727.

Lindeberg, M., Cunnac, S. and Collmer, A. (2012) Pseudomonas syringae type III effector repertoires: last words in endless arguments. *Trends Microbiol.*, **20**, 199–208.

Liu, J., Elmore, J.M., Lin, Z.-J.D. and Coaker, G. (2011) A receptor-like cytoplasmic kinase phosphorylates the host target RIN4, leading to the activation of a plant innate immune receptor. *Cell Host Microbe*, **9**, 137–146.

Ma, S. and Bohnert, H.J. (2007) Integration of Arabidopsis thaliana stress-related transcript profiles, promoter structures, and cell-specific expression. *Genome Biol.*, **8**, R49.

Mackey, D., Holt, B.F., Wiig, A. and Dangl, J.L. (2002) RIN4 interacts with Pseudomonas syringae type III effector molecules and is required for RPM1-mediated resistance in Arabidopsis. *Cell*, **108**, 743–754.

Meng, X., Zhang, S. (2013) MAPK cascades in plant disease resistance signaling. *Ann. Rev. Phytopath.* **51**, 245-266.

Mukherjee, K., Sharma, M., Jahn, R., Wahl, M.C. and Südhof, T.C. (2010) Evolution of CASK into a Mg2+-sensitive kinase. *Sci. Signal.*, **3**, ra33.

Navarro, L., Navarro, L., Zipfel, C., et al. (2004) The transcriptional innate immune response to flg22. Interplay and overlap with Avr gene-dependent defense responses and bacterial pathogenesis. *Plant Physiol.*, **135**, 1113–1128.

Rasmussen, S., Barah, P., Suarez-Rodriguez, M.C., Bressendorff, S., Friis, P., Costantino, P., Bones, A.M., Nielsen, H.B. and Mundy, J. (2013) Transcriptome responses to combinations of stresses in Arabidopsis. *Plant Physiol.*, **161**, 1783–1794.

Singh, D.K., Calviño, M., Brauer, E.K., et al. (2014) The tomato kinome and the tomato kinase library ORFeome: novel resources for the study of kinases and signal transduction in tomato and Solanaceae species. *Mol. Plant-Microbe Interact.*, **27**, 7–17.

Tena, G., Asai, T., Chiu, W.-L. and Sheen, J. (2001) Plant mitogen-activated protein kinase signaling cascades. *Curr. Opin. Plant Biol.*, **4**, 392–400.

Thomma, B.P.H.J., Nürnberger, T. and Joosten, M.H. a J. (2011) Of PAMPs and effectors: the blurred PTI-ETI dichotomy. *Plant Cell*, **23**, 4–15.

Tsuda, K. and Katagiri, F. (2010) Comparing signaling mechanisms engaged in pattern-triggered and effector-triggered immunity. *Curr. Opin. Plant Biol.*, **13**, 459–465.

Tsuda, K., Mine, A., Bethke, G., Igarashi, D., Botanga, C.J., Tsuda, Y., Glazebrook, J., Sato, M. and Katagiri, F. (2013) Dual regulation of gene expression mediated by extended MAPK activation and salicylic acid contributes to robust innate immunity in Arabidopsis thaliana. *PLoS Genet.*, **9**, e1004015.

Tsugama, D., Liu, S. and Takano, T. (2012) Drought-induced activation and rehydration-induced inactivation of MPK6 in Arabidopsis. *Biochem. Biophys. Res. Commun.*, **426**, 626–629.

Ubersax, J.A. and Ferrell Jr, J.E. (2007) Mechanisms of specificity in protein phosphorylation. *Nat. Rev. Mol. cell Biol.*, **8**, 530–541.

Underwood, W., Zhang, S. and He, S.Y. (2007) The Pseudomonas syringae type III effector tyrosine phosphatase HopAO1 suppresses innate immunity in Arabidopsis thaliana. *Plant J.*, **52**, 658–672.

Walley, J.W., Coughlan, S., Hudson, M.E., Covington, M.F., Kaspi, R., Banu, G., Harmer, S.L. and Dehesh, K. (2007) Mechanical stress induces biotic and abiotic stress responses via a novel cis-element. *PLoS Genet.*, **3**, e172.

Zhang, J., Shao, F., Li, Y., et al. (2007) A Pseudomonas syringae effector inactivates MAPKs to suppress PAMP-induced immunity in plants. *Cell Host Microbe*, **1**, 175–185.

Zipfel, C., Kunze, G., Chinchilla, D., Caniard, A., Jones, J.D.G., Boller, T. and Felix, G. (2006) Perception of the bacterial PAMP EF-Tu by the receptor EFR restricts Agrobacterium-mediated transformation. *Cell*, **125**, 749–760.

CHAPTER 2

Experimental and analytical approaches to characterize plant kinases using protein microarrays*

ABSTRACT

Comprehensive analysis of protein kinases and cellular signaling pathways requires the identification of kinase substrates and other interaction partners using large-scale amenable approaches. Here, we describe our methods for producing plant protein microarrays (PMAs) and discuss various parameters critical to the quality of PMAs. Next, we describe methods for detecting protein-protein interactions and kinase activity including auto-phosphorylation and substrate phosphorylation. We have provided a short video demonstrating how to conduct an interaction assay and how to properly handle a protein microarray. Finally, a set of methods are presented for the acquisition of PMA data and statistical decisions for selecting PMA candidates. The experimental and analytical protocols described here outline the steps to produce and utilize PMAs to analyze signaling networks.

*****This chapter is adapted from Brauer, E.K., Popescu, S.C. & Popescu, G.V. (2014) Experimental and analytical approaches to characterize plant kinases using protein microarrays. *Methods in Molecular Biology* 1171: 217-235. Copyright Springer Publishing. All data in this chapter was generated by E.K.B. with the exception of figure 2.3 which was generated by S.C.P.

INTRODUCTION

Understanding the function of proteins, both individually and in protein interaction networks, is the next great challenge of the post-genomic era. Protein Microarrays (PMAs) represent a relatively new approach that has significantly contributed to our understanding of protein networks in model organisms (Popescu *et al.*, 2007a; Popescu *et al.*, 2007b; Popescu, Popescu *et al.*, 2009a; Popescu *et al.*, 2009b; Wolf-Yadlin *et al.*, 2009). PMA technology consists of depositing minute quantities of full-length or truncated proteins on a modified microscope slide (MacBeath and Schreiber, 2000; Zhu *et al.*, 2000). Functional PMAs can contain thousands of proteins and are used for high-throughput probe-protein interaction screens and kinase activity screens *in vitro* (Figure 2.1). PMAs assays are a more rapid and precise method for determining probe-protein interactions than *in vivo* methods such as the yeast-two-hybrid assay (MacBeath and Schreiber, 2000; Chen *et al.*, 2010).

PMAs can be a powerful resource to generate hypotheses regarding a protein of interest or a network of protein interactions. To produce reliable results, several parameters should be optimized prior to experimentation. A first critical factor that needs consideration is the quality of the proteins used for PMA probing or printing. The model organism used to produce the purified recombinant proteins may have an effect on the protein activity, particularly in the case of kinases (Popescu *et al.*, 2009b). To circumvent this problem, plant proteins should be purified when possible from plant tissue as described below. Another important parameter is the slide surface chemistry on which the PMA is printed. Commercial glass slides are overlaid with various chemicals that allow efficient protein immobilization. The most commonly used slide surfaces for producing PMAs include nitrocellulose, silans, aldehides,

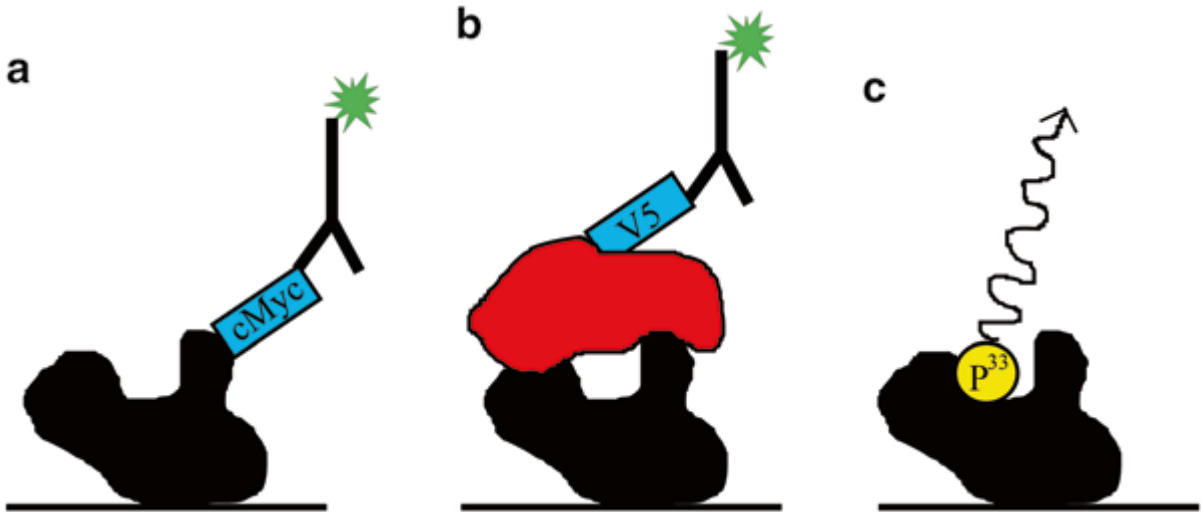

Figure 2.1 Protein microarrays can be used in three types of assays: in an immunoassay, in an interaction assay and in a kinase assay.
(a) In an immunoassay, the amount of printed cMyc-tagged protein is quantified by probing with an anti-cMyc Cy3-conjugated antibody and recording the relative fluorescence.
(b) In an interaction assay, the PMA is incubated with a V5-tagged probe protein followed by an anti-V5 Cy3-conjugated antibody. The resulting signal indicates probe-protein interaction provided the spotted protein does not show signal with the anti-V5 antibody alone (control slide).
(c) If the spotted protein on the array is a kinase, autophosphorylation or substrate phosphorylation can be measured by providing the kinase with cofactors and radioactive ^{33}P γ-ATP, washing and detecting the bound P^{33} using film.

resins, silicons, and polyacrilamide (Ptacek and Snyder, 2007; Zhu and Snyder, 2003). The type and thickness of the slide surface will determine the quantity of protein which can be immobilized, the amount of background signal and the activity of the proteins on the slide. To illustrate the importance of considering slide surface chemistry in designing a PMA experiment, we compared the performance of three commercially available slides in protein immobilization and in retaining the activity of immobilized proteins. Three types of slides, UltraGAPS, PATH and FAST, were used to demonstrate differences in immobilization of a dilution series of Cy5-labelled Anti-V5 antibodies (Figure 2.2). UltraGAPS have an amino silane-covered hydrophobic surface (Corning), while PATH and FAST slides are covered with a proprietary nitrocellulose polymer (Grace biolabs, Schleichell & Schuell BioScience). The FAST slides have the thickest slide surface, and bind the most protein as demonstrated by significantly higher signal in all six concentrations of printed antibody (Figure 2.2). However, the FAST slides also showed the highest level of background, visualized by the red color surrounding the spots in Figure 2.2A. PATH and UltraGAPS slides have thinner slide surfaces compared to FASTs, and demonstrated lower protein binding and signal intensity with the printed antibody. These slides also have the best non-saturated range of detection with minimal background and are recommended for the assays described below.

Slide surface chemistry also has a direct impact on the outcome of either an interaction assay or a kinase assay. To illustrate this effect, PMAs containing 558 *Arabidopsis* protein preparations, including over 300 kinases, were printed on GAPS II and UltraGAPS amino silane covered slides, Full Moon 3-D polymer covered slides (Full Moon Biosystems) and FAST slides. The PMAs were used in kinase autophosphorylation assays and the number of phosphorylated proteins was compared in Figure 2.3A. We found that 42% of the immobilized kinases displayed

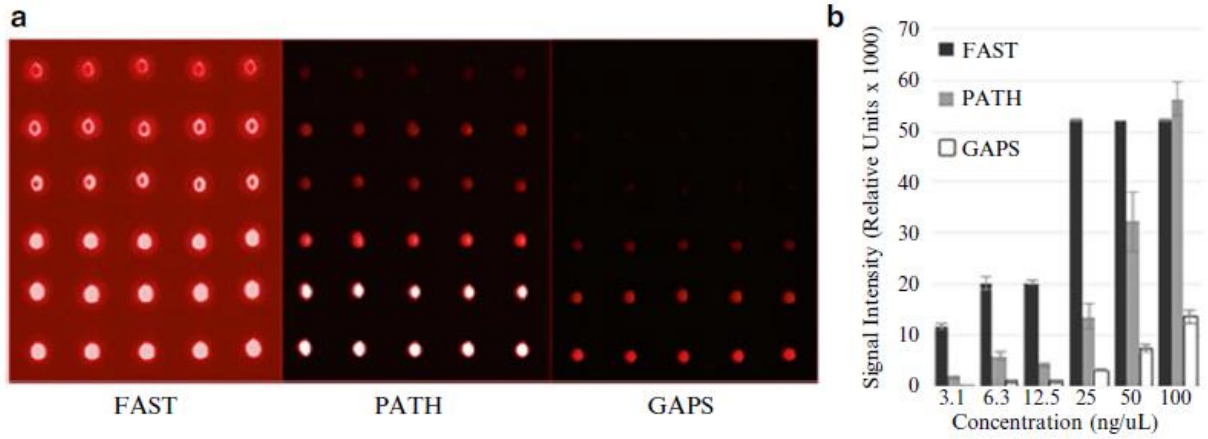

Figure 2.2 Protein binding capacity in commercially available PMA slides.
(a) Signal intensity was measured for 5 replicate spots of Cy-3 labelled anti-V5 antibody in a dilution series (100, 50, 25, 12.5, 6.3, 3.1 ng/µL) printed on FAST, PATH and GAPS slides. The range of florescence is visualized from low to high by black to red to white coloration in slides scanned at 50 % PMT immediately following printing.
(b) Quantification of the signal on arrays shown in a. Background signal was subtracted from the median signal of five replicate spots. The resulting intensities were averaged and graphed for each dilution level of the antibody along with the standard deviation.

autophosphorylation activity on GAPS, 28 % on Full Moon, and 14 % on FAST (Figure 2.3B). Quantification of signal intensity showed that kinases immobilized on GAPS slides exhibited a higher activity overall compared to the other types of slides (Figure 2.3C). These results indicate that GAPS, followed closely by the Full Moon slides, have the best kinase activity detection properties among the tested slides. Thus, while GAPS bind less protein, their surface chemistry is conducive for kinase assays. This may be due to the better availability of active protein domains for biochemical reactions or to preservation of the native folding of the proteins. A number of other parameters can be optimized for PMA assays including minimizing non-specific binding of antibodies to proteins on the array, assay conditions and probe concentration. These parameters have been discussed elsewhere and should be optimized depending on the probe and experimental design.

The protocols described below have been designed to be compatible with a broad range of plant protein kinases. Protein kinases are core components of signal transduction pathways that mediate cellular communication and fundamental processes such as growth, development and the immune response. Phosphorylation of protein substrates by kinases is one the best understood post-translational modifications and is a universal regulatory mechanism of enzymatic function. Applications of PMAs in this area are numerous and include identification of kinase phosphorylation substrates, interaction partners and substrate specificity (Popescu *et al.*, 2009b; Jones *et al.*, 2006; Mok *et al.*, 2009; Popescu and Popescu, 2011; Lee *et al.*, 2011).

Phosphorylation is a chemically simple enzymatic reaction catalyzed by a kinase, in which a phosphoryl group from the donor molecule ATP is transferred to specific serine, threonine or tyrosine residues in the protein substrate (Adams, 2001). The reaction requires

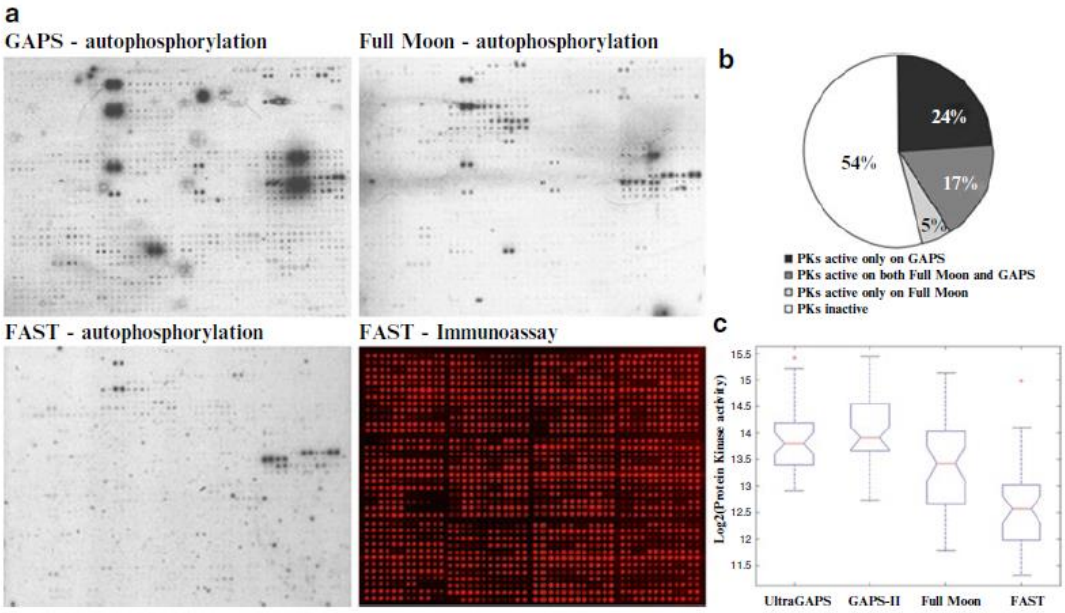

Figure 2.3 Variation of kinase activity as a function of slide surface chemistry.
(a) Autophosphorylation activity assays were performed to assess kinase activity on protein microarrays (PMAs). The PMAs containing 558 *Arabidopsis* proteins were printed in duplicate on two types of GAPS, Full Moon and FAST slides. A representative PMA area is shown for kinase assays and immunoassays, performed as described in the protocols. For the immunoassays, the PMAs were probed with anti c-Myc primary antibody, a Cy5-labeled secondary antibody, and scanned at 635 nm at PMT 400.
(b) Quantification of the results from the kinase assays performed on various PMAs.
(c) Quantification of the activity of *A. thaliana* MAPKs on PMAs. The box plots show the distribution of MAPK activity on the four types of slides.

divalent metal ions, usually Mg^{2+}, which correctly position the ATP in the kinase active site and facilitate the phosphoryl transfer reaction (Adams, 2001). An active protein kinase overlaid on the PMA is able to complete the transfer of the phosphoryl group from the ^{33}P γ-ATP donor molecule to the immobilized proteins on the slide. In general, kinases and their substrates establish transient and/or low affinity interactions, and thus kinase-substrate complexes are difficult to detect on PMAs or when using other classical molecular biology approaches such as co-immunoprecipitation. To identify putative kinase substrates on the PMAs, the enzymatically modified proteins labeled with P^{33} are visualized by exposing the probed PMA to X-ray film. Autophosphorylation can be visualized with or without a probe of interest depending on the experimental design. Interaction assays can be used to detect protein complexes formed between a probe (kinase) and the proteins immobilized on PMAs.

Here we present a comprehensive guide for generating plant PMAs, characterizing protein-protein interactions and kinase activity using PMAs, and analyzing PMA data.

MATERIALS

Prepare all materials using ultrapure water and analytical grade reagents at room temperature unless indicated otherwise. Of great importance to the workflow is a solid plan and good organization. For example, ensure that the proteins to be spotted on the PMA contain an appropriate tag (V5, cMyc, HA) which is different from the tag used on the probe protein. In the Popescu lab, we use the pYL436 vector (GenBank: AY737283.1) to purify the proteins to be printed on the PMA (cMyc tag) and the SPDK1433 vector to purify the protein probe (V5 tag)

(Lee *et al.*, 2011). Both vectors were developed from the pLIC vector backbones and are identical except for the cMyc or V5 tag. All clones should be transformed into *Agrobacterium* GV2260 and single colonies should be selected by plating transformants on antibiotic-containing plates. Protocols describing infiltration of *N. benthamiana* with clones for transient protein expression have been described elsewhere (Popescu, Popescu, *et al.*, 2007; Ratcliff *et al.*, 2001). All of the PMA assays described below have been optimized to test a wide range of protein kinases. Buffer components can be added or excluded depending on the proteins of interest.

1. Protein Purification

1. Extraction buffer: A stock of 0.1 M Tris-HCl pH 7.5, 0.1 M NaCl, 0.005 M EDTA, 0.005 M EGTA, 0.1% Triton-X, 10% glycerol, can be made and stored at 4$_{o}$C for up to 6 months. Add 0.001 M PMSF dissolved in ethanol, 0.0001 M sodium orthovanadate, 0.01 M β-glycerophosphate, protease inhibitor, 0.1% β-mercaptoethanol and 0.01 M NaF immediately preceding the extraction. Sodium orthovanadate must also be activated prior to use. Keep the buffer on ice.

2. Wash buffer: A stock of 0.1 M Tris-HCl pH 7.5, 0.5 M NaCl, 0.005 M EDTA, 0.005 M EGTA, 0.1% Triton-X, 10% glycerol, can be made and stored at 4^{o}C for up to 6 months. Add 0.001 M PMSF dissolved in ethanol, 0.0001 M sodium orthovanadate, 0.01 M β-glycerophosphate, protease inhibitor, 0.1% β-mercaptoethanol and 0.01 M NaF immediately preceding the extraction. Keep the buffer on ice.

3. Cleavage buffer: 0.05 M Tris-HCl pH 7.0, 0.15 M NaCl, 0.001 M EDTA, 0.001 M DTT, 0.1% Triton-X. Keep the buffer on ice.

4. TURBO 3C cleavage protease (catalog number H0101S, Accelagen).

5. IgG Sepharose 6 Fast Flow beads (catalog number 17-0969-01, GE Healthcare). Wash the beads three times with extraction buffer and resuspend the beads with the buffer at a 1:1 ratio. Store for up to 1 year at 4ºC.

6. Zirconia or silica beads (0.5 mm).

7. Glutathione-conjugated beads (catalog number 88821, Pierce).

2. Printing the Protein Microarrays

1. Slides: use PATH slides for immunoassay or interaction assays, (catalog number 805020, Grace biolabs), and UltraGAPS for kinase assays (catalog number 40017, Corning).

2. Purified protein preparations in 20% glycerol, stored at -80 ºC.

3. Microarray printing instrument.

4. Buffer for cleaning microarrayer pins: 0.1% SDS.

5. Negative controls: 30% BSA in 20% glycerol.

6. Positive control: 30 ug/mL Cy3 or Cy5-conjugated antibodies in 20% glycerol.

7. 96- or 384-well microarray sample plates (catalog number 7020, Genetix).

3. PMA Immunoassay

1. Protein microarray on a PATH slide.

2. Clean, empty tip box.

3. Incubation chamber; a square tissue culture plate or other small container that has two to three layers of wetted blotting paper lining the bottom.

4. Blocking buffer: PBS buffer, 0.1% Tween 10, 1% BSA.

5. Washing buffer: PBS buffer, 0.1% Tween 10.

6. Primary and labeled secondary antibody against the spotted protein tag.

7. Scanner and detection software.

4. Screening for kinase-protein interactions on PMAs

1. All the materials listed in 2.4.

2. Probing buffer: 0.01 M Tris-HCl pH 6, 0.0002 M ATP (Cell Signaling, 9804S), 0.002 M $MgCl_2$, 0.002 M $MnCl_2$, 0.0001 M $CaCl_2$, 0.2% BSA, 0.0002 M DTT. It may be desirable to make a concentrated (4x) buffer in order to not dilute the purified probe protein.

3. Slide cover slips - HibriSlip hybridization covers (Sigma, GBL716024). The cover slips are only necessary when less than 300 µL of probing buffer will be used on the arrays, to prevent drying of the slide.

4. Purified probe protein. V5-tagged protein probes should be used at a final concentration of 10 nM to 1 µM, and some experimentation with different concentrations of probe may be necessary.

5. Primary and fluorescently-labeled secondary antibody against the probe protein tag.

6. Scanner and detection software.

5. PMA-based kinase auto-phosphorylation assay

1. Protein microarray printed on a GAPS slide.

2. Clean, empty pipette tip box.

3. Incubation chamber; a square tissue culture plate or other small container which has two to three layers of wetted blotting paper lining the bottom.

4. Purified probe protein.

5. Blocking buffer: PBS buffer, 0.1% Tween 10, 1% BSA.

6. Kinase buffer: 0.05 M Tris-HCl pH 7.5, 0.01 M $MgCl_2$, 0.01 M $MnCl_2$, 0.001 M $CaCl_2$, 1% BSA, 0.001 M DTT, purified probe protein, 0.5% ATP^{33}.

7. Washing buffer: 0.05 M Tris-HCl pH 7.5, 0.5% SDS.

8. X-ray Film (Kodak)

METHODS

1. Generating PMAs using plant proteins

In this section, we describe the production of protein preparations using a plant-based expression system, generation of PMAs by contact printing onto commercial slides and visualization of the printed proteins on the array.

1.1 Protein Purification

1. Cool centrifuges to 4°C and prepare extraction buffer on ice.

2. Grind leaf tissue expressing the protein of interest very finely in liquid nitrogen and add tissue to the 0.5 mL mark on a 1.5 mL microcentrifuge tube. Fill to the 1.0 mL mark with extraction buffer and vortex immediately. Add 0.2 g of chilled zirconia beads. Incubate on ice.

3. Place the tubes in a rack under a layer of paper towels and shake using a paint shaker to further disrupt the tissue. Shake four to five times for one minute each followed by a one minute incubation on ice until large pieces of tissue are macerated.

4. Centrifuge for 10 minutes at maximum speed at 4°C. Transfer supernatant to a new tube and centrifuge again for 5 minutes. Transfer supernatant to a new tube taking care not to transfer any tissue.

5. Add 40 µL of IgG Sepharose beads and invert the tube 3-4 times to mix. Incubate for two hours at 4°C with 360° rotation.

6. Centrifuge for 5 minutes at 1000 rpm at 4°C and remove supernatant. Wash the beads with 0.5 mL of wash buffer three times.

7. Wash the beads with 1 mL of cleavage buffer without cleavage protease, centrifuge (5 min, 1000 rpm, 4^{o}C) and remove supernatant.

8. Add 50 µL of cleavage buffer containing the cleavage protease (40 µL/mL) and incubate overnight with 360^{o} rotation at 4^{o}C.

9. Optional: To remove the cleavage protease, centrifuge and add 1/10 of the total volume of glutathione-conjugated beads to the supernatant. Incubate with 360^{o}C rotation at 4^{o}C for 1 hour.

10. Harvest the supernatant and add sterile glycerol to a final concentration of 20%. Aliquot the purified protein into 15-30 µL samples, flash freeze the protein in liquid nitrogen and store at -80^{o}C until use.

11. Run a Western to visualize the purity and abundance of your protein of interest in the total extract, on the IgG Sepharose beads and in the final purified sample. A size difference should be apparent between the cleaved (+12 kDa) and uncleaved protein (+25 kDa).

12. Perform a Bradford assay to determine the approximate amount of protein in the sample.

1.2 Printing the Protein Microarrays

1. Prior to printing the PMA, determine the parameters and layout. For example, it is necessary to know the number of proteins to be printed, the number of replicate protein spots within a slide and the number of slides to be printed. It is useful to include a positive and negative control at a specific location within each block of spotted proteins. These controls help with data normalization between slides and provide a reference point during scanning. We typically use a fluorescently labeled antibody as a positive control and BSA as a negative control but other controls may be more appropriate, depending on the experiment.

2. Create an excel file with the name of the protein and the placement of the sample on the sample source plate.

3. Create a layout file using the excel spreadsheet as input into the microarray printing software. Open the output file to visualize where samples are going to be printed on the PMA based on the parameters that you have specified (replicate spot number, number of pins, number of blocks, and distance between spots).

4. Adjust your setup as necessary to print the PMAs on an appropriate number of slides. Typically, there is variation both within and between slides and thus the experimenter should consider using a minimum of three replicate slides per treatment and three replicate control slides within an experiment. Each microarray printer is different and thus a number of parameters need to be optimized ahead of printing such as the height of the printing pins during sample transfer and the number and pattern of pins that are used. We recommend spacing spots 0.3 mm apart in duplicate with 3 mm unprinted area at the periphery of the slide. Wash the printing pins after printing each sample and maintain room humidity above 50% if possible.

5. Create a GAL file and save that file for future data analysis.

6. Place samples in a 96 or 384-well plate in the order you specified in the Excel file.

7. Print the PATH or GAPS slides using the instructions provided by the microarray manufacturer.

8. Clean the pins following printing with 0.1% SDS solution and sonication for 30 minutes.

9. Carefully place your microarrays in slide holders and allow them to set overnight at 4^{o}C prior to long-term storage at -80^{o}C.

1.3 Immunoassay

Please watch the video associated with this chapter to see how to correctly handle the slides during an immunoassay.

1. Defrost the PMA by placing it on ice for 5-10 minutes.

2. Block the slides in SuperBlock buffer by carefully submerging each slide such that the buffer covers the slide all at once. Incubate for 1-2 hours, without shaking, at 4°C.

3. Remove the slide using tweezers by grasping on the barcode edge and drain excess liquid by tapping one side of the slide onto a paper towel. Do not allow the slide to dry.

4. Apply 300 μL of a 1:1000 dilution of primary antibody in blocker reagent to the slide by dripping the solution onto the slide without touching the surface. Incubate in the incubation chamber at 4°C for 1 h without shaking.

5. Drain excess liquid as before and wash slides three times in PBS-T for 5 minutes each, with shaking at 50 rpm at 4°C.

6. Apply 300 μL of a 1:1000 dilution of Cy3 or Cy5-conjugated secondary antibody in blocker reagent to the slide by dripping the solution onto the slide without touching the surface. Incubate in the incubation chamber at 4°C for 1 h without shaking.

7. Drain excess liquid as before and wash slides three times in PBS-T for 5 minutes each, with shaking at 50 rpm at 4°C.

8. Wash once by dipping the slide into a 50mL tube containing deionized water.

9. Drain excess liquid in a 50 mL Falcon tube with a Kimwipe at the bottom, and centrifuge for 3 minutes at 800xg. Allow the array to dry completely (1-2 minutes).

10. Scan for fluorescence at an appropriate PMT and resolution. Alter the PMT in order to minimize the number of saturated spots, and scan all slides at the same PMT from each experiment. Refer to section 4.1 for more information on scanning.

***2.* PMA-based methods for characterizing kinases**

Once PMAs have been produced or obtained commercially, they can be used in the two assays described below. The kinase assay is used to identify candidate phosphorylation

substrates and the interaction assay is used to test for protein-protein interactions with a kinase probe of interest. Please refer to that attached video for a demonstration of the interaction assay.

2.1 Kinase Autophosphorylation Assay

1. Block the slides in SuperBlock buffer by carefully submerging the slide such that the buffer covers the slide all at once. Incubate for 1-2 hours without shaking at 4^{o}C.

2. Remove the slide using tweezers by grasping on the barcode edge and drain excess liquid by tapping one side of the slide onto a paper towel. Do not allow the slide to dry. Apply 300 µL of kinase buffer without touching the surface of the slide.

3. Incubate in a wet chamber at 30^{o}C for 1 hour without shaking. Make sure the slides are flat and not tilted. Check back periodically to make sure that the slides are not drying on one side if a coverslip is not being used.

4. Drain excess liquid and wash slides three times in PBS-T for 5 minutes each (50 rpm, 4^{o}C).

5. Wash once by dipping the slide into a 50mL tube containing deionized water.

6. Centrifuge at 800 rpm for 1 min in a 50 mL Falcon tube, with a tissue paper at the bottom of the tube. Allow the array to dry completely (1-2 minutes).

7. Place slides in a cassette on top of a piece of paper, cover carefully with Saran wrap (no wrinkles) and tape entire unit down so nothing moves. Do not re-adjust the Saran wrap as this will dislodge the proteins on the slide.

8. Expose the slides to film for 1, 3, and 7 days in an exposure cassette.

2.2 Protein-Protein Interaction Assay

1. Defrost PMA placing on ice for 5-10 minutes.

2. Block the slides in SuperBlock buffer by carefully submerging the slide such that the buffer covers the slide all at once. Incubate for 1-2 hours without shaking at 4^{o}C.

3. Remove the slide using tweezers by grasping on the barcode edge and drain excess liquid by tapping one side of the slide onto a paper towel. Do not allow the slide to dry. Apply 300 µL of probing buffer containing the V5-labelled purified protein probe (10 nM – 1 µM probe final concentration) by dripping the solution without touching the surface of the slide. Cover the slide with a coverslip by touching the end of the slide with the edge of the coverslip and allowing the coverslip to fall on to the surface of the buffer.

4. Incubate in the incubation chamber for 90 minutes at 4^{o}C without shaking.

5. Wash the slide three times in PBS-T for 5 minutes each, with shaking at 50 rpm at 4^{o}C. Remove the coverslip.

6. Drain excess liquid and apply 300 µL of a 1:1000 dilution of primary antibody in blocker reagent. Incubate in incubation chamber at 4^{o}C for 1 h without shaking.

7. Drain excess liquid and wash slides three times in PBS-T for 5 minutes each (50 rpm, 4^{o}C).

8. Apply 300 µL of a 1:1000 dilution of Cy3 or Cy5-conjugated secondary antibody in blocker reagent. Incubate in incubation chamber at 4^{o}C for 1 h without shaking.

9. Drain excess liquid and wash slides three times in PBS-T for 5 minutes each, (50 rpm, 4^{o}C).

10. Wash once by dipping the slide into a 50mL tube containing deionized water.

11. Drain excess liquid and centrifuge in 50 mL Falcon tube with a Kimwipe at the bottom for 3 minutes at 800xg. Allow the array to dry completely (1-2 minutes).

12. Scan for fluorescence at an appropriate PMT and resolution. Alter the PMT in order to minimize the number of saturated spots, and scan all slides from the same experiment at the same PMT. Refer to section 4.1 for more information on scanning.

3. Protein microarray data acquisition

Here we describe the methods needed to acquire protein microarray data. These methods can be used to identify kinase-binding proteins from interaction assay data and phosphorylation substrates from kinase assay data.

PMAs can measure thousands of protein-protein interactions in parallel. However each interaction is measured a limited number of times, necessitating a robust method for minimizing detection error and selecting interactors which perform consistently. Here, we present methods for PMA analysis including data acquisition including scanning the PMA, aligning features to the scanned image, filtering outliers and generating the results report. Many of the acquisition and preprocessing steps are automated in commercially available software suites such as GenePix and ScanArray/ QuantArray.

3.1 Protein microarray data acquisition and processing

1. Select the wavelength for the scanning laser according to the fluorophore used for detection (i.e. 633 nm for Cy5 and 543 for Cy3, etc.); pre-scan the probed PMAs at low resolution, optimizing photomultiplier (PMT) intensity such that the positive controls do not saturate. In most cases that corresponds to an intensity between 50% and 90% of the maximum. Scan the PMA at high resolution (typically 10 microns), at the same PMT for each slide within an experiment. Save the image as a TIFF (.tif) file for further analysis and export JPG (.jpg) images for graphic illustration of the probed PMA.

2. Load the layout file (.gal file for GAL GenePix format) used to map PMA features to protein identifiers. The layout file can be generated from the clone list file describing the content of the samples used for array printing using the robotic printing software, the scanning software (i.e. Array List Generator), custom scripts, or it is simply provided by the PMA vendor. The layout

includes printing details such as position of printed blocks, rows, column, printed feature size, distance between pins, etc.

3. Align the layout features on the PMA using GenePix: for best results align all blocks first, then detect and align features in each block (pay attention to correct setting of the printing head parameters such as feature size and pin distance). Depending on the noise on the arrays and the quality of the printing, it is best to constrain the variation of the feature size to 50% from the spot diameter indicated in the layout file. Alternatively, one can use free feature segmentation (irregular shape). Review the alignment and manually adjust feature position and size if needed.

4. Perform the quality control of detected features. Validate detected features and mark features corresponding to slide artifacts (use the provided QC code, i.e. Good/Bad/Absent/Not Found). Use the provided tools to identify and mark additional outliers (i.e. features where the background is too high) if necessary. Save the GPS (.gps) file containing the optimal layout alignment for each PMA slide.

5. Generate the GPR report file (.gpr) after selecting the relevant data columns (i.e. signal intensity mean, median, standard deviation, background mean, median, standard deviation, flags, log ratios, other statistics).

SUMMARY

The protocols presented here provide detailed instructions to produce and use PMAs to examine protein kinase activity and interactions in plants. Commercially available *Arabidopsis* PMAs contain approximately 50% of the proteome (http://abrc.osu.edu/protein-chip), providing the field of plant science with an invaluable resource. Using these PMAs, the experimenter is

able to probe thousands of proteins within one day, using resources that are available in a typical molecular biology lab. PMA-based assays provide testable hypotheses for the cellular function of individual proteins and produce valuable insights into the system-level properties of kinases and cellular signaling. However, sub-optimal PMA probing conditions and inappropriate slide chemistry may facilitate spurious phosphorylation events or interactions. Like other *in vitro* methods, PMAs may produce false positive or false negatives since interactions are being measured outside of context of the cell where post-translational modifications, compartmentalization or additional protein interactions may have an influence (Wolf-Yadlin *et al.*, 2009; Zhu *et al.*, 2000; MacBeath and Schreiber, 2000). Further verification experiments using complementary methods followed by *in vivo* functional validation are required to establish the functional relevance of the PMA-obtained hits.

Moving forward, there is a need in the plant research community for shared proteomic resources such as PMAs for not only model organisms, but important crops as well. Continued production of PMAs and availability of results will enhance our understanding of protein networks and signal transduction in plants.

REFERENCES

Adams, J.A. (2001) Kinetic and catalytic mechanisms of protein kinases. *Chem. Rev.*, **101**, 2271–2290.

Chen, L.-Q., Hou, B.-H., Lalonde, S., et al. (2010) Sugar transporters for intercellular exchange and nutrition of pathogens. *Nature*, **468**, 527–32.

Jones, R.B., Gordus, A., Krall, J.A. and MacBeath, G. (2006) A quantitative protein interaction network for the ErbB receptors using protein microarrays. *Nature*, **439**, 168–174.

Lee, H.Y., Bowen, C.H., Popescu, G.V., Kang, H.-G., Kato, N., Ma, S., Dinesh-Kumar, S., Snyder, M. and Popescu, S.C. (2011) Arabidopsis RTNLB1 and RTNLB2 Reticulon-like proteins regulate intracellular trafficking and activity of the FLS2 immune receptor. *Plant Cell*, **23**, 3374–91.

MacBeath, G. and Schreiber, S.L. (2000) Printing proteins as microarrays for high-throughput function determination. *Science (80-.).*, **289**, 1760–1763.

Mok, J., Im, H. and Snyder, M. (2009) Global identification of protein kinase substrates by protein microarray analysis. *Nat. Protoc.*, **4**, 1820–1827.

Popescu, G. V and Popescu, S.C. (2011) Complexity and Modularity of MAPK Signaling Networks.

Popescu, S.C., Popescu, G. V, Bachan, S., Zhang, Z., Seay, M., Gerstein, M., Snyder, M. and Dinesh-Kumar, S.P. (2007b) Differential binding of calmodulin-related proteins to their targets revealed through high-density Arabidopsis protein microarrays. *Proc. Natl. Acad. Sci. U. S. A.*, **104**, 4730–4735.

Popescu, S.C., Popescu, G. V, Snyder, M. and Dinesh-Kumar, S.P. (2009a) Integrated analysis of co-expressed MAP kinase substrates in Arabidopsis thaliana. *Plant Signal. Behav.*, **4**, 524–527.

Popescu, S.C., Popescu, G. V., Bachan, S., Zhang, Z., Gerstein, M., Snyder, M. and Dinesh-Kumar, S.P. (2009b) MAPK target networks in Arabidopsis thaliana revealed using functional protein microarrays. *Genes Dev.*, **23**, 80–92.

Popescu, S.C., Snyder, M. and Dinesh-Kumar, S.P. (2007b) Arabidopsis Protein Microarrays for the High-Throughput Identification of Protein-Protein Interactions. *Plant Signal. Behav.*, **2**, 416–420.

Ptacek, J. and Snyder, M. (2007) 14 Yeast Protein Microarrays. In I. S. and M. J. R. S. B. T.-M. in Microbiology, ed. *Yeast Gene Analysis Second Edition*. Academic Press, pp. 303–705.

Ratcliff, F., Martin- Hernandez, A.M. and Baulcombe, D.C. (2001) Technical advance: tobacco rattle virus as a vector for analysis of gene function by silencing. *Plant J.*, **25**, 237–245.

Wolf-Yadlin, A., Sevecka, M. and MacBeath, G. (2009) Dissecting protein function and signaling using protein microarrays. *Curr. Opin. Chem. Biol.*, **13**, 398–405.

Zhu, H., Klemic, J.F., Chang, S., et al. (2000) Analysis of yeast protein kinases using protein chips. *Nat. Genet.*, **26**, 283–289.

Zhu, H. and Snyder, M. (2003) Protein chip technology. *Curr. Opin. Chem. Biol.*, **7**, 55–63.

CHAPTER 3

Regulation of plant immunity by effector-interacting kinase networks*

ABSTRACT

The pathogen *Pseudomonas syrinage* pv. *tomato* DC3000 evades recognition of extracellular pathogen-associated molecular patterns (PAMP) by injecting effector proteins into the cell. A subset of effectors such as AvrPto and HopAI1, suppress pattern-triggered immunity (PTI) induced by PAMPs, by modulating the function of host protein kinases by altering phosphorylation status or complex formation. To understand the role of protein kinases which may be targeted by four PTI-repressing effectors, we tested the functional relevance of 36 kinases with multiple effector interactors in *N. benthamiana.* All but one of these kinases had a role in basal immunity, effector-triggered immunity (ETI), or MAPK signaling. A subset of these kinases altered basal immunity only in the presence of the *HopAI1*, *AvrPto*, *HopA1* and *HopAF1* effectors demonstrating that effector context has a significant impact on kinase-dependent pathways. Only one kinase was required for both basal immunity and ETI, while MAPK signaling and ETI responses employed an overlapping set of 10 kinases. Together, this

---

*****This chapter is currently in preparation for submission to *PLOS Pathogens*. All data in this chapter was generated by E.K.B. in collaboration Kamala Gupta, Bhaskar Gupta and Mauricio Calvino. E.K.B., George Popescu and S.C.P performed the analysis and interpretation of the data and E.K.B and S.C.P. contributed to writing. This work is based on protein interaction screens performed by Dharmendra Singh and pathogen strains were graciously provided by Suma Chakravarthy and Alan Collmer.

study identifies novel immunity components and indicates that basal immunity and ETI responses require distinct sets of kinases and supports the hypothesis that multiple layers of kinases promote basal immunity.

INTRODUCTION

Uncovering the architecture and signal flow of immune response networks in plants is central to understanding how plants respond to pathogens. Pathogens overcome these partially functionally redundant protein kinase-based signaling networks by perturbing kinase function using effectors (Kvitko *et al.*, 2009). While some of these effectors and their functional targets have been functionally validated, the breadth and the depth of effector-host interactions is only beginning to be understood (Mukhtar *et al.*, 2011). Unravelling the complexity of these interactions can reveal important components in plant immunity and help to elucidate how plants defend themselves against diverse pathogens.

Plants basal immunity is comprised of constitutive and inducible forms of protection, which help to limit the growth of a wide range of pathogens. One branch of the inducible immune system involves detection of conserved molecular signatures called pathogen-associated molecular patterns (PAMPs), which triggers PAMP-triggered immunity (PTI). A second level of inducible immunity is initiated by detection of effector proteins in the cytoplasm, which triggers effector-triggered immunity (ETI). While PTI confers resistance to a broad range of microbes which share a PAMP, ETI provides resistance to only those pathogens which carry a recognizable effector. PAMP recognition is typically mediated by complexes of receptor-like kinases (RLKs), receptor kinases and receptor-like cytosolic kinases (RLCK) which activate

downstream MAPK cascades and other cytosolic kinases (Macho and Zipfel, 2014). In contrast, effector recognition is mediated by NB-LRR proteins which also activate MAPK and cytosolic kinases (Meng and Zhang, 2013). While some transcriptomic and genetic evidence suggest ETI and PTI require similar groups of kinases, only MPK3 and MPK6 have been shown to have a significant role in both levels of immunity in Arabidopsis (Tsuda *et al.*, 2013; Navarro *et al.*, 2004).

Bacterial pathogens subvert the robust PTI and ETI responses by injecting effectors into the cytosol, some of which target kinase-mediated immune signaling. For example, the AvrPto and AvrPtoB effectors have a significant effect on *Pseudomonas syringae* virulence and seem to play redundant roles in blocking PAMP perception through direct interaction with the RLKs FLS2 and EFR (Martin, 2012). Several effectors including AvrPto appear to be able to bind multiple kinases, which is thought to contribute to their PTI-suppressing function (Singh *et al.*, 2014). For example, the HopAI1 effector is a phosphothreonine lyase that binds and inactivates MPK3 and MPK6 and represses host defense gene induction in response to PAMPs (Li *et al.*, 2005; Zhang *et al.*, 2007). Other effectors such as AvrB and AvrRpm1 depend on host kinases to modulate phosphorylation status of host proteins like RIN4, thereby altering PTI responses (Liu *et al.*, 2011).

We hypothesized that protein kinases which interact with effectors may be involved in immune response and that study of several such kinases is likely to generate insights into the architecture and signal flow in plant immunity. To test this hypothesis, we set to explore the interface between the tomato kinome and effectors from the bacterial pathogens *P. syringae* pv. *tomato* and *P. syringae* pv. *phaselicola*. We recently developed a tomato protein kinase clone library and a robust screening assay to identify kinase-effector interactions in tomato cells

(Singh, Calviño et al. 2014). To determine if these kinases are required for immunity, we examined the function of their homologs in the closely related *N. benthamiana*, which is more consistently and easily transformed compared to tomato. Here we report the functional characterization of 36 effector-interacting kinases in *N. benthamiana* and their role in basal immunity, ETI, MAPK responses and response to specific effectors.

RESULTS

Effector-interacting kinases contribute to basal immunity

A previously performed screen to identify tomato kinases that interact with four *Pseudomonas syringae* effectors – HopA1, HopAI1, HopAF1, AvrPto – revealed that of the 139 kinase-effector interactors (*KEI*s), 76% interacted with multiple effectors (Singh *et al.*, 2014, data not shown). Based on recent studies demonstrating that proteins targeted by multiple effectors are important for immunity, we hypothesized that the *KEI*s play a role in immune responses (Mukhtar *et al.*, 2011; Weßling *et al.*, 2014). A focus group of 36 *KEI*s, representing 49% of the highly-targeted *KEI*s including four known immune kinases (FLS2, BAK1, SOBIR1 and MPK6) was selected for functional characterization (Table 3.1). To characterize the *KEIs'* potential functions in immune-related signaling pathways, the expression of individual *KEIs* was silenced in *Nicotiana benthamiana* using viral-induced gene silencing (VIGS)(Figure 3.1, Table 3.2) and plant responses to various immunity- or PCD-inducing treatments were probed. A VIGS construct containing a gene fragment from *Escherichia coli* (EC1) was included as a negative control.

Table 3.1 Description of the selected *KEI*s for further functional analysis in *N. benthamiana.* Information on the tomato ortholog used to design primers for silencing, the *Arabidopsis* ortholog and gene name, and kinase classification according to the PlantsP classification system are presented (PPC code, www.plantsp.genomics.purdue.edu/).

***KEI* ID**	**Tomato ID**	**Classification**	**PPC code**	**Arabidopsis ID**	**Gene name**
KEI143	Solyc02g081070	Strubbelig Receptor Family 1	PPC:1.1.1	AT4G22130	*SRF8*
KEI37	Solyc02g065520	Putative receptor-like protein kinase	PPC:1.1.3	AT2G33580	*LYK5*
KEI188	Solyc02g089900	Putative receptor-like protein kinase	PPC:1.1.3	AT2G23770	*LYK4*
KEI150	Solyc02g068300	Legume Lectin Domain Kinase	PPC:1.11.1	AT5G06740	*LecRK-S4*
KEI151	Solyc02g087460	Leucine Rich Repeat Kinase X	PPC:1.12.1	AT3G28450	*BIR2*
KEI342	Solyc10g047140	Leucine Rich Repeat Kinase II & X	PPC:1.12.2	AT4G33430	*BAK1*
KEI156	Solyc07g006110	Leucine Rich Repeat Kinase II & X	PPC:1.12.2	AT2G23950	
KEI279	Solyc08g074760	Leucine Rich Repeat Kinase II & X	PPC:1.12.2	AT2G35620	*FEI1*
KEI91	Solyc03g113450	Leucine Rich Repeat Kinase II & X	PPC:1.12.2	AT5G62710	
KEI92	Solyc05g056370	Leucine Rich Repeat Kinase II & X	PPC:1.12.2	AT5G63710	
KEI153	Solyc05g010400	Leucine Rich Repeat Kinase II & X	PPC:1.12.2	AT5G16000	*NIK1*
KEI72	Solyc06g071810	Leucine Rich Repeat Kinase X	PPC:1.12.5	AT2G31880	*SOBIR1*
KEI160	Solyc08g081940	Leucine Rich Repeat Kinase III	PPC:1.13.3	AT4G23740	
KEI163	Solyc03g095490	Leucine Rich Repeat Kinase	PPC:1.13.3	AT5G58300	

		III			
KEI161	Solyc06g068910	Leucine Rich Repeat Kinase III	PPC:1.13.3	AT1G48480	*RLK1*
KEI7	Solyc07g042590	Receptor Like Cytoplasmic Kinase VII	PPC:1.2.2	AT2G07180	*PBL17*
KEI86	Solyc11g072660	Receptor Like Cytoplasmic Kinase VII	PPC:1.2.2	AT1G07870	*PBL5*
KEI196	Solyc10g012170	Receptor Like Cytoplasmic Kinase VII	PPC:1.5.3	AT4G00330	*CRCK2-like*
KEI149	Solyc03g006890	Receptor Like Cytoplasmic Kinase VI	PPC:1.10.1	AT3G15890	*PTI1-like*
KEI104	Solyc11g064890	Receptor Like Cytoplasmic Kinase II	PPC:1.16.1	AT1G63500	*BSK7*
KEI221	Solyc05g013070	Ankyrin Repeat Domain Kinase (Raf-related in Group C1 of MAP3K group)	PPC:2.1.2	AT1G14000	*VIK*
KEI20	Solyc01g097980	CTR1/EDR1 Kinase (Raf in Group B2 of MAP3Ks)	PPC:2.1.3	AT1G08720	*EDR1/ AtMAP3 Kδ3*
KEI25	Solyc02g078140	GmPK6/AtMRK 1 Family (Raf-related in Group C5 of MAP3K group)	PPC:2.1.4	AT5G58950	
KEI304	Solyc03g123800	MAP2K	PPC:4.1.3	AT3G21220	*MKK5*
KEI327	Solyc12g019460	MAPK	PPC:4.5.1	AT2G43790	*MPK6*
KEI33	Solyc06g082440	SNF1 Related Protein Kinase (SnRK)	PPC:4.2.4	AT2G30360	*SIP4/ SNRK3.22*
KEI250	Solyc12g010130	SNF1 Related Protein Kinase (SnRK)	PPC:4.2.4	AT4G30960	*CIPK6*
KEI255	Solyc06g068450	SNF1 Related Protein Kinase (SnRK)	PPC:4.2.4	AT5G25110	*CIPK25*

KEI311	Solyc03g115700	SNF1 Related Protein Kinase (SnRK)	PPC:4.2.4	AT3G01090	*AKIN10*
KEI318	Solyc04g012160	SNF1 Related Protein Kinase (SnRK)	PPC:4.2.4	AT4G33950	*OST1*
KEI376	Solyc01g103940	SNF1 Related Protein Kinase (SnRK)	PPC:4.2.4	AT1G60940	*SNRK2.10*
KEI323	Solyc06g071210	IRE/NPH/PI dependent/S6 Kinase	PPC:4.2.6	AT3G08720	*S6K2*
KEI259	Solyc06g008330	IRE/NPH/PI dependent/S6 Kinase	PPC:4.2.6	AT2G20470	
KEI272	Solyc12g062870	GSK3/Shaggy Like Protein Kinase Family	PPC:4.5.4	AT5G14640	*SK13*
KEI339	Solyc06g069330	Other Kinase	PPC:5.1.1	AT5G08160	*ATPK3*

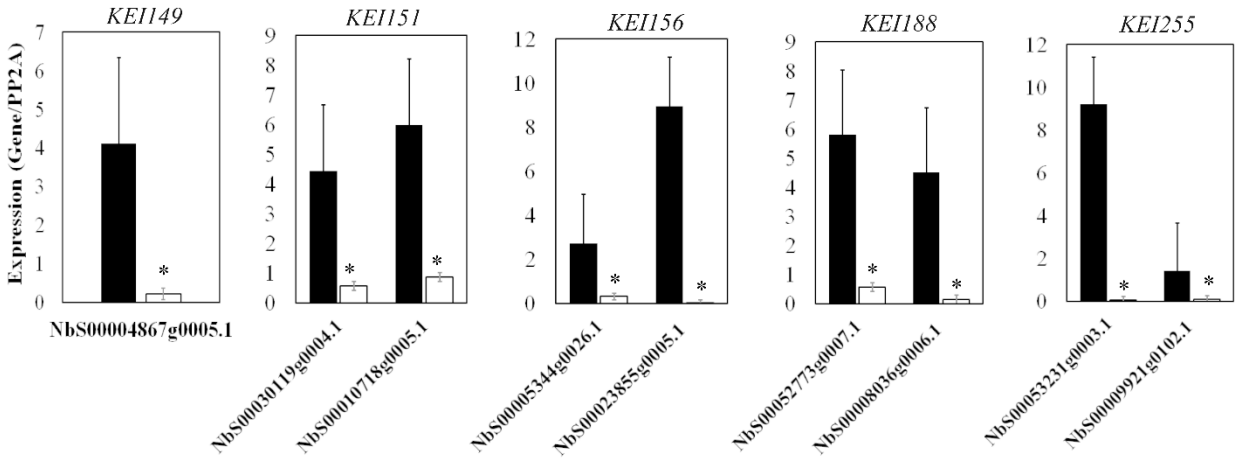

Figure 3.1 Verification of gene silencing of kinases in *KEI* lines.
The genes which are predicted to be silenced by individual VIGS constructs are described in Table 3.2. The expression of these genes were then quantified by qRT PCR where expression was normalized to the PP2A gene. The asterisk indicates significantly altered expression relative to the EC1 control line.

Table 3.2 Predicted *N. benthamiana* silencing targets for *KEI* lines using the Sol Genomics VIGS design tool (www.solgenomics.net).

***KEI* line ID**	**Tomato Gene ID**	**Predicted Targets**	**Predicted off-targets**
KEI143	Solyc02g081070	NbS00055518g0003.1	
KEI37	Solyc02g065520	NbS00012824g0002.1 NbS00006810g0118.1	
KEI188	Solyc02g089900	NbS00052773g0007.1 NbS00008036g0006.1	NbS00008036g0004.1 NbC26073808g0002.1
KEI150	Solyc02g068300	NbS00004867g0005.1	
KEI151	Solyc02g087460	NbS00030119g0004.1 NbS00010718g0005.1	NbS00056452g0008.1 NbS00056452g0009.1
KEI342	Solyc10g047140	NbS00044412g0010.1 NbS00003411g0018.1	
KEI156	Solyc07g006110	NbS00005344g0026.1 NbS00023855g0005.1	
KEI279	Solyc08g074760	NbS00032709g0016.1 NbS00056913g0001.1	NbS00016190g0006.1 NbS00035814g0001.1
KEI91	Solyc03g113450	NbS00042791g0006.1 NbS00049670g0007.1	
KEI92	Solyc05g056370	NbS00019122g0004.1 NbS00025463g0012.1	
KEI153	Solyc05g010400	NbS00012058g0007.1	
KEI72	Solyc06g071810	NbS00037616g0014.1 NbS00033954g0002.1 NbS00006092g0015.1	NbS00005491g0024.1
KEI160	Solyc08g081940	NbS00027675g0005.1 NbS00030754g0008.1	
KEI163	Solyc03g095490	NbS00007294g0015.1 NbS00005729g0009.1	NbS00018948g0003.1
KEI161	Solyc06g068910	NbS00005919g0003.1	
KEI7	Solyc07g042590	NbS00046910g0007.1 NbS00040223g0007.1	NbS00032837g0003.1
KEI86	Solyc11g072660	NbS00031691g0018.1 NbS00046018g0001.1 NbS00003259g0009.1 NbS00037822g0005.1	
KEI196	Solyc10g012170	NbS00001871g0010.1 NbS00012422g0010.1	NbS00040530g0013.1 NbS00005966g0012.1 NbS00038795g0005.1
KEI149	Solyc03g006890	NbS00004867g0005.1	

KEI104	Solyc11g064890	NbS00049297g0008.1 NbS00008710g0016.1	NbS00025065g0006.1 NbS00010386g0020.1 NbS00034642g0001.1 NbS00035104g0006.1 NbS00023423g0007.1
KEI221	Solyc05g013070	NbS00002505g0024.1 NbS00017293g0010.1	
KEI20	Solyc01g097980	NbS00017432g0014.1 NbS00011737g0001.1	
KEI25	Solyc02g078140	NbS00033220g0003.1 NbS00035332g0004.1	
KEI304	Solyc03g123800	NbS00012713g0030.1 NbS00006609g0002.1	
KEI327	Solyc12g019460	NbS00060107g0004.1 NbS00036924g0003.1 NbS00003284g0009.1 NbS00003284g0006.1	
KEI33	Solyc06g082440	NbS00033396g0001.1 NbS00057370g0001.1	
KEI250	Solyc12g010130	NbS00006911g0001.1 NbS00044379g0001.1	
KEI255	Solyc06g068450	NbS00053231g0003.1 NbS00009921g0102.1	
KEI311	Solyc03g115700	NbS00001056g0057.1	NbS00006811g0001.1
KEI318	Solyc04g012160	NbS00013414g0001.1 NbS00061263g0003.1	NbS00027230g0001.1
KEI376	Solyc01g103940	NbS00001404g0029.1 NbS00005219g0010.1	NbS00054246g0008.1
KEI323	Solyc06g071210	NbS00015787g0004.1 NbS00003311g0003.1 NbS00054087g0006.1	
KEI259	Solyc06g008330	NbS00002051g0010.1 NbS00023439g0002.1 NbS00006379g0032.1 NbS00025105g0013.1	NbS00041702g0008.1 NbS00057232g0004.1 NbS00040185g0011.1
KEI272	Solyc12g062870	NbS00003134g0111.1 NbS00000901g0007.1	
KEI339	Solyc06g069330	NbS00043523g0017.1 NbS00030449g0013.1	

To explore the potential roles of *KEI*s in basal immunity, we generated a set of mutant *P. syringae pv. tomato* (*Pst*) strains which included one effectorless strain, D29E, and four single-effector strains in the D29E background expressing AvrPto, HopA1, HopAF1 or HopAI1. To determine the relative virulence of these strains, we infiltrated the EC1 control line with the five strains and quantified bacterial growth at 6 days post-infiltration (dpi). The D29E effectorless strain and the D29E + HopA1 strain grew to similar levels while strains containing AvrPto, HopAI1 and HopAF1, grew to significantly higher levels (3%)(Figure 3.2a).

To determine the contribution of the focus *KEIs* to the plant immune response, we quantified the growth of the five *Pst* strains in silenced plants using the method described above. Following infection with the effectorless D29E strain, 7 lines (19%) supported significantly different levels of growth relative to the EC1 control (Figure 3.2b). The majority of *KEIs*, including RLKs and RLCKs, promoted higher bacterial growth counts when silenced, indicating a positive role in immunity. Silencing of *KEI339* resulted in decreased bacterial growth, outlining *KEI339* as a susceptibility gene. Susceptibility genes were postulated to function as either positive determinants of pathogen virulence or negative modulators of plant defenses (Eckardt, 2002; Pavan *et al.*, 2010).

Following inoculations with individual D29E + effector strains, 72% of the *KEIs* were revealed to have an immune phenotype relative to EC1 (Figure 3.2c-f). Within these *KEI* lines, 62% demonstrated increased bacterial growth while 38% demonstrated decreased growth. The *KEI* lines often demonstrated significant phenotypes in response to multiple strains including *SOBIR1* and *MPK6*, while *BAK1* was only required for response to *D29E+HopA1*. Lines which were silenced for RLKs demonstrated some of the largest increases in bacterial growth though all kinase groups demonstrated significant immune phenotypes (Figure 3.2g). Some of the *KEI* lines

Figure 3.2 Bacterial growth in *KEI* lines infected with strains of the effectorless *P. syringae* pv. *tomato* D29E pathogen.
(a) Growth of the D29E strain in the control line transformed with a vector targeting the bacterial EC1 gene. The N indicates the number of biological replicates.
(b) – (f) Growth of the indicated D29E strain or D29E strain containing an effector in the indicated *KEI* line on the horizontal axis relative to the EC1 control line in grey. All of the lines indicated in the graphs show significantly altered bacterial growth relative to the EC1 control ($p<0.05$) and the number of biological replicates is indicated (N).
(g) The p-values for all *KEI* lines, arranged by kinase classification under all bacterial growth conditions. Bars which extend above the central axis indicate significant difference from EC1 at $p<0.05$.

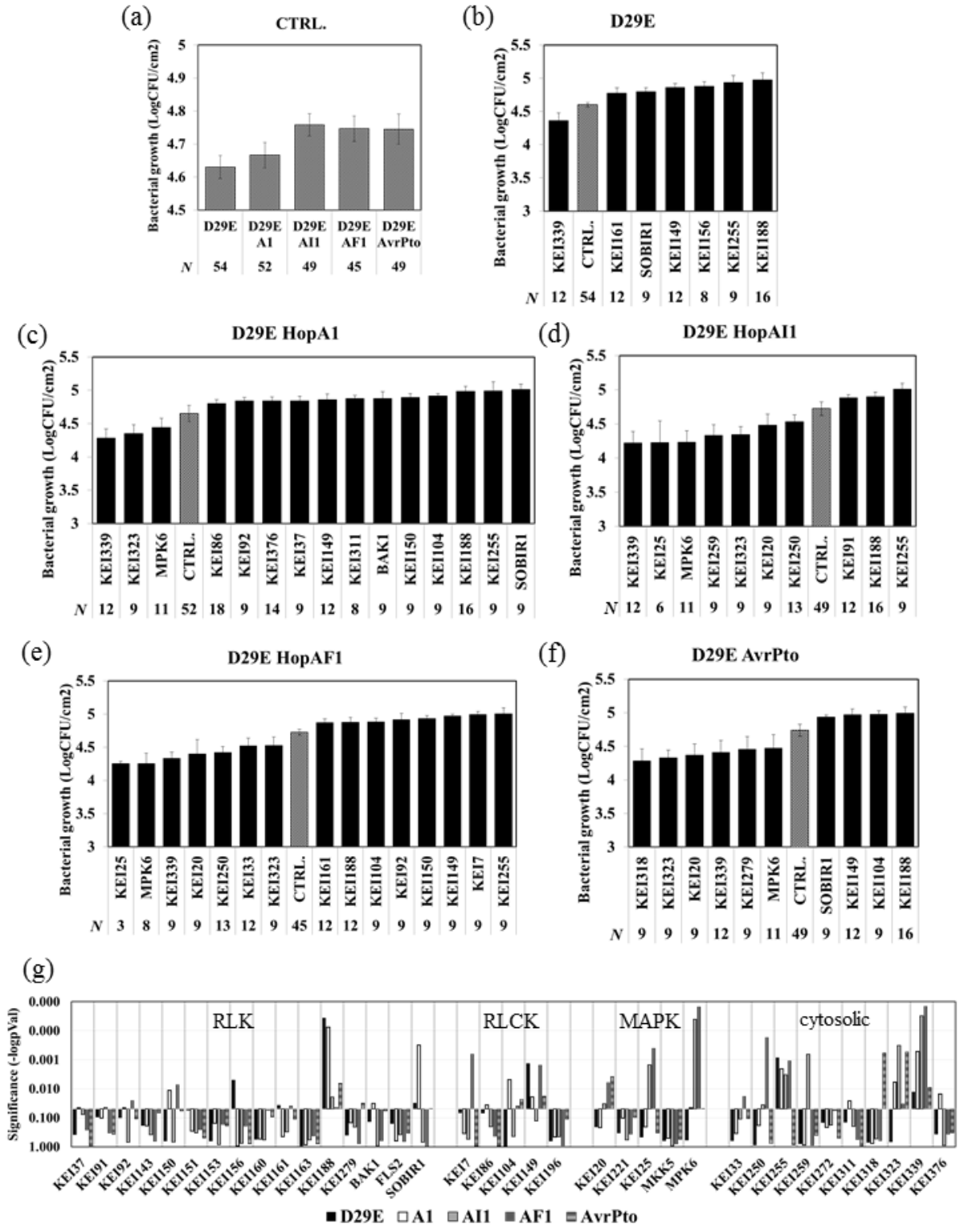
(a)
CTRL.
Bacterial growth (LogCFU/cm2)
D29E
D29E A1
D29E AI1
D29E AF1
D29E AvrPto
N 54 52 49 45 49
(b)
D29E
KEI339 CTRL. KEI161 SOBIR1 KEI149 KEI156 KEI255 KEI188
N 12 54 12 9 12 8 9 16
(c)
D29E HopA1
KEI339 KEI323 MPK6 CTRL. KEI86 KEI92 KEI376 KEI37 KEI149 KEI311 BAK1 KEI150 KEI104 KEI188 KEI255 SOBIR1
N 12 9 11 52 18 9 14 9 12 8 9 9 9 16 9 9
(d)
D29E HopAI1
KEI339 KEI25 MPK6 KEI259 KEI323 KEI20 KEI250 CTRL. KEI91 KEI188 KEI255
N 12 6 11 9 9 9 13 49 12 16 9
(e)
D29E HopAF1
KEI25 MPK6 KEI339 KEI20 KEI250 KEI33 KEI323 CTRL. KEI161 KEI188 KEI104 KEI92 KEI150 KEI149 KEI7 KEI255
N 3 8 9 9 13 12 9 45 12 12 9 9 9 9 9 9
(f)
D29E AvrPto
KEI318 KEI323 KEI20 KEI339 KEI279 MPK6 CTRL. SOBIR1 KEI149 KEI104 KEI188
N 9 9 9 12 9 11 49 9 12 9 16
(g)
Significance (-logpVal)
RLK
RLCK
MAPK
cytosolic
KEI37 KEI91 KEI92 KEI143 KEI150 KEI151 KEI153 KEI156 KEI160 KEI161 KEI163 KEI188 KEI279 BAK1 FLS2 SOBIR1
KEI7 KEI86 KEI104 KEI149 KEI196
KEI20 KEI221 KEI25 MKK5 MPK6
KEI33 KEI250 KEI255 KEI259 KEI272 KEI311 KEI318 KEI323 KEI339 KEI376
D29E A1 AI1 AF1 AvrPto

including *MPK6* demonstrated decreased bacterial growth in the presence of multiple effectors but no phenotype with the D29E strain.

Together, our results demonstrate that: *(i)* individual effectors are able to confer a small, but significant functional advantage to the pathogen; and *(ii) KEIs* have distinct quantitative contributions to the growth of *Pst*, which are influenced by the presence of effectors.

Comparison of the D29E and effector-influenced immune kinases

Within the focus group, more *KEIs* (72%) participated in responses to effector-containing strains compared to *D29E* (19%). When considering each *Pst* strain separately (Figure 3.3a), the *D29E HopA1* and *HopAF1* triggered the highest *KEI* participation – an over 2-fold increase over the *D29E* and 1.5-fold increase over the other strains. *D29E HopAI1* and *AvrPto* triggered each a 1.4-fold increase in *KEI* participation over *D29E*.

Bacterial growth was significantly correlated between strains across all of the *KEI* lines (Figure 3.3b) where the HopAI1-AvrPto combination had the highest (R=0.76) and D29E-AvrPto the lowest (R=0.44) correlation. RLKs represented the majority of critical *KEIs* (57%) in the response to *Pst D29E* (Figure 3.3c) while for D29E + effector strains, the class distribution of *KEIs* was not clear-cut. With the exception of *D29E HopA1*, for which RLKs and cytosolic *KEIs* (RLCKs, MAPK, and other cytosolic kinases) participated in comparable numbers, for the *D29E HopAI1*, *HopAF1* or *AvrPto* strains, the cytosolic *KEIs* were preponderant – showing 4-, 2.8- and 2.3-fold enrichment, respectively (Figure 3.3c). Considering the *KEIs'* impact in promoting or inhibiting immunity, we found that RLKs or RLCKs promoted immunity (47% and 21% of positive regulators, respectively), while cytosolic and MAPK-like kinases inhibited immunity (60% and 30% of negative regulators, respectively)(Figure 3.3d).

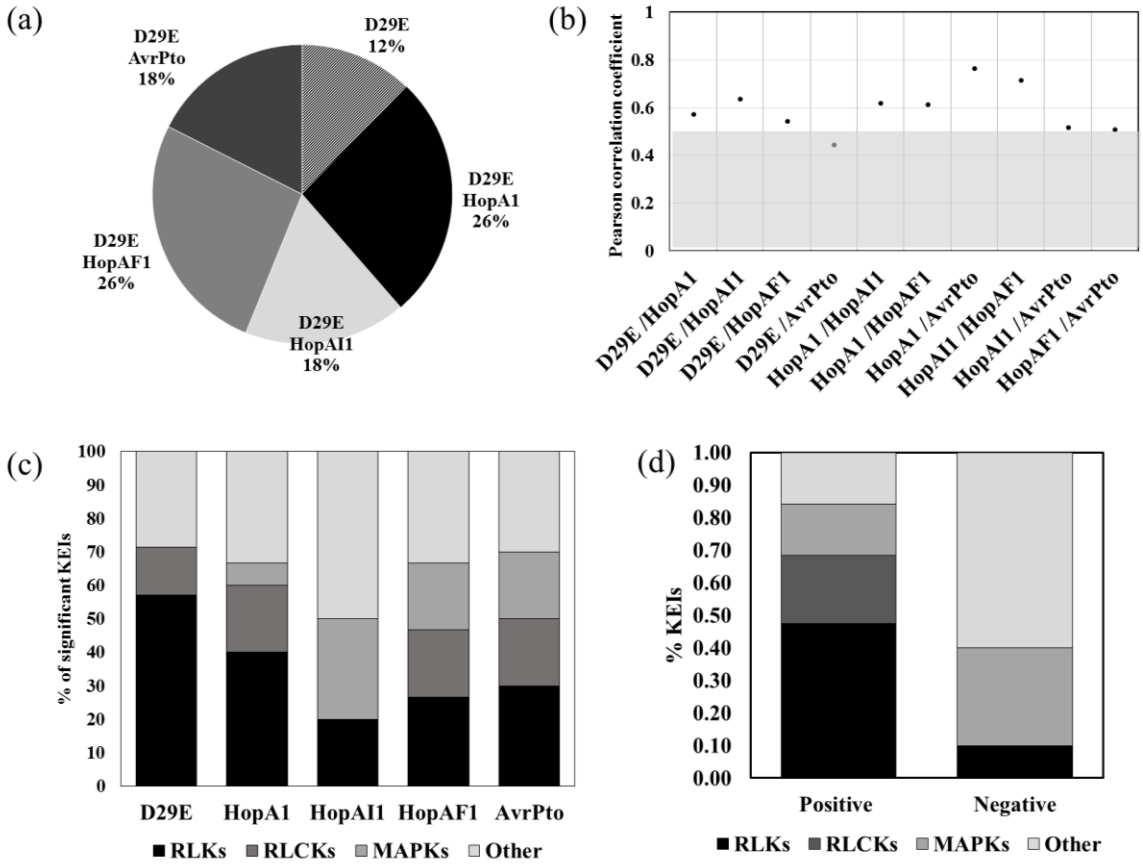

Figure 3.3 Analysis of the contribution of *KEI*s to bacterial growth by strain and functional category.
(a) A chart demonstrating the proportion of *KEI* lines (out of 36) which had a significantly altered bacterial growth compared to the EC1 line for each of the five tested bacterial strains.
(b) Correlation analysis across the 37 lines for bacterial growth during infection with pairs of bacterial strains. Values above the grey line indicate a significant correlation between variables.
(c) Functional categories of the *KEI*s which demonstrated a role in modulating bacterial growth.
(d) Type of regulation and functional category of the significant *KEI* lines across all bacterial growth experiments.

Overall, these results indicate that a larger number and more diverse group of kinases are involved in immune responses when effectors are present during infection compared to bacterial infection with an effectorless strain.

Diverse classes of kinases facilitate programmed cell death

We asked whether these *KEIs*, the majority of which play a role in basal immunity, also participate in the effector-triggered PCD signaling pathways. First, we tested the roles of *KEIs* in the recognition of *HopQ1-1* and induction of ETI (Wei *et al.*, 2007) by quantifying the level of cell death triggered by the infiltration of *D29E+HopQ1-1* in *KEI*-silenced *N. benthamiana* plants (Figure 3.4a).We found that 12 *KEIs* were needed for full cell death, including RLKs, MAP3K and calcium-dependent kinases (CDPKs). Silencing of known genes required for PCD or ETI – *SOBIR1*, *MKK5, MPK6,* and *FLS2* – resulted in impaired *Pst HopQ1-1*-triggered PCD confirming their importance. Silencing of the negative cell death modulator *BAK1* did not significantly impact the cell death intensity triggered by *D29E + HopQ1-1*.

To further analyze the *KEI*s' roles in PCD, we analyzed their contributions to constitutively active $MKK7^{DD}$ and $MKK9^{DD}$-induced cell death (Popescu *et al.*, 2009). *MKK7* and *MKK9* participate in immune-related signaling in coordination with distinct hormonal pathways and were predicted to activate distinct signaling pathways (Xu *et al.*, 2008; Bethke *et al.*, 2009). To test *KEI* involvement in this process, *KEI* lines were infiltrated with Agrobacteria containing the $MKK7^{DD}$ or $MKK9^{DD}$ clones driven by a 35S promoter, and the cell death intensity at the infiltration site was quantified (Figure 3.4b,c). PCD was significantly altered in 64% of the tested *KEI*-silenced lines following transformation with $MKK7^{DD}$ and/or $MKK9^{DD}$. While $MKK7^{DD}$-triggered PCD was inhibited in 1/3 of the lines and enhanced in 2/3 of them

Figure 3.4 Programmed cell death induction in *KEI* lines.
(a) Cell death in arbitrary units (AU) following induction of ETI with a strain containing the HopQ1-1 avirulence gene. The *KEI* lines that are significantly different from to the EC1 control line in grey are plotted and the number of biological replicates is indicated below the plot.
(b) & (c) Cell death is presented as described in (a), in response to Agrobacteria-mediated transformation with activated $MKK7^{DD}$ and $MKK9^{DD}$.
(d) Comparison of the *KEI* functional category and positive or negative regulation of cell death induced by activated MAPKKs.
(e) The p-values for all *KEI* lines, arranged by kinase classification under all cell death-inducing conditions. Bars which extend above the central axis indicate significant difference from EC1 at $p<0.05$.

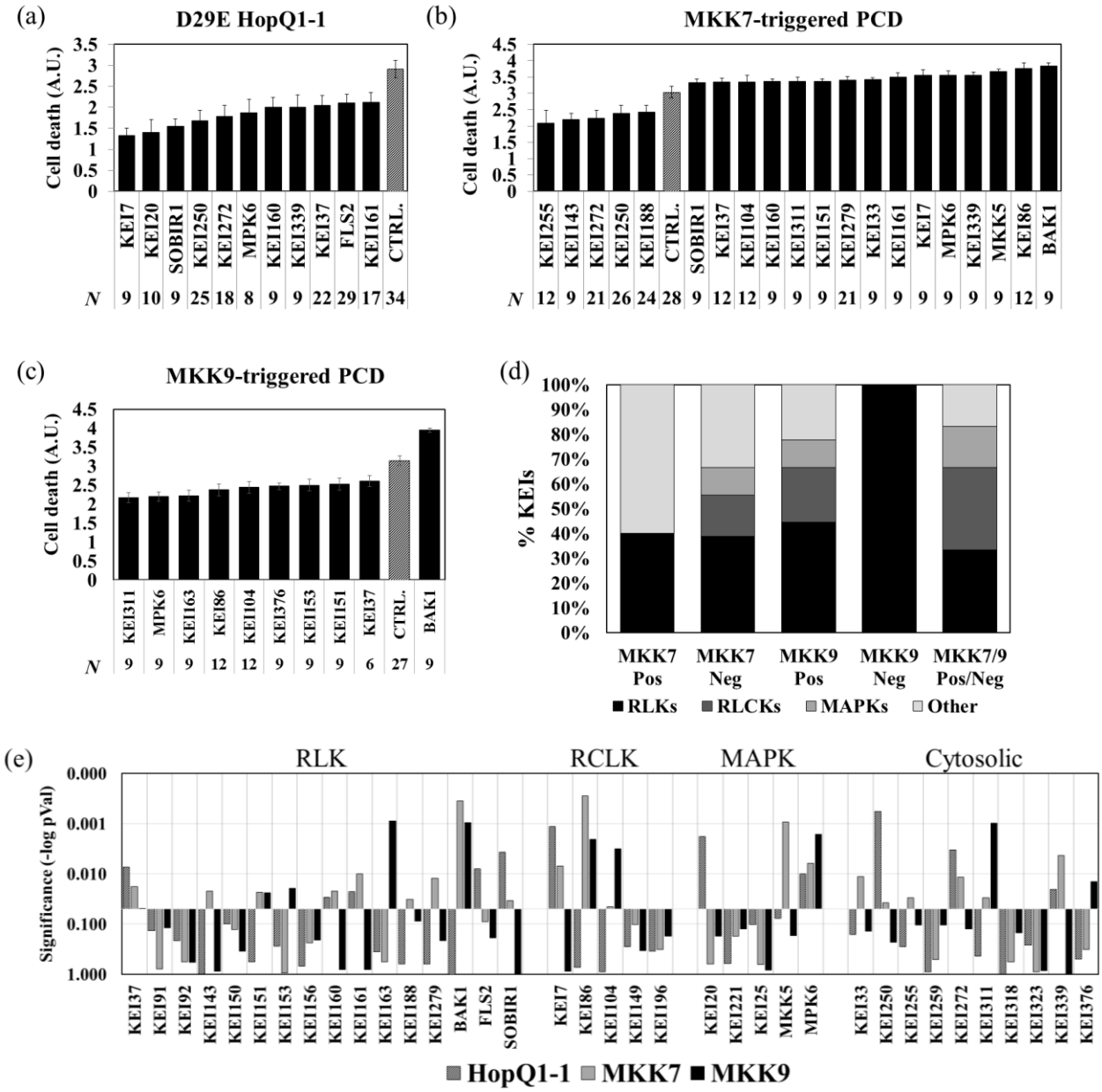
(a)
D29E HopQ1-1
Cell death (A.U.)
KEI7 KEI20 SOBIR1 KEI250 KEI272 MPK6 KEI160 KEI339 KEI37 FLS2 KEI161 CTRL.
N 9 10 9 25 18 8 9 9 22 29 17 34
(b)
MKK7-triggered PCD
Cell death (A.U.)
KEI255 KEI143 KEI272 KEI250 KEI188 CTRL. SOBIR1 KEI37 KEI104 KEI160 KEI311 KEI151 KEI279 KEI33 KEI161 KEI7 MPK6 KEI339 MKK5 KEI86 BAK1
N 12 9 21 26 24 28 9 12 12 9 9 9 21 9 9 9 9 9 9 12 9
(c)
MKK9-triggered PCD
Cell death (A.U.)
KEI311 MPK6 KEI163 KEI86 KEI104 KEI376 KEI153 KEI151 KEI37 CTRL. BAK1
N 9 9 9 12 12 9 9 9 6 27 9
(d)
% KEIs
MKK7 Pos
MKK7 Neg
MKK9 Pos
MKK9 Neg
MKK7/9 Pos/Neg
RLKs RLCKs MAPKs Other
(e)
RLK
RCLK
MAPK
Cytosolic
Significance (-log pVal)
KEI137 KEI191 KEI192 KEI143 KEI150 KEI151 KEI153 KEI156 KEI160 KEI161 KEI163 KEI188 KEI279 BAK1 FLS2 SOBIR1 KEI7 KEI186 KEI104 KEI1149 KEI196 KEI20 KEI221 KEI25 MKK5 MPK6 KEI33 KEI250 KEI255 KEI259 KEI272 KEI311 KEI318 KEI323 KEI339 KEI376
HopQ1-1 MKK7 MKK9

compared to the control, *MKK9*-triggered PCD was almost exclusively inhibited in the nine *KEI*-silenced lines; the exception was *BAK1* who's silencing enhanced PCD by both $MKK7^{DD}$ and $MKK9^{DD}$. Overall, the kinases showing both positive and negative effects on MAPK-mediated PCD were mostly RLKs and RLCKs (Figure 3.4d,e).

These results indicate that *KEIs* have variable quantitative contributions to PCD activated by *Pst HopQ1-1*, *MKK7* or *MKK9* expression, and that the sign of the regulatory input of *KEIs* varies with the type of stimulus.

Contributions of *KEI* lines to distinct immune processes

While less than 3% of the tomato kinome was functionally analyzed here, all of the *KEI*s except *KEI196* and *KEI221* demonstrated a significant contribution to basal immunity or PCD (Table 3.3). A higher number of *KEI*s were positive regulators across most processes while fewer kinases were negative regulators (Figure 3.5a). A number of kinases also demonstrated an inversion of regulatory roles in different assays, for example the *BAK1* line positively regulated basal immune response but negatively regulated PCD. Interestingly, the RLKs & RLCKs were more likely to be positive regulators ($p=0.001$) while other cytosolic kinases were equally likely to regulate processes positively or negatively ($p=0.409$)(Figure 3.5b). The majority of *KEI*s were required for multiple processes and no significant enhancement of *KEI* sharing was observed between basal immunity and ETI ($p=0.705$)(Figure 3.5c). Only three *KEI*s (*SOBIR1*, *KEI161*, *KEI339*) were required for both D29E-triggered immunity and ETI response and only *MPK6* and *KEI37/LYK5* were required for basal immunity, ETI and PCD in response to both MKK7 and MKK9. Consistent with this observation, no correlations were observed between bacterial growth, ETI, MKK7 or MKK9 treatments with the exception of the ETI response compared to

Table 3.3: Summary of phenotypes exhibited by *KEI* lines. Blank cells indicate no significant difference from the EC1 control while + and – indicate the *KEI* positively or negatively regulates the response, respectively.

Kinase group	ID	Name	BI	eBI	ETI	MKK7	MKK9
RLK	***KEI143***	SRF8				+	
	KEI37	LYK5		+	+	-	+
	KEI188	LYK4	+	+		+	
	KEI150	LecRK-S4		+			
	KEI151	BIR2				-	+
	KEI342	BAK1		+		-	-
	KEI156		+				
	KEI279	FEI1		-		-	
	KEI91			+			
	KEI92			+			
	KEI153	NIK1					+
	KEI72	SOBIR1	+	+	+	-	
	KEI160				+	-	
	KEI163						+
	KEI161	RLK1	+	+	+	-	
	FLS2				+		
RLCK	***KEI7***	PBL17		+	+	-	
	KEI86	PBL5		+		-	+
	KEI196	CRCK2-like					
	KEI149	PTI1-like	+	+			
	KEI104	BSK7		+		-	+
MAPK	***KEI221***	VIK					
	KEI20	EDR1		-	+		
	KEI25			-			
	KEI304	MKK5				-	
	KEI327	MPK6		-	+	-	+
Other	***KEI33***	SIP4		-		-	
	KEI250	CIPK6		-	+	+	
	KEI255	CIPK25	+	+		+	
	KEI311	AKIN10		+		-	+
	KEI318	OST1		-			
	KEI376	SNRK2.10		+			+
	KEI323	S6K2		-			
	KEI259	NDR1		-			
	KEI272	SK13			+	+	
	KEI339	ATPK3	-	-	+	-	

Figure 3.5 Summary of *KEI* line phenotypes across assays.

(a) Summary table presenting the number of *KEI* lines with phenotypes for each assay and their regulation of processes across all assays.
(b) Comparison of *KEI*s and their regulation across assays according to functional category.
(c) Venn diagram demonstrating the overlap between *KEI* lines in multiple assays.
(d) Correlation analysis across all 37 lines for response to each pair of assays. Significant correlations are highlighted in green.
BI= basal immunity, eBI= basal immunity in the presence of an effector, ETI= PCD induced by the HopQ1-1 effector, MKK7= PCD induced by $MKK7^{DD}$, MKK9= PCD induced by $MKK9^{DD}$

(a)

Assay	BI	eBI	ETI	MKK7	MKK9	Total
Total number	7	25	11	20	10	34
Positive regulators	86%	60%	100%	25%	90%	35%
Negative regulators	14%	52%	0%	25%	0%	21%
Both positive and negative regulation						44%

(b)

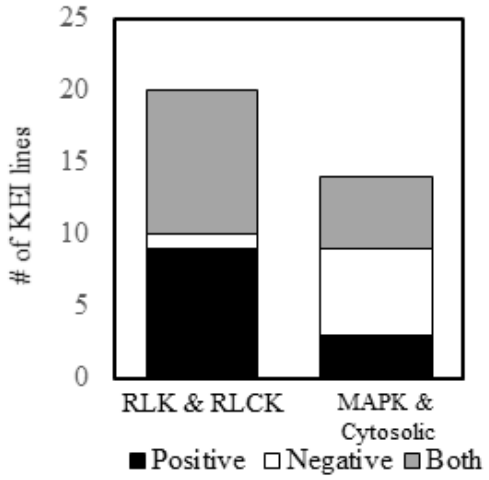

(c)

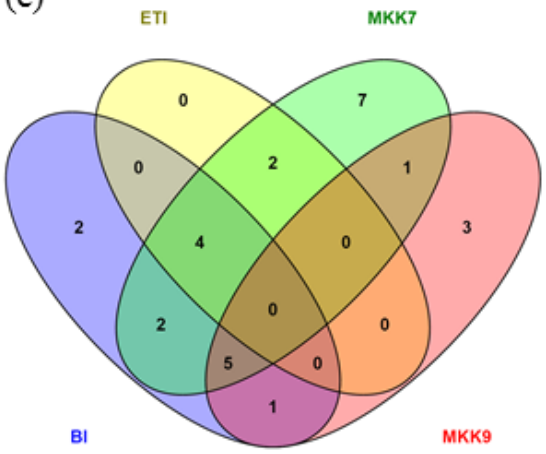

(d)

	D29E + HopA1	D29E + HopAI1	D29E + HopAF1	D29E + AvrPto	ETI	MKK7	MKK9
D29E	0.574	0.638	0.546	0.446	0.250	0.009	0.038
D29E + HopA1		0.621	0.616	0.765	0.327	0.051	-0.034
D29E + HopAI1			0.717	0.520	0.349	-0.106	0.104
D29E + HopAF1				0.509	0.430	-0.149	0.101
D29E + AvrPto					0.080	0.169	0.148
ETI						-0.021	-0.193
MKK7							-0.162

D29E + HopAI1 or HopAF1 bacterial responses (Figure 3.5d). Together, this demonstrates that these processes rely on a partially overlapping set of kinases, and that the regulatory role of the kinases in these processes may be different.

We conclude that (*i*) a majority of the *KEI*s are involved in immune and PCD responses (*ii*) RLKs and RLCKs function as positive regulators of these responses while cytosolic kinases may be positive or negative regulators (*iii*) these do not support the hypothesis that ETI and basal immunity rely on the same signaling pathways to suppress bacterial growth and produce PCD.

DISCUSSION

The relentless tug-of-war between plants and pathogens during evolution has generated a complex and proficient immune system in plants, and equally multifaceted assault and endurance mechanisms in pathogens. Here we compared the immune function and network architecture of 36 kinases which interact with multiple pathogen effectors. This approach allowed us to discover both novel immune-associated kinases and to gain an understanding of the hierarchy of the kinase repertoire which underlies multiple levels of immune response.

The immunity-associated *KEI*s include multiple receptors and modulators of ion/nutrient-mediated processes

Our previous interaction screen uncovered a set of tomato kinases that associate with 3 or 4 *P. syringae* effectors. With the assumption that the interaction of a kinase with many effectors may signify its importance in host immunity or potential as a virulence determinant, we tested the roles of a subset of multi-effector interacting kinases in basal immunity, ETI and PCD using

kinase-silenced *KEI* lines. The majority of the *KEI* lines (95%) demonstrated a phenotype in at least one functional assay, supporting the hypothesis that effectors converge on critical immune elements (Mukhtar *et al.*, 2011).

Previous analysis of signaling pathways suggest that collectively, these networks have a characteristic 'bow-tie' architecture in which the pathways contributing to response are both multi-layered and directional (Friedlander *et al.*, 2014). It is noteworthy that 30% of the tested *KEIs* participated in the plant's response to most treatments, revealing that kinases may be involved in more signaling responses than previously appreciated. In considering what is currently known about PAMP triggered immunity, signal flow is generally mediated by RLK → RLCK → MAPK/cytosolic pathways (Macho and Zipfel, 2014). For example, the pattern-recognition receptor (PRR) RLKs directly bind PAMPs to activate immunity associated signal transduction cascades. However the high percentage of RLK-encoding genes in plants relative to other organisms have prompted questions regarding their potential non-PRR function in immunity (Böhm *et al.*, 2014).

Our results indicate that RLKs modulate PCD and response to specific effectors, processes which are typically thought to rely on cytosolic-based signaling. As such, the fungal chitin-responsive LysM receptors *KEY37/LYK5* and *KEI188/LYK4* (Cao *et al.*, 2014) and the legume lectin *KEI150*, may offer alternative signaling pathways and modulate the duration or timing of bacterial-induced signaling. Recently observed similarities in signaling pathways activated by the fungal chitin and bacterial flagellin (Wan *et al.*, 2012) or bacterial peptidoglycan (Yamaguchi *et al.*, 2013) supports this hypothesis. We identified the RLKs *KEI161/RKL1* and *KEI156* as promoting D29E-induced basal immunity, and interestingly these RLKs have been

associated with vascular patterning and differentiation in other plant species (Sakaguchi *et al.*, 2010; Song *et al.*, 2011), suggesting a potential role for vasculature-specific pathways in defense.

Cytosolic *KEI*s also contributed to immune responses, including a group of kinases which are associated with apoplastic or intracellular ion and nutrient homeostasis, such as *KEI250/CIPK6* (Tripathi *et al.*, 2009; Held *et al.*, 2011; de la Torre *et al.*, 2013), *KEI33/PKS5/CIPK11* (Fuglsang *et al.*, 2007), *KEI318/OST1* (Brandt *et al.*, 2012; Imes *et al.*, 2013; Wang *et al.*, 2015), *KEI255/CIPK25* (Zhang *et al.*, 2013), *KEI259/NDR1* (Knepper *et al.*, 2011), *KEI323/S6K2* (Xiong and Sheen, 2012) and *KEI339* (Goodwin and Sutter, 2009). The pathways for the ion/nutrient homeostasis function coordinately with the kinase-mediated signaling and are critical for adjusting plant growth and metabolic rates under stress (Robaglia *et al.*, 2012). Most *KEIs* in this group act as plant susceptibility factors, suggesting that ion or nutrient availability in plant cells is critical for *P. syringae* pathogenesis or repression of plant immunity.

***KEI*s regulation of cell death is complex and changes depending on the initial stimuli**

The composition of kinase-mediated signaling pathways that contribute to ETI and PCD is not known. A current model which is based on similarities between PTI/ETI transcriptional reprogramming patterns and hormone-mediated immune signaling, considers that basal immunity and ETI signaling occur via shared pathways (Tsuda and Katagiri, 2010; Qi *et al.*, 2011). Our data reveals marginal intersection in the *KEI*-mediated signaling between the HopQ1-1 ETI and other effector-triggered signaling pathways; it appears that, although shared components exist between basal immunity and ETI, these shared components constitute a minority of the *KEI*s with immune phenotypes.

A group of *KEIs* were found to function as both positive and negative modulators of cell death. Notably, the energy sensor *KEI311/KIN10*, which facilitates physiological adaptation of plants to environmental stresses (Im *et al.*, 2014), enabled HopQ1-1 ETI-PCD and inhibited MKK7 cell death, while *KEI160/IRK*, previously associated with anti-viral defense and regulation of R-gene mediated PCD (Caplan *et al.*, 2009), facilitated MKK9 and inhibited MKK7 cell death. These dual-function *KEIs* are especially informative as they underscore the importance of the initial stimulus in determining the composition of downstream signaling pathways; they also reveal the ability of kinases to participate in multiple signaling pathways that may lead to opposed physiological outcomes. Furthermore, the commonality in composition and sign of regulation of the basal immune *KEI*s are in contrast with the more complex regulation of PCD by *KEI*s. The differences in *KEI* requirement between HopQ1-1 and MKK9-mediated PCD alongside the overwhelming positive regulatory outputs of their component *KEIs*, predicts spatially separated signaling networks which are able to function simultaneously. By contrast, although many *KEIs* are shared by MKK7 and MKK9 networks, the opposing regulatory outputs of the shared *KEIs* suggest partially overlapping pathways which function sequentially – *e.g.* the activation of MKK9 signaling is coupled with the repression of MKK7 pathways and vice versa. These observations substantiate a current model of plant immunity, comprising multiple sectors connected by positive or negative regulatory relationships (Sato *et al.*, 2010), by providing it with a possible foundation in kinase-mediated signaling.

Effector repression and activation of immunity

We asked whether individual effectors are able to suppress host immunity in the absence of any other effectors. Most effectors tested, with the exception of HopA1, increased pathogen's

virulence to a similar degree, indicating that individual effectors contribute to pathogen virulence. The contribution of these individual effectors is still smaller than the changes induced by deletion of multiple clusters of effectors suggesting that their contribution to pathogen virulence is only one part of a larger story in the effector repertoire (Kvitko *et al.*, 2009). The inability of HopA1, a negative regulator of PTI and suppressor of ROS production (Oh *et al.*, 2010), to augment pathogen virulence in our experimental system may signify a requirement for synergies with other effectors to execute its functions.

Interestingly, although the single-effector strains elicited similar responses in the host, as shown by the correlation analysis across *KEI*s, a high number of *KEI* lines demonstrated a phenotype in the presence of an effector-carrying D29E strain but not in the D29E strain alone. This indicates that effectors have an influence on immune pathways that are also influenced by the *KEI*s. This observation is consistent with the previously described notion that plant immune networks are made up of highly interconnected signaling pathways in which some players play a more dominant role while others are only important under specific scenarios (ie. when an effector is blocking one of the pathways (Tsuda *et al.*, 2009). We predict that the composition and structure of the immune signaling pathways is determined by the host's ability to perceive and respond appropriately to the presence of the effectors, in a context in which the effectors act to undermine these host functions.

With this in mind, we noted a lower number of susceptibility-type *KEIs* in response to the HopA1-containing strain relative to the HopAI1, HopAF1 and AvrPto-containing strains which have a larger effect on bacterial growth. This may reflect a difference either in how the effector is modulating the immune response (Nomura *et al.*, 2006) or how kinases may be required to activate the effector's function (Axtell *et al.*, 2003). Similarly, addition of effectors actually

reduced bacterial virulence in a number of *KEI* backgrounds relative to the D29E strain (*KEI339, KEI327, KEI318, KEI250, KEI259, KEI323*). This suggests that either the effector required the *KEI* to exert its virulence function or that the loss of a kinase combined with the effector activity triggered an otherwise hidden immune response. Both explanations are plausible since kinase-dependence has been demonstrated for other effectors (Liu *et al.*, 2011) and deletion of individual effectors from *P. syringae* pv. *syringae* has been shown to increase bacterial virulence (Vinatzer *et al.*, 2006). Nevertheless, when considering the contribution of individual effectors to pathogen virulence, substantial contributions may come from factors not accounted for in our experimental pipeline, such as the timing of effector deployment or activity during infection (Lindeberg *et al.*, 2006).

Together, we performed a comprehensive analysis of effector-interacting kinases to identify novel immune kinases and provides insights into overlap between response pathways. Our data indicate that kinases which play a role in basal immunity are not more likely to be involved in effector-triggered immunity, relative to other kinases. This suggests that these two forms of immunity are dependent on partially discrete groups of kinases. Surprisingly, some kinases promote susceptibility in the presence of specific effectors. This may indicate that effectors trigger an undescribed form of immunity which is only visible in certain backgrounds or that these kinases are required for effector function. Future mechanistic studies will help to untangle these possibilities and may provide promising gene targets for development of crop resistance.

METHODS

Bacterial strains

To generate the D29E bacterial strains, the coding region of effectors without the stop codon was cloned into the Gateway entry vector pENTR/SD/D-TOPO. The sequence for hopAI1 was amplified from *P. syringae* pv. *tomato* T1 using primers 5'-caccatgctcagtttaaagctgaacacccag and 5'-gcgagtccagggcggtggcatcag. All other effectors were from *P. syringae* pv. *tomato* DC3000. Hrp promoter-driven effectors fused at the C-terminus with the HA tag were generated in the destination vector pCPP5372 (Oh *et al.*, 2007) using Gateway cloning (Hai-Lei Wei and Joanne Morello). pCPP5372 carrying different effectors was mobilized into DC3000 D29E, a derivative of DC3000 D28E (Cunnac *et al.*, 2011) lacking HopAD1 (Hai-Lei Wei), by triparental mating using the helper plasmid pRK2013 (Ditta *et al.*, 1980). Transconjugants were selected on KB medium with appropriate antibiotics. DC3000D28E::ShcM HopM1 has been described previously (Cunnac *et al.*, 2011). Bacteria were maintained on King's B medium at 37ºC.

KEI cloning

Cloning of the TOKN library, from which *KEI*s were identified has been described previously (Singh *et al.*, 2014). To create clones for virus-induced gene silencing of orthologous kinases in *N. benthamiana*, tomato gene sequences were analyzed using the Sol Genomics VIGS tool (http://vigs.solgenomics.net/) and the optimal gene fragment with the fewest off-targets was used to design primers. The gene fragment was generated from *N. benthamiana* cDNA using PCR and was cloned into the TOPO pER8 donor vector using a kit (Invitrogen K2500-20). The fragment

was subcloned into the TRV2 expression vector and transformed into Agrobacterium GV2260 for expression *in planta*.

KEI line production and maintenance

The *KEI* lines were produced by syringe-infiltrating leaves of two-week old *N. benthamiana* plants with the TRV2-*KEI* Agrobacterium clones along with TRV1-containing Agrobacterium at a 1:1 ratio as described previously (Chakravarthy *et al.*, 2010). The EC1 and FLS2 constructs were identical those cited in Chakravarthy et al., 2010 which served as controls and were included in each round of *KEI* line testing. Once transformed, the *KEI* lines were grown (16 light, >50% humidity) in 6 inch diameter pots for three weeks prior to testing. All functional assays were done using the third or fourth fully expanded leaf.

Bacterial growth

Bacterial growth was assayed 6 days after direct infiltration of the pathogen into the leaf as described previously (Kvitko *et al.*, 2009). Each plant was tested once with each strain and three plants were tested per round of *KEI* line production. Each *KEI* line was tested over a minimum of three experiments and a maximum of 18 experiments (EC1, FLS2), resulting in between 9-55 biological replicates.

Programmed cell death induction using $MKK7^{DD}$, $MKK9^{DD}$ or *HopQ1-1*

One or two leaves of *KEI* lines were syringe-infiltrated with Agrobacterium carrying the $MKK7^{DD}$, $MKK9^{DD}$ genes as described previously (Popescu 2009). The D29E + HopQ1-1 strain was applied by syringe inoculation at a level of $3x10^8$ CFU/mL. For both MPKK and HopQ1-1

induction, the area of infiltration was carefully marked and PCD was quantified relative to this area over the three days following infiltration. The PCD was scored as; 1=0-25%, 2=26-50%, 3=51-75%, 4=76-100% of the infiltration area as demonstrating necrosis. The data presented here is using PCD one day post-infiltration for HopQ1-1 and 2 days post-infiltration for MPKK treatments. All three treatments were applied to the same leaf and three plants were infiltrated per round of VIGS. A minimum of three experiments were done and the total number of biological replicates used per treatment was between 9-34.

Statistical analysis

To compare the *KEI* response to the EC1 response to various treatments, we used 2-tailed t-tests at the α=0.05 level. Correlation between treatments was calculated using a Pearson's correlation coefficient (Lawrence and Lin, 1989).

REFERENCES

Axtell, M.J., Chisholm, S.T., Dahlbeck, D. and Staskawicz, B.J. (2003) Genetic and molecular evidence that the *Pseudomonas syringae* type III effector protein AvrRpt2 is a cysteine protease. *Mol. Microbiol.*, **49**, 1537–1546.

Bethke, G., Unthan, T., Uhrig, J.F., Pöschl, Y., Gust, A.A., Scheel, D. and Lee, J. (2009) Flg22 regulates the release of an ethylene response factor substrate from MAP kinase 6 in *Arabidopsis thaliana* via ethylene signaling. *Proc. Natl. Acad. Sci.*, **106**, 8067–8072.

Böhm, H., Albert, I., Fan, L., Reinhard, A. and Nürnberger, T. (2014) Immune receptor complexes at the plant cell surface. *Curr. Opin. Plant Biol.*, **20**, 47–54.

Brandt, B., Brodsky, D.E., Xue, S., et al. (2012) Reconstitution of abscisic acid activation of SLAC1 anion channel by CPK6 and OST1 kinases and branched ABI1 PP2C phosphatase action. *Proc. Natl. Acad. Sci.*, **109**, 10593–10598.

Cao, Y., Liang, Y., Tanaka, K., Nguyen, C.T., Jedrzejczak, R.P., Joachimiak, A. and Stacey, G. (2014) The kinase LYK5 is a major chitin receptor in Arabidopsis and forms a chitin-induced complex with related kinase CERK1. *Elife*, **3**, e03766.

Caplan, J.L., Zhu, X., Mamillapalli, P., Marathe, R., Anandalakshmi, R. and Dinesh-Kumar, S.P. (2009) Induced ER chaperones regulate a receptor-like kinase to mediate antiviral innate immune response in plants. *Cell Host Microbe*, **6**, 457–469.

Chakravarthy, S., Velásquez, A.C., Ekengren, S.K., Collmer, A. and Martin, G.B. (2010) Identification of Nicotiana benthamiana genes involved in pathogen-associated molecular pattern-triggered immunity. *Mol. plant-microbe Interact.*, **23**, 715–726.

Cunnac, S., Chakravarthy, S., Kvitko, B.H., Russell, A.B., Martin, G.B. and Collmer, A. (2011) Genetic disassembly and combinatorial reassembly identify a minimal functional repertoire of type III effectors in Pseudomonas syringae. *Proc. Natl. Acad. Sci.*, **108**, 2975–2980.

Ditta, G., Stanfield, S., Corbin, D. and Helinski, D.R. (1980) Broad host range DNA cloning system for gram-negative bacteria: construction of a gene bank of *Rhizobium meliloti*. *Proc. Natl. Acad. Sci.*, **77**, 7347–7351.

Eckardt, N.A. (2002) Plant disease susceptibility genes? *Plant Cell Online*, **14**, 1983–1986.

Friedlander, T., Mayo, A.E., Tlusty, T. and Alon, U. (2014) Evolution of bow-tie architectures in biology. *arXiv Prepr. arXiv1404.7715*.

Fuglsang, A.T., Guo, Y., Cuin, T.A., et al. (2007) Arabidopsis protein kinase PKS5 inhibits the plasma membrane H^+-ATPase by preventing interaction with 14-3-3 protein. *Plant Cell Online*, **19**, 1617–1634.

Goodwin, S.B. and Sutter, T.R. (2009) Microarray analysis of Arabidopsis genome response to aluminum stress. *Biol. Plant.*, **53**, 85–99.

Held, K., Pascaud, F., Eckert, C., et al. (2011) Calcium-dependent modulation and plasma membrane targeting of the AKT2 potassium channel by the CBL4/CIPK6 calcium sensor/protein kinase complex. *Cell Res.*, **21**, 1116–1130.

Im, J.H., CHO, Y., KIM, G., KANG, G., HONG, J. and YOO, S. (2014) Inverse modulation of the energy sensor Snf1- related protein kinase 1 on hypoxia adaptation and salt stress tolerance in Arabidopsis thaliana. *Plant. Cell Environ.*, **37**, 2303–2312.

Imes, D., Mumm, P., Böhm, J., Al- Rasheid, K.A.S., Marten, I., Geiger, D. and Hedrich, R. (2013) Open stomata 1 (OST1) kinase controls R–type anion channel QUAC1 in Arabidopsis guard cells. *Plant J.*, **74**, 372–382.

Knepper, C., Savory, E.A. and Day, B. (2011) Arabidopsis NDR1 is an integrin-like protein with a role in fluid loss and plasma membrane-cell wall adhesion. *Plant Physiol.*, **156**, 286–300.

Kvitko, B.H., Park, D.H., Velásquez, A.C., Wei, C.-F., Russell, A.B., Martin, G.B., Schneider, D.J. and Collmer, A. (2009) Deletions in the repertoire of *Pseudomonas syringae* pv. *tomato* DC3000 type III secretion effector genes reveal functional overlap among effectors. *PLoS Pathog.*, **5**, e1000388.

la Torre, F. de, Gutiérrez-Beltrán, E., Pareja-Jaime, Y., Chakravarthy, S., Martin, G.B. and Pozo, O. del (2013) The tomato calcium sensor Cbl10 and its interacting protein kinase Cipk6 define a signaling pathway in plant immunity. *Plant Cell Online*, **25**, 2748–2764.

Lawrence, I. and Lin, K. (1989) A concordance correlation coefficient to evaluate reproducibility. *Biometrics*, 255–268.

Li, X., Lin, H., Zhang, W., Zou, Y., Zhang, J., Tang, X. and Zhou, J.-M. (2005) Flagellin induces innate immunity in nonhost interactions that is suppressed by Pseudomonas syringae effectors. *Proc. Natl. Acad. Sci. U. S. A.*, **102**, 12990–12995.

Lindeberg, M., Cartinhour, S., Myers, C.R., Schechter, L.M., Schneider, D.J. and Collmer, A. (2006) Closing the circle on the discovery of genes encoding Hrp regulon members and type III secretion system effectors in the genomes of three model Pseudomonas syringae strains. *Mol. plant-microbe Interact.*, **19**, 1151–1158.

Liu, J., Elmore, J.M., Lin, Z.-J.D. and Coaker, G. (2011) A receptor-like cytoplasmic kinase phosphorylates the host target RIN4, leading to the activation of a plant innate immune receptor. *Cell Host Microbe*, **9**, 137–146.

Macho, A.P. and Zipfel, C. (2014) Plant PRRs and the activation of innate immune signaling. *Mol. Cell*, **54**, 263–272.

Martin, G.B. (2012) Suppression and activation of the plant immune system by *Pseudomonas syringae* effectors AvrPto and AvrPtoB. *Eff. Plant-Microbe Interact.*, 123–154.

Meng, X., Zhang, S. (2013) MAPK cascades in plant disease resistance signaling. *Ann. Rev. Phytopath.* **51**, 245-266.

Mukhtar, M.S., Carvunis, A.-R., Dreze, M., et al. (2011) Independently evolved virulence effectors converge onto hubs in a plant immune system network. *Science* **333**, 596–601.

Navarro, L., Navarro, L., Zipfel, C., et al. (2004) The transcriptional innate immune response to flg22: interplay and overlap with Avr gene-dependent defense responses and bacterial pathogenesis. *Plant Physiol.*, **135**, 1113–1128.

Nomura, K., DebRoy, S., Lee, Y.H., Pumplin, N., Jones, J. and He, S.Y. (2006) A bacterial virulence protein suppresses host innate immunity to cause plant disease. *Science (80)*, **313**, 220–223.

Oh, H.-S., Kvitko, B.H., Morello, J.E. and Collmer, A. (2007) *Pseudomonas syringae* lytic transglycosylases coregulated with the type III secretion system contribute to the translocation of effector proteins into plant cells. *J. Bacteriol.*, **189**, 8277–8289.

Oh, H.-S., Park, D.H. and Collmer, A. (2010) Components of the *Pseudomonas syringae* type III secretion system can suppress and may elicit plant innate immunity. *Mol. plant-microbe Interact.*, **23**, 727–739.

Pavan, S., Jacobsen, E., Visser, R.G.F. and Bai, Y. (2010) Loss of susceptibility as a novel breeding strategy for durable and broad-spectrum resistance. *Mol. Breed.*, **25**, 1–12.

Popescu, S.C., Popescu, G. V., Bachan, S., Zhang, Z., Gerstein, M., Snyder, M. and Dinesh-Kumar, S.P. (2009) MAPK target networks in *Arabidopsis thaliana* revealed using functional protein microarrays. *Genes Dev.*, **23**, 80–92.

Qi, Y., Tsuda, K., Glazebrook, J. and Katagiri, F. (2011) Physical association of pattern-triggered immunity (PTI) and effector-triggered immunity (ETI) immune receptors in Arabidopsis. *Mol. Plant Pathol.*, **12**, 702–708.

Robaglia, C., Thomas, M. and Meyer, C. (2012) Sensing nutrient and energy status by SnRK1 and TOR kinases. *Curr. Opin. Plant Biol.*, **15**, 301–307.

Sakaguchi, J., Itoh, J., Ito, Y., Nakamura, A., Fukuda, H. and Sawa, S. (2010) COE1, an LRR–RLK responsible for commissural vein pattern formation in rice. *Plant J.*, **63**, 405–416.

Sato, M., Tsuda, K., Wang, L., Coller, J., Watanabe, Y., Glazebrook, J. and Katagiri, F. (2010) Network modeling reveals prevalent negative regulatory relationships between signaling sectors in Arabidopsis immune signaling. *PLoS Pathog.*, **6**, e1001011.

Singh, D.K., Calviño, M., Brauer, E.K., et al. (2014) The tomato kinome and the tomato kinase library ORFeome: novel resources for the study of kinases and signal transduction in tomato and Solanaceae species. *Mol. Plant-Microbe Interact.*, **27**, 7–17.

Song, D., Xi, W., Shen, J., Bi, T. and Li, L. (2011) Characterization of the plasma membrane proteins and receptor-like kinases associated with secondary vascular differentiation in poplar. *Plant Mol. Biol.*, **76**, 97–115.

Thomma, B.P.H.J., Nürnberger, T. and Joosten, M.H. a J. (2011) Of PAMPs and effectors: the blurred PTI-ETI dichotomy. *Plant Cell*, **23**, 4–15.

Tripathi, V., Parasuraman, B., Laxmi, A. and Chattopadhyay, D. (2009) CIPK6, a CBL-interacting protein kinase is required for development and salt tolerance in plants. *Plant J.*, **58**, 778–790.

Tsuda, K. and Katagiri, F. (2010) Comparing signaling mechanisms engaged in pattern-triggered and effector-triggered immunity. *Curr. Opin. Plant Biol.*, **13**, 459–465. Available at: http://dx.doi.org/10.1016/j.pbi.2010.04.006.

Tsuda, K., Mine, A., Bethke, G., Igarashi, D., Botanga, C.J., Tsuda, Y., Glazebrook, J., Sato, M. and Katagiri, F. (2013) Dual regulation of gene expression mediated by extended MAPK activation and salicylic acid contributes to robust innate immunity in Arabidopsis thaliana. *PLoS Genet.*, **9**, e1004015.

Tsuda, K., Sato, M., Stoddard, T., Glazebrook, J. and Katagiri, F. (2009) Network properties of robust immunity in plants. *PLoS Genet.*, **5**.

Vinatzer, B.A., Teitzel, G.M., Lee, M., Jelenska, J., Hotton, S., Fairfax, K., Jenrette, J. and Greenberg, J.T. (2006) The type III effector repertoire of *Pseudomonas syringae* pv. *syringae* B728a and its role in survival and disease on host and non-host plants. *Mol. Microbiol.*, **62**, 26–44.

Wan, J., Tanaka, K., Zhang, X.-C., Son, G.H., Brechenmacher, L., Nguyen, T.H.N. and Stacey, G. (2012) LYK4, a lysin motif receptor-like kinase, is important for chitin signaling and plant innate immunity in Arabidopsis. *Plant Physiol.*, **160**, 396–406.

Wang, P., Du, Y., Hou, Y.-J., et al. (2015) Nitric oxide negatively regulates abscisic acid signaling in guard cells by S-nitrosylation of OST1. *Proc. Natl. Acad. Sci.*, **112**, 613–618.

Wei, C., Kvitko, B.H., Shimizu, R., Crabill, E., Alfano, J.R., Lin, N., Martin, G.B., Huang, H. and Collmer, A. (2007) A *Pseudomonas syringae* pv. *tomato* DC3000 mutant lacking the type III effector HopQ1-1 is able to cause disease in the model plant Nicotiana benthamiana. *Plant J.*, **51**, 32–46.

Weßling, R., Epple, P., Altmann, S., et al. (2014) Convergent targeting of a common host protein-network by pathogen effectors from three kingdoms of life. *Cell Host Microbe*, **16**, 364–375.

Xiong, Y. and Sheen, J. (2012) Rapamycin and glucose-target of rapamycin (TOR) protein signaling in plants. *J. Biol. Chem.*, **287**, 2836–2842.

Xu, J., Li, Y., Wang, Y., Liu, H., Lei, L., Yang, H., Liu, G. and Ren, D. (2008) Activation of MAPK kinase 9 induces ethylene and camalexin biosynthesis and enhances sensitivity to salt stress in Arabidopsis. *J. Biol. Chem.*, **283**, 26996–27006.

Yamaguchi, K., Yamada, K., Ishikawa, K., et al. (2013) A receptor-like cytoplasmic kinase targeted by a plant pathogen effector is directly phosphorylated by the chitin receptor and mediates rice immunity. *Cell Host Microbe*, **13**, 347–357.

Zhang, H., Lv, F., Han, X., Xia, X. and Yin, W. (2013) The calcium sensor PeCBL1, interacting with PeCIPK24/25 and PeCIPK26, regulates Na+/K+ homeostasis in Populus euphratica. *Plant Cell Rep.*, **32**, 611–621.

Zhang, J., Shao, F., Li, Y., et al. (2007) A Pseudomonas syringae effector inactivates MAPKs to suppress PAMP-induced immunity in plants. *Cell Host Microbe*, **1**, 175–185.

CHAPTER 4

Integrin-linked kinase 1 is required for potassium-mediated processes at the plasma membrane during innate immunity and osmotic stress*

ABSTRACT

Plants combat bacterial infection by detecting conserved molecular signatures called pathogen-associated molecular patterns (PAMPs) and producing defensive compounds to restrict pathogen entry and reproduction. Numerous ion fluxes are activated within minutes of PAMP perception, including Ca^{2+} influx and anion efflux, which are required for depolarization and gene induction. However the molecular components that mediate these ion fluxes are unknown. Here, we report that the *INTEGRIN-LINKED KINASE1 (ILK1)* promotes signaling responses to the PAMP flg22 through its contribution to K^+ homeostasis and plasma membrane depolarization. We confirmed our previous findings that ILK1 interacts with CML9, a Ca^{2+}-sensing calmodulin-like protein, and demonstrate that ILK1 activity is repressed by CML9. *ILK1* promotes basal immunity and response to osmotic stress and flg22. ILK1 also interacts with the HAK5 high affinity K^+ transporter and contributes to dynamic changes in ion homeostasis induced by flg22

---

* This chapter has been submitted to *The Plant Journal* and is currently in revision. All data in this chapter was generated by E.K.B. with the exception of Figure 4.1d, 4.4a, Tables 4.1, 4.3 which were generated in collaboration with Nagib Ahsan and Jay Thelen at the University of Missouri, Figure 4.1e, 4.5a generated by Renee Dale and Naohiro Kato at Louisiana State University and Figure 4.5b generated by Alison Coluccio, Miguel Pineros and Leon Kochian at the Robert W. Holley Center for Agriculture and Health.

and NaCl, including changes in K^+ content. Both *HAK5* and *ILK1* affect the rate of flg22-induced plasma membrane depolarization, K^+ transport and gene induction in leaf cells where depolarization could also be delayed by applying chemical K^+ transport inhibitors. Furthermore, we demonstrated that HAK5 protein accumulation is significantly enhanced by the presence of both ILK1 and CML9 *in planta*. Together, our data indicate that flagellin-induced signaling responses are influenced by *ILK1*- and *HAK5*-mediated K^+ transport at the plasma membrane. These findings reveal a previously unidentified role for potassium nutrition in modulating PAMP-activated gene expression and shed light on the mechanisms regulating membrane depolarization dynamics during immunity.

INTRODUCTION

Plant survival is dependent on the activation of multiple signaling pathways during pathogen infection and environmental stress. The earliest immune signaling responses are induced within minutes of stress perception and include changes in ion fluxes, reactive oxygen species (ROS) production, membrane depolarization and kinase phosphorylation (Boller and Felix, 2009). A clear interdependence of some of these responses has been demonstrated, though the mechanisms underlying this dependence are not clear in some cases. For example, a critical component upstream of stress-induced kinase signaling involves plasma membrane (PM) ion transport, which causes membrane depolarization and cytosolic Ca^{2+} spiking (Nürnberger *et al.*, 1994). Early studies in cultured parsley cells established that inducible ion fluxes are one of the first responses to the oomycete elicitor Pep-13 (Nürnberger *et al.*, 1994). These fluxes were

required to activate immune responses such as reactive oxygen species (ROS) production, MAPK activation and gene expression (Jabs *et al.*, 1997; Ligterink *et al.*, 1997). Later studies demonstrated that elicitor-induced Ca^{2+} influx precedes activation of both ROS production and anion channels in several plant species (Wendehenne *et al.*, 2002; Kuchitsu *et al.*, 1997; Felle *et al.*, 2000; Jeworutzki *et al.*, 2010). Anion channels in particular are thought to play a major role in depolarizing the PM in response to the bacterial elicitor flg22, since blocking Cl^- efflux reduces depolarization (Jeworutzki *et al.*, 2010). Chemical blockage of anion channels also abolished defense compound production suggesting that these ion fluxes may also be important for cellular signaling (Jabs *et al.*, 1997). However, the role of PM depolarization in immunity is unclear since the identity of cellular elements and pathways facilitating this process remain unknown.

The calmodulins (CaM) and calmodulin-like proteins (CMLs) constitute a significant subset of Ca^{2+}-sensing proteins that detect cytosolic Ca^{2+} signals to activate downstream signaling pathways. Some CMLs, including *CML9*, *CML24*, and *CML42*, coordinate responses to both biotic and abiotic stress (Bender and Snedden, 2013). In particular, the Arabidopsis *cml9* knockout line is more susceptible to virulent pathogens and is also more sensitive to high NaCl and KCl supply during germination (Leba *et al.*, 2012; Magnan *et al.*, 2008). Ectopic *CML9* expression suppressed basal immunity and immune responses to flg22, a bacterial pathogen-associated molecular pattern (PAMP) derived from flagellin (Leba *et al.*, 2012). The mechanisms underlying *CML9*'s function in PAMP perception and salt stress are yet to be determined.

In this study, we confirm that a previously identified CML9 interactor, the *Integrin-linked kinase 1* (*ILK1*)(Popescu *et al.*, 2007), interacts with CML9 *in vivo* and promotes osmotic stress response, basal immunity and response to flg22. We next identified the high-affinity K^+

transporter *HAK5* as an *ILK1* interactor and demonstrate that changes in *HAK5* and *ILK1*-regulated K^+ transport modulate flg22-induced membrane depolarization, ion transport and signaling responses.

RESULTS

The ILK1 pseudokinase is a functional kinase

ILKs are classified as pseudokinases because they contain substitutions in conserved amino acid motifs (Figure 4.1a)(Adams, 2003). However, metazoan and plant ILKs have been shown to be active *in vitro* with an unusual dependence on Mn as a cofactor (Maydan *et al.*, 2010; Chinchilla *et al.*, 2008). To determine if the Arabidopsis ILK1 is a functional kinase, a radioactive kinase assay with purified recombinant ILK1-cMyc was performed. The 75 kDa ILK1 exhibited autophosphorylation activity with either Mn or Mg as cofactors, though higher activity was consistently observed with Mn (Figure 4.1b). ILK1-dependent phosphorylation increased with higher Mn concentration while no relationship between Mg concentration and activity was observed (Figure 4.1c, 4.2). Mass spectrometry analysis confirmed that ILK1 autophosphorylates at residues near the N-terminus – Ser17 and Ser26 in the presence of Mn, and only Ser17 in the presence of Mg (Figure 4.1d, Table 4.1). To determine if ILK1 was producing the observed phosphorylation, we generated two mutant ILK1 isoforms, ILK1 ^{K222A} and ILK1 ^{D319N}, which showed decreased and increased activity, respectively (Figure 4.3a). The ILK1 and ILK1 ^{D319N} protein preparations were digested with trypsin and analyzed by tandem mass spectrometry and no additional 75 kDa kinases were detected in these preparations (Figure 4.3b) . The 75 kDa autophosphorylation signal was also absent in empty vector control extracts,

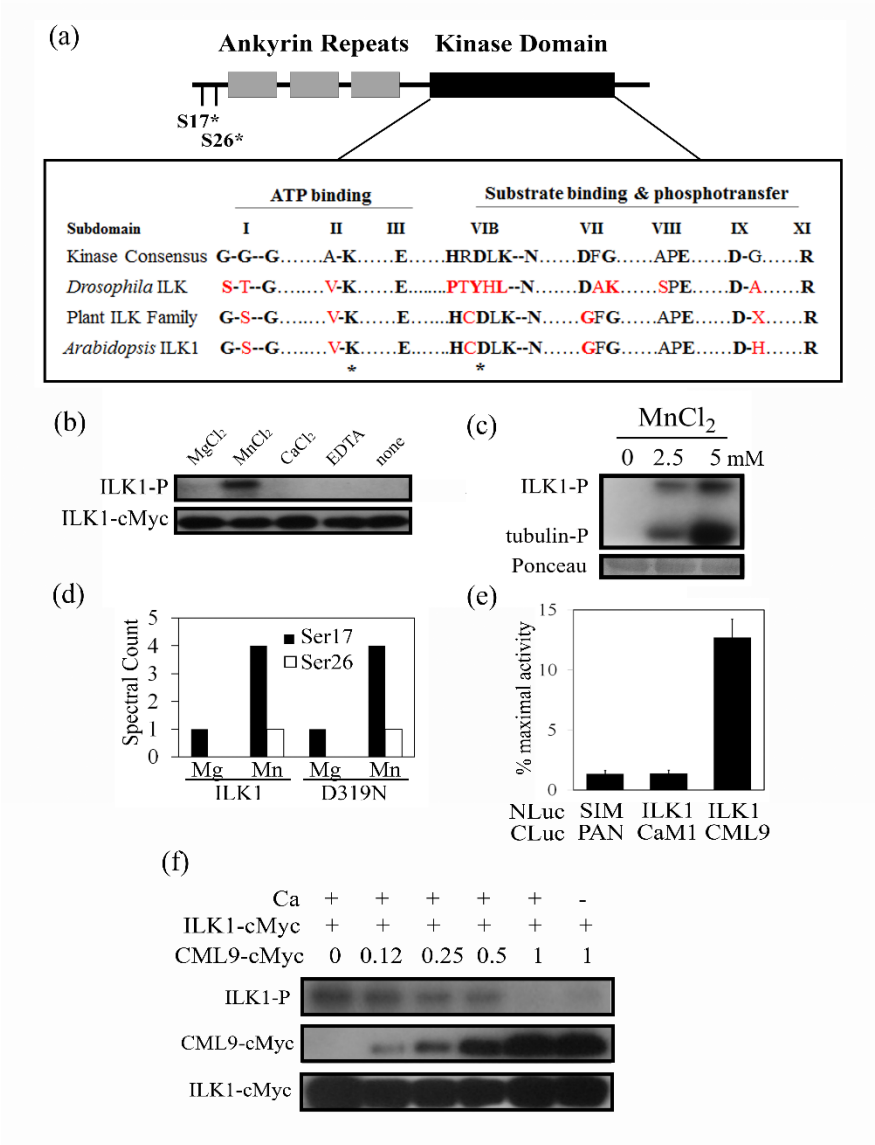

Figure 4.1 ILK1 kinase activity is repressed by interactions with CML9.
(a) Alignment of the plant ILK1 family revealed conservation of an aberrant GFG motif in place of the conserved cofactor-binding DFG motif.
(b) Autophosphorylation of purified recombinant ILK1 is highest with 5 mM Mn, relative to 5 mM Mg, Ca or EDTA. Equal loading was determined by Western blot.
(c) ILK1 activity with increasing concentrations of Mn. Equal loading was verified by Ponceau staining.
(d) Location and amount of autophosphorylated serines on ILK1 isoforms in the presence of Mn or Mg as determined by mass spectrometry.
(e) Interaction between bait (NLuc) and pray (CLuc) fusion proteins were quantified by measuring luciferase activity in *Arabidopsis* protoplasts relative to the positive control (NLuc-H2A, CLuc-H2B) and compared to the negative control (NLuc-SIM, CLuc-PAN).
(f) ILK1 autophosphorylation activity with 5 mM Mn decreases in the presence of purified CML9 and 1 mM Ca, and is partially regained when calcium is absent.

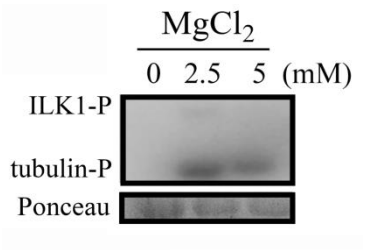

Figure 4.2 ILK1 kinase activity in the presence of Mg.
ILK1 auto- and substrate phosphorylation does not increase in the presence of increased Mg concentration. Equal loading of the kinase was determine by Ponceau stain.

Table 4.1 Identification of phosphorylated serines in purified ILK1 and ILK1^{D319N} protein using mass spectrometry.

Phospho site	Peptide	ΔM [ppm]	pRS Score [a)]	pRS site probability [b)]	ΔCn	Xcorr	m/z [Da]	RT [min]	Ion matched
Ser^{17}	GISRQFs TGSIRR	1.34	200	S(7): 99.6; T(8): 0.4	0	3.35	516	20	21/48
Ser^{26}	RTLsRQ FTR	2.20	218	T(2): 0.0; S(4): 100.0	0	3.00	416	13	17/32

[a)] pRS score: This peptide score is based on the cumulative binomial probability that the observed match is a random event. The value of the pRS score strongly depends on the data scored, but usually scores above 50 give good evidence for a good PSM.

[b)] pRS site probabilities: For each phosphorylation site this is an estimation of the probability (0-100%) for the respective site being truly phosphorylated. pRS site probabilities above 50% are good evidence that the respective site is truly phosphorylated.

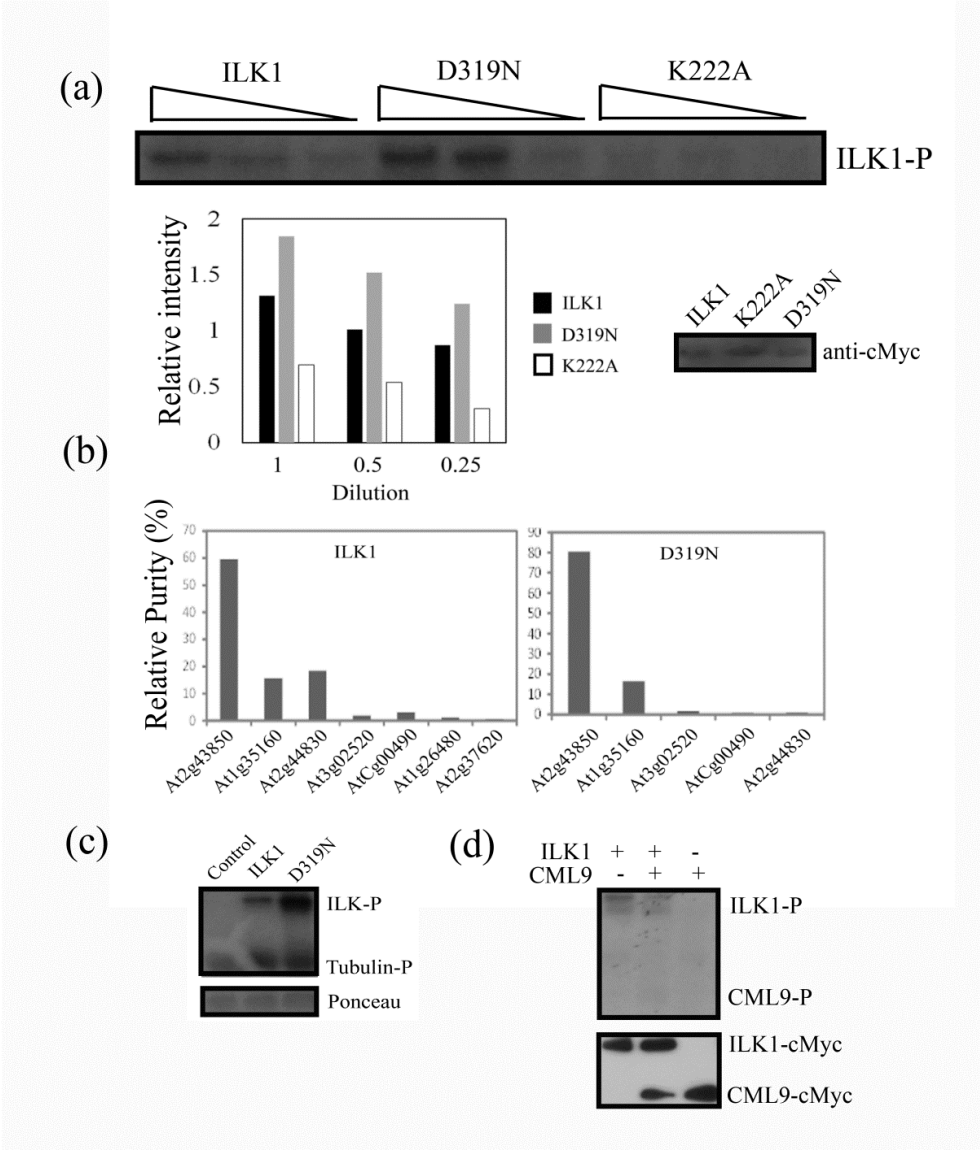

Figure 4.3 Relative purity of ILK1 isoforms used to conduct kinase assays.
(a) Three isoforms of cMyc-tagged ILK1 were purified and confirmed to be approximately 75 kDa by Western blot. Autophosphorylation of ILK1, ILK1^{K222A} or ILK1^{D319N} across a dilution series (1, 0.5, 0.25) was quantified across two experiments in the presence of 5 mM Mn using ImageJ relative to the background.
(b) Identity and relative amount of non-ILK1 proteins in purified samples used for kinase assays, as determined by mass spectrometry.
(c) Autophosphorylation activity is not present in the empty vector control tissue relative to ILK1, or ILK1^{D319N} in the presence of 5 mM Mn. Equal loading is confirmed by Ponceau staining.
(d) Adding purified CML9 to ILK1 protein reduces autophosphorylation activity of ILK1, and no phosphorylation at the CML9 position is observed in the presence of 5 mM Mn (upper blot). The presence of the cMyc-tagged protein was confirmed by Western (lower blot).

indicating that the observed activity is not due to contaminating plant kinases extracted during the purification process (Figure 4.3c). Together, these results indicate that ILK1 functions as a kinase and that Ser residues near the N-terminus may be important for ILK1 activity.

The kinase activity of ILK1 is inhibited by CML9

To confirm the reported interactions between ILK1 and CML9 or CaM1 (Popescu *et al.*, 2007), we used the split-luciferase complementation assay (SLCA) in *Arabidopsis* protoplasts (Kato and Jones, 2010). Reconstitution of the *Renilla reniforms* luciferase (Luc) activity with NLuc-ILK1 and CLuc-CML9 co-expression indicated interaction of these proteins *in vivo,* while NLuc-ILK1 and CLuc-CaM1 did not produce significant activity above the negative control (Figure 4.1e). Next, to determine if CML9 is a phosphorylation target of ILK1, we performed a radioactive kinase assay with recombinant CML9 as a substrate. No phosphorylation of CML9 was observed and instead, we saw a decrease in ILK1 autophosphorylation in the presence of CML9 (Figure 4.3d). The reduced ILK1 activity correlated with increasing CML9 concentrations and was not dependent on the presence of Ca^{2+} (Figure 4.1f). Our results indicate that ILK1 and CML9 interact *in vivo* and that the interaction dampens the activity of ILK1.

A mutant with reduced *ILK1* expression exhibits defects in immunity and osmotic stress response

Since *CML9* negatively regulates basal immunity and ionic stress responses, we evaluated the role of *ILK1* in these stresses using a reverse genetics approach. One T-DNA insertion line was available for *ILK1*, with the insertion site in the promoter region. The *ilk1* homozygous T-DNA insertion line was generated following one round of backcrossing and

selection using PCR (Table 4.2) and expressed on average 80% less *ILK1* mRNA relative to azygous (WT) plants (Figure 4.4a). This *ilk1* line was transformed with the three *ILK1-CFP* isoforms under control of the 35S promoter (*ilk1/ILK1*, *ilk1/ ILK1*^{K222A} (kinase attenuated), *ilk1/ ILK1*^{D319N} (kinase overactive) to restore *ILK1* expression above *ilk1* levels, in two separate lines per construct (Figure 4.4a).

The role of *ILK1* in ionic or osmotic stress was tested by exposing seeds to high levels of NaCl or mannitol on solid media and recording germination. While all of the lines exhibited high germination rates under control conditions (Figure 4.4b), both NaCl and mannitol treatment inhibited WT germination by over 60% (Figure 4.5a). Germination was less inhibited by these treatments in *ilk1* seeds while lines with ectopic *ILK1* expression exhibited higher germination inhibition relative to the WT (Figure 4.5a). Transgenic lines overexpressing *ILK1* in the *ilk1* background also complemented the *ilk1* phenotype (Figure 4.4c), suggesting that *ILK1* expression correlates with sensitivity to osmotic and ionic stress.

To test basal immunity in *ilk1* lines, the knockdown and overexpression lines were infected with *Pseudomonas syringae* pv. *tomato* (*Pst*) DC3000 *hrcQ-U* bacteria which lack a functional type-three secretion system. The bacteria grew to significantly higher levels in *ilk1* and *ilk1/ ILK1*^{K222A} plants indicating an impaired immune response while *ilk1/ILK1*, and *ilk1/ ILK1*^{D319N} plants performed like WT (Figure 4.5b). To determine if impaired immunity in *ilk1* lines correlated with a defective ability to induce PAMP-mediated responses, the transgenic lines were grown on media containing flg22 which inhibits root growth (Gómez-Gómez *et al.*, 1999). In accordance with results from the bacterial growth assay, the *ilk1* and *ilk1/ ILK1*^{K222A} plants demonstrated less root growth inhibition, indicating altered flg22-induced responses (Figure 4.5c). In addition, no differences between WT and *ilk1* were observed upon infection with the

Table 4.2 The primer pairs used in this study.

Gene	Use	Forward Primer	Reverse Primer
ILK1 T-DNA insert	Mutant selection	CCAGAAAGACAAAGCAGAATC	GCCTTTCAGAAATGGATAAATA GCCTTG
ILK1	Cloning	ATGGAGAACATAACCGCGCA	CCAGAAAGACAAAGCAGAATC
K222A mutation	Cloning	TTCAGTCGCAATACTTGATAA AGA	ATCAAGTATTGCGACTGAAA CCCG
D319N mutation	Cloning	CAATCATTCACTGTAACCTAA AGCCAAAAAATATTTTG	ATTTTTTGGCTTTAGTTGACAGT GAATGATTGG
FRK1	qRTPCR	TGCAGCTCAGTTTCAATCAAGT GG	CCTTTGCCTCTCGGCGTCGG
CFP	Mutant selection	GAGCAAAGACCCCAACGAGA	GGTACCGTCGACTGCAGAAT
PP2A	qRTPCR	TAACGTGGCCAAAATGATGC	GTTCTCCACAACCGCTTGGT
WRKY29	qRTPCR	ACGAGTACGCACCAAGCGGC	GGAAAAGTTCCGCTCCCGGACA
CYP81F2	qRTPCR	CTATCGTCGGCCATCTCCAC	TATTTTTCAGCGAAGCGGCG
NHL10	qRTPCR	GCCTACTACGAGGGAAAGCG	AACGTTGGTGTGAGAACGGT
PHI-I	qRTPCR	GGTGGCCAAAGCTACGCGGT	CAGTCCCGTGTGACCCGCAT
RD29A	qRTPCR	AGTGATCGATGCACCAGGCGT	CGGAAGACACGACAGGAAACAC
RD29B	qRTPCR	GGGGAAAGGACATGGTGAGG	GGTTTACCACCGAGCCAAGA
HAK5	qRTPCR	CCGTCCACTCGGTGTTTGTA	GAATCCTTTGGCCCCACGTA
ILK1	qRTPCR	CATCATCTTGATGGCCGGA	GTACTTTGCATCAGCAGCCG

Figure 4.4 Analysis of *ILK1* expression and stress responses in *ilk1* transgenic lines.

(a) Expression of the *ILK1* gene in the *ilk1* T-DNA insert line relative to WT and *ilk1* plants ectopically expressing *ILK1*, *ILK1*^{K222A} or *ILK1*^{D319N} normalized to *PP2A* expression. The average of 3-5 biological replicates are presented relative to WT expression (set to 1).
(b) Germination rates of the *ilk1* lines 3 days after vernalization on solid medium (n=100).
(c) Germination inhibition of additional lines ectopically expressing *ILK1* on plates containing 150 mM NaCl 3 days after vernalization (n=120).
(d) Bacterial growth of *Pst* DC3000, DC3000 *hrcQ-U* and DC3000 avrRpt2 in rosette leaves 2 days after flood inoculation. The box plot represents the average of 25-36 plants where the *rps2* line is unable to induce *avrRpt2*-induced immunity.
(e) Expression of the *ILK1* gene in WT two-week old seedlings in control and stress conditions calculated as described in (a). Stress treatments included 300 mM NaCl for 5h or 400 mM mannitol for 5h or 1 µM flg22 for 3 or 24 h (n=3).
(f) ROS production in relative light units was measured immediately following exposure to water, 10 µM flg22 (n=27-36).
(g) Average induction of Ca^{2+}-dependent genes following treatment with 1 µM flg22 for 3h to untreated controls (n=6). Expression was normalized to *PP2A* expression and presented as the induction relative to the untreated control (set to 1).

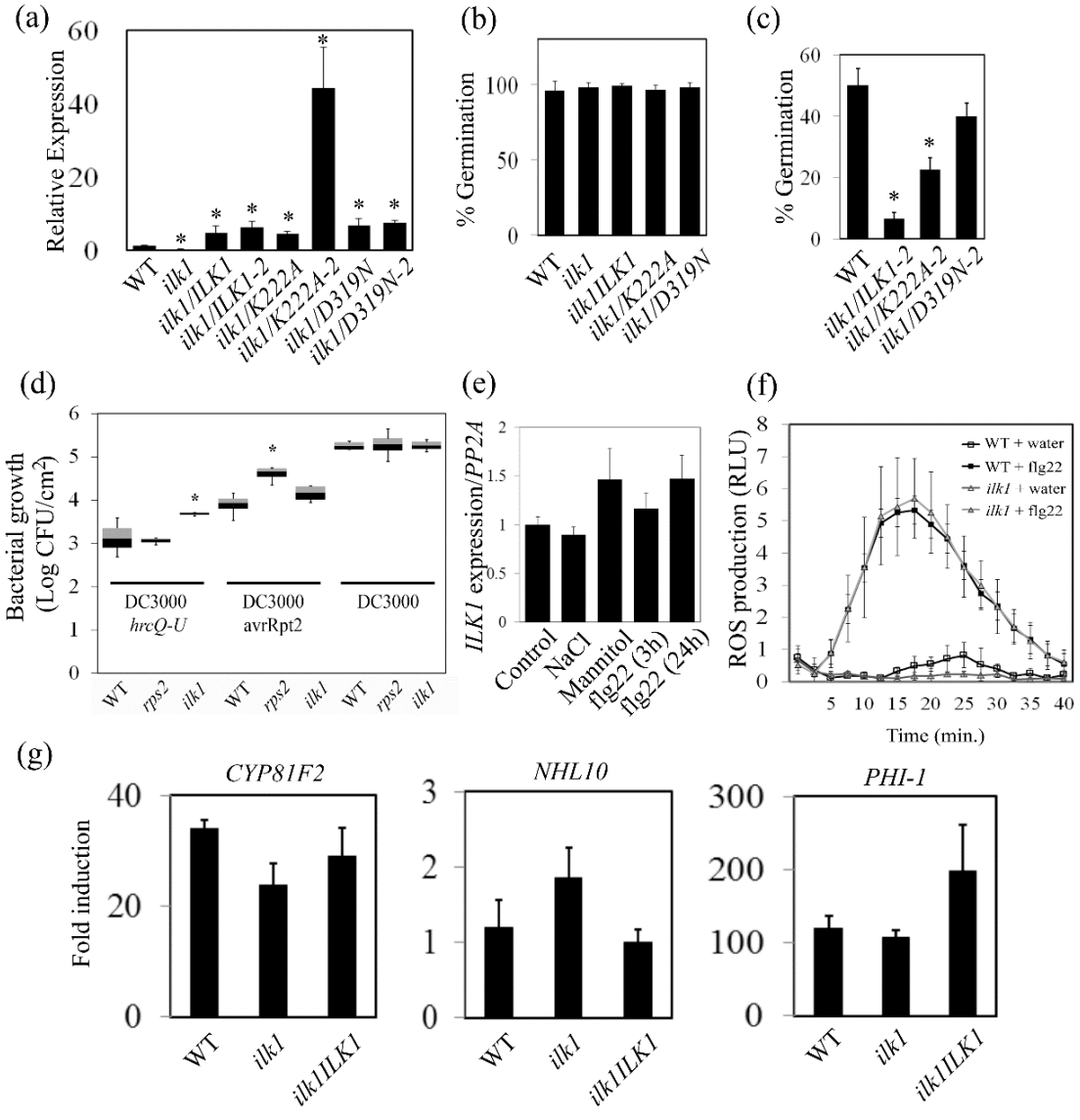
(a)
Relative Expression
WT
ilk1
ilk1/ILK1
ilk1/ILK1-2
ilk1/K222A
ilk1/K222A-2
ilk1/D319N
ilk1/D319N-2
(b)
% Germination
WT
ilk1
ilk1ILK1
ilk1/K222A
ilk1/D319N
(c)
% Germination
WT
ilk1/ILK1-2
ilk1/K222A-2
ilk1/D319N-2
(d)
Bacterial growth (Log CFU/cm2)
DC3000 hrcQ-U
DC3000 avrRpt2
DC3000
WT
rps2
ilk1
(e)
ILK1 expression/PP2A
Control
NaCl
Mannitol
flg22 (3h)
flg22 (24h)
(f)
ROS production (RLU)
WT + water
WT + flg22
ilk1 + water
ilk1 + flg22
Time (min.)
(g)
CYP81F2
NHL10
PHI-1
Fold induction
WT
ilk1
ilk1ILK1

Figure 4.5 *ILK1* promotes immunity and ionic or osmotic stress responses.
(a) Seed germination (radicle emergence) on plates containing 150 mM NaCl or 300 mM mannitol 3 days after vernalization. The average is expressed as a percentage of germination on control plates (n=100).
(b) Bacterial growth of *Pst* DC3000 *hrcQ-U* in rosette leaves 2 days after syringe inoculation (n=25-36).
(c) Root growth inhibition of 6-day-old seedlings in the presence or absence of 10 µM flg22 normalized to control plate root lengths (n=15).
(d) Detection of MPK3 or MPK6 phosphorylation in seedlings treated with 1 µM flg22. Ponceau staining was used to determine equal loading and the experiment was repeated twice.
(e) Average gene induction following treatment with 1 µM flg22 for 3h or 300 mM NaCl for 8 h (n=6). Expression was normalized to *PP2A* expression and presented as the induction relative to the untreated control (set to 1).

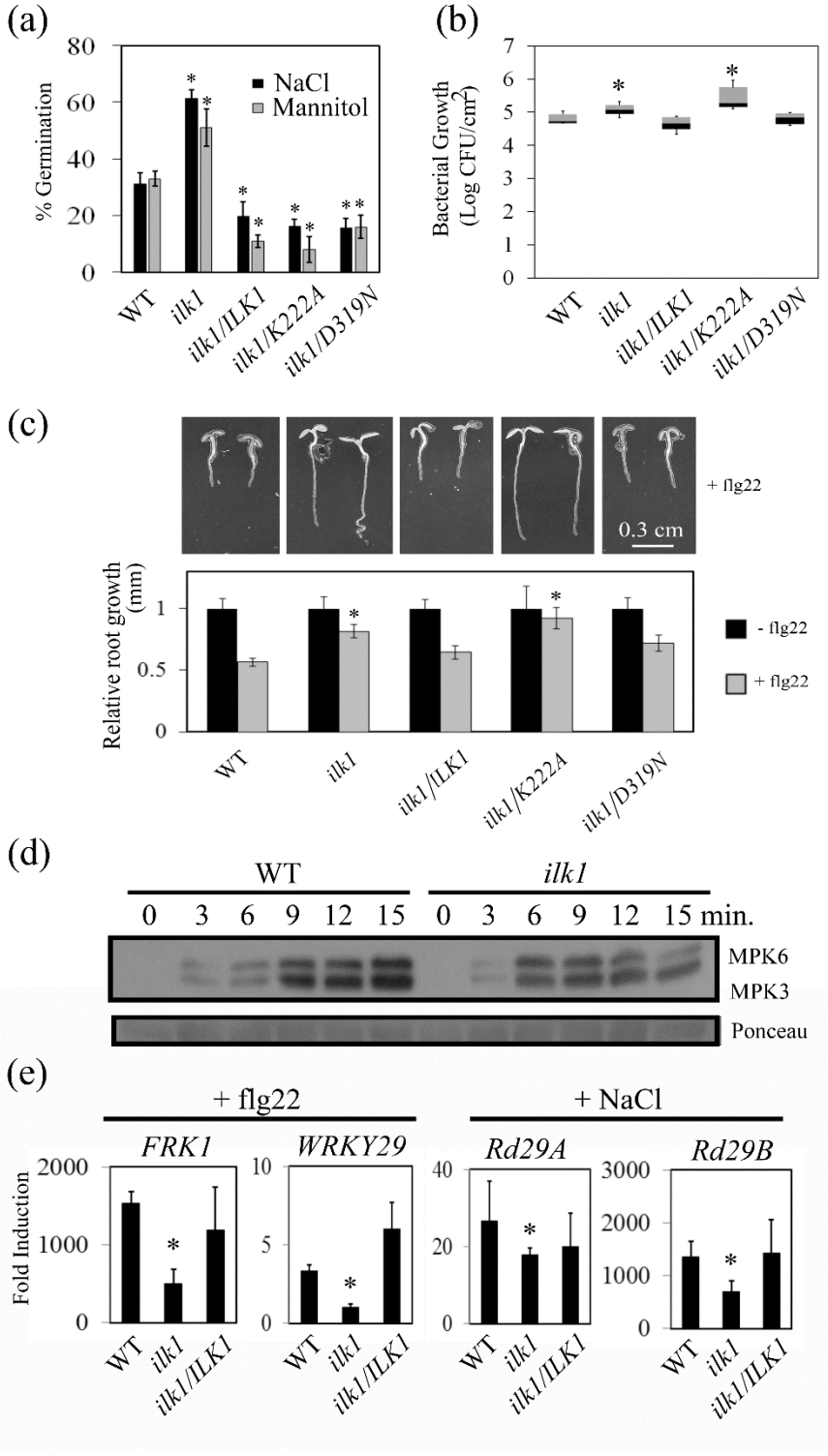
(a)
% Germination
NaCl
Mannitol
WT
ilk1
ilk1/ILK1
ilk1/K222A
ilk1/D319N
(b)
Bacterial Growth (Log CFU/cm2)
(c)
+ flg22
0.3 cm
Relative root growth (mm)
- flg22
+ flg22
(d)
WT
ilk1
0 3 6 9 12 15 0 3 6 9 12 15 min.
MPK6
MPK3
Ponceau
(e)
+ flg22
+ NaCl
FRK1
WRKY29
Rd29A
Rd29B
Fold Induction

virulent DC3000 or avirulent DC3000 *avrRpt2* strains (Figure 4.4d). These results suggest that ILK1 functions as a kinase to promote basal immunity and responses to flg22.

To determine how *ILK1* is contributing to PAMP and osmotic stress sensitivity, a number of signaling responses were quantified. First, *ILK1* expression was compared in plants treated with NaCl, mannitol, flg22 or water, and no changes were observed (Figure 4.4e). Flg22-induced ROS production also did not differ between WT and *ilk1* plants (Figure 4.4f). In contrast, MPK3 and MPK6 phosphorylation dynamics were altered within the first 15 minutes following flg22 application in *ilk1* plants (Figure 4.5d). Phosphorylation of MPK3 and MPK6 occurred at low levels at 3 minutes and gradually increased to a maximum at 15 minutes in the WT, while maximum phosphorylation was observed at 6 minutes and was sustained until 12 minutes in the *ilk1* plants. MAPKs have been shown to regulate *FRK1* and *WRKY29* gene induction in response to flg22 (Boudsocq *et al.*, 2010), and consistent with a disruption in MAPK signaling, *FRK1* and *WRKY29* induction was lower in *ilk1* mutants compared to either WT or *ilk1/ILK1* plants (Figure 4.5e); by contrast, the CDPK-regulated gene expression (Boudsocq *et al.*, 2010), was unaffected (Figure 4.4g). Salt-induced gene expression was also significantly reduced in *ilk1* relative to WT and *ilk1/ILK1* plants (Figure 4.5e). Together, this indicates that *ILK1* influences MAPK-mediated responses to flg22 and that *ILK1* a positive regulator of basal immunity and ionic stress response.

ILK1 fusion proteins localize to cellular membranes and the cytoplasm

To gain further insight into ILK1's role in stress, the cellular localization of ILK1 fluorescent fusion proteins was recorded in transiently expressing *N. benthamiana* or stably expressing *Arabidopsis* tissue. In *N. benthamiana*, the ILK1::GFP chimera protein co-localized

with both the PM (BDCaM53::mCherry)(Rodríguez-Concepción *et al.*, 2000) and endoplasmic reticulum (ER) HDEL::mCherry markers (Figure 4.6a, Pearson correlation coefficient R = 0.84 and 0.70 respectively). Cellular fractionation of these samples revealed that ILK1::GFP signal was observed in both membrane and cytosolic protein fractions on a Western blot (Figure 4.6b). In addition, ILK1::GFP was detected in Hechtian strands and at the cell periphery external to chloroplast autofluorescence following plasmolysis (Figure 4.6c). A similar localization pattern was observed in leaf and root tissues of the *ilk1/ILK1* line where ILK1::CFP localized to the cell periphery, as well as the helical structure which is consistent with proto-xylem (Figure 4.6d)((Mähönen *et al.* 2000). No ILK1::CFP signal was detected when *ILK::CFP* was expressed under control of the endogenous *ILK1* promoter. Together, these findings indicate that ectopically-expressed ILK1 can be found in the cytoplasm, PM and ER.

ILK1 is required for the flg22-mediated fluctuations in cellular ion homeostasis

Since ILK1 does not contain transmembrane domains and is not predicted to be myristoylated or palmitoylated, it is possible that ILK1 interacts with a membrane-bound protein to produce the observed localization pattern in the PM and ER. To identify these potential interactors, we used two unbiased proteomic approaches including functional protein microarrays. The microarrays contained 15,000 purified proteins and were probed with purified ILK1-V5 and anti-V5 Cy3-labelled antibody, allowing identification of protein-ILK1 complexes (Brauer *et al.*, 2014). A kinase client assay (KiC) was also performed, where purified ILK1-cMyc was incubated with a peptide library and phosphorylation of the peptides was quantified by mass spectrometry (Ahsan *et al.*, 2013). These two approaches identified seven transporters as putative ILK1 interaction partners including two K^+ uptake transporters (Figure 4.7a, Table 4.3).

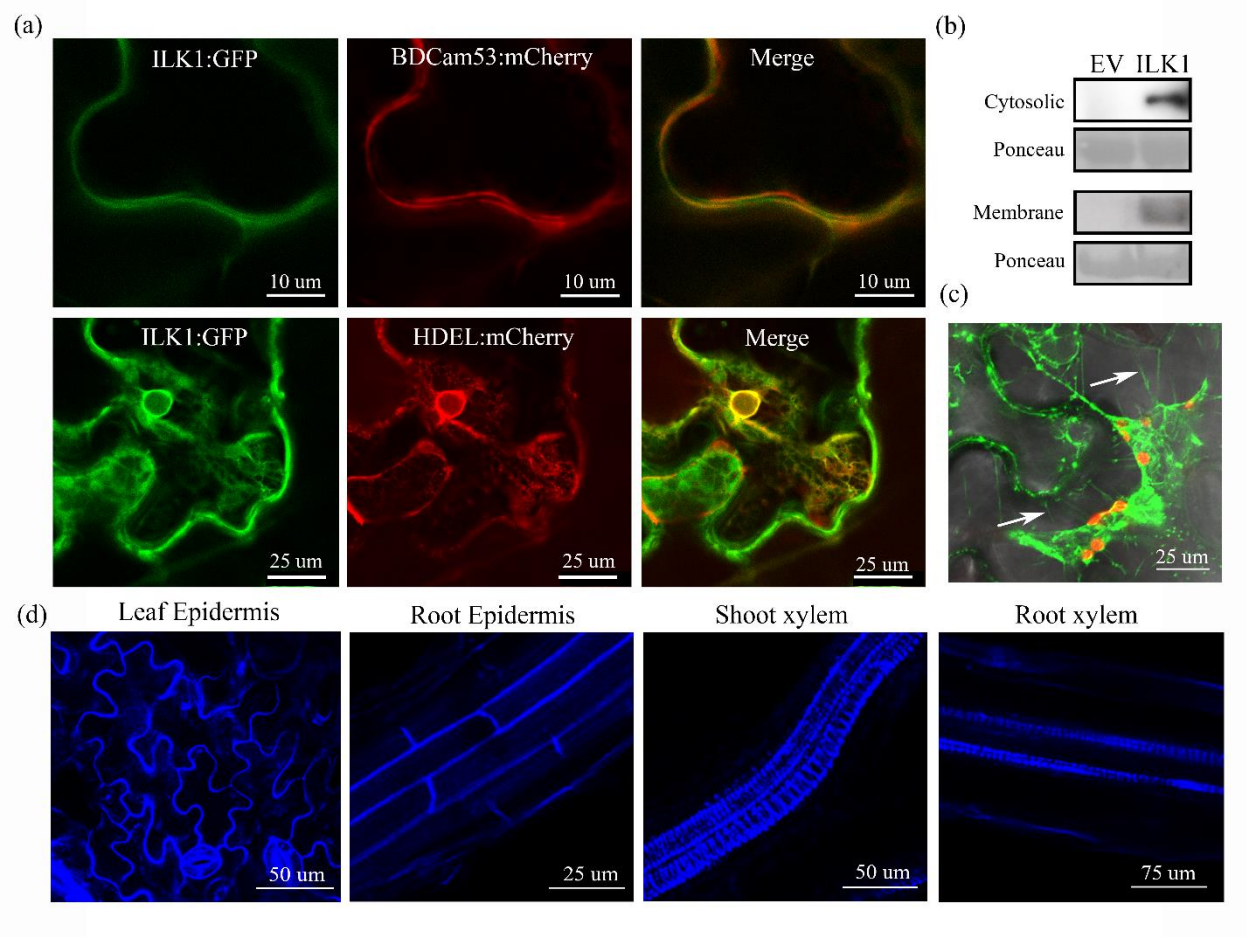

Figure 4.6 ILK1 fusion proteins localize to both the cytosol and membrane.
(a) Transiently expressed ILK1-GFP co-localizes with the plasma membrane BDCam53:mCherry marker and the endoplasmic reticulum HDEL:mCherry marker (n=5).
(b) Membrane fractionation of ILK1-GFP-expressing tissue indicates that ILK1-GFP is found in both membrane and cytosolic fractions.
(c) The ILK1-GFP fusion proteins localized to Hetchian strands (indicated by white arrows) in *N. benthamiana* leaf epidermis cells following treatment with 1 M NaCl (n=4).
(d) Stably expressed ILK1-CFP localized to the cell periphery and xylem tissue in *Arabidopsis* leaves and roots in three-week-old seedlings (n=5-10).

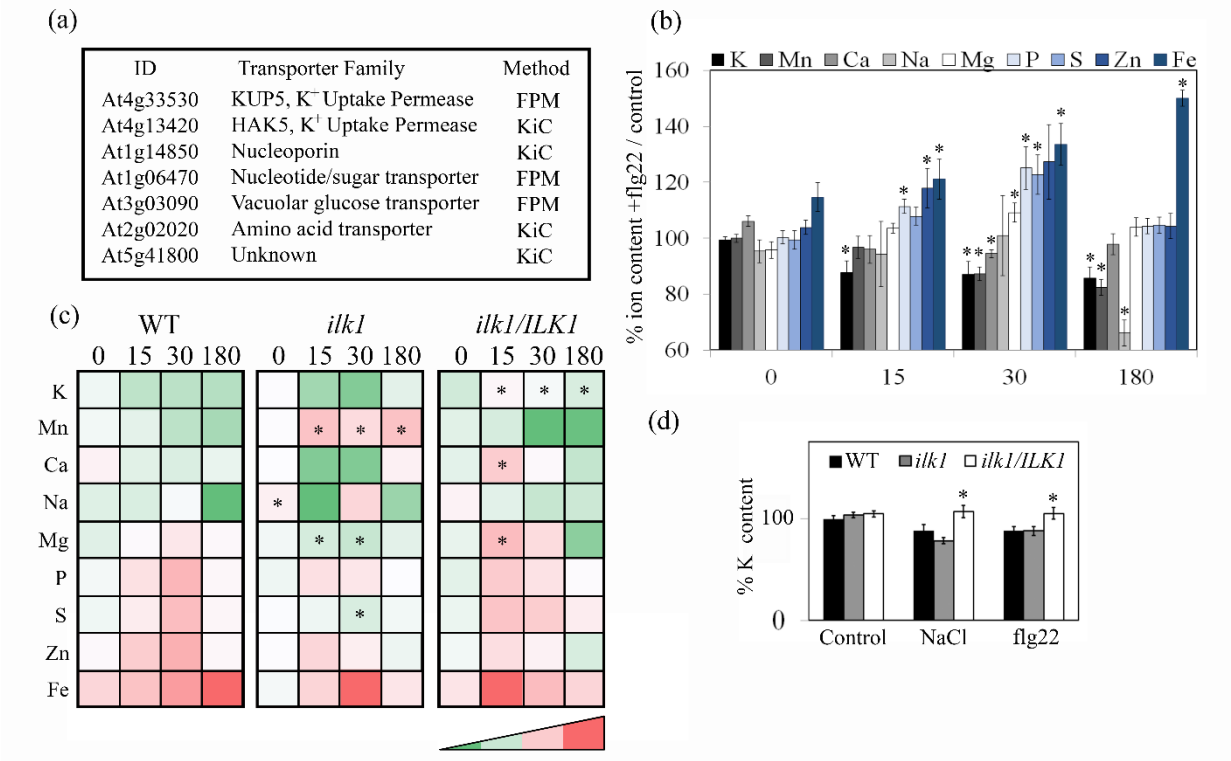

Figure 4.7 *ILK1* modulates ion homeostasis during flg22 and NaCl treatments.
(a) Identification of putative ILK1-interacting transporters *in vitro* using functional protein microarrays (FPM) or the kinase client assay (KiC).
(b) Ionomic profile of 1 µM flg22-treated WT seedlings normalized to the untreated control over 15, 30 and 180 minutes following treatment (n=4).
(c) A heat map indicating the relative ion content of two-week old seedlings treated with 1 µM flg22. Each ion is normalized to the untreated control and red indicates higher content while green indicates lower content (n=4). The asterisks indicate significantly different ion content from the WT line at the given time.
(d) Comparison of K^+ content in NaCl (300 mM, 8 h) and flg22-treated (1 µM, 15 min) seedlings relative to control conditions (set at 100%, n=4-20).

Table 4.3 Analysis of transporters identified as putative ILK1 phosphorylation targets and protein interaction targets using the kinase client assay (KiC) and functional protein microarrays (FPM). The average signal with ILK1 represents the fluorescence signal in relative light units across three independent arrays for the FPM and the number of phosphopeptides observed and number of peptides detected overall in parentheses for the KiC.

ID	Assay	Phospho -peptide	pRS Score [a)]	pRS site probability [b)]	p-value	Average signal with ILK1	Average signal in control
At4g33530	FPM	-	-	-	0.0002	45051	1590
At1g06470	FPM	-	-	-	0.0001	39483	1469
At3g03090	FPM	-	-	-	0.0044	17531	1566
At4g13420	KiC	YRPDSFIIEAGQT	46	Y(1): 98.8; T(13): 100.0		1 (7)	0 (10)
At1g14850	KiC	NLFGAYSNGGESANKRQ	44	Y(6): 50.0; S(7): 50.0		1 (10)	0 (24)
At5g41800	KiC	PFPVTRLDSDAGALFVLQ	101	S(9): 98.8		2 (28)	0 (26)
At1g11260	KiC	IRGVDDVSQEFDDLVAASKE	39	S(18): 98.6		1 (28)	0 (23)

[a)] pRS score: This peptide score is based on the cumulative binomial probability that the observed match is a random event where scores above 50 give good evidence for a match.

[b)] pRS site probabilities: Estimate of probability (0-100%) that the phosphorylation site is phosphorylated where a score of 50% or above is considered evidence of phosphorylation.

Together with our genetic data indicating that ILK1 is important for osmotic stress sensitivity, these finding suggest that *ILK1* may play a role in modulating cellular ion homeostasis.

Little is known about the effect of PAMPs on ion homeostasis in intact plants. To determine if ion homeostasis is altered in response to flg22, we determined ion content in WT seedlings between 15 to 180 minutes after PAMP treatment (Figure 4.7b). Flg22 treatment produced significant changes in ion accumulation as early as 15 min, including a net K^+ loss and P, Zn and Fe accumulation. We next measured how *ILK1* influences these changes, and found a significant effect of *ILK1* expression on K^+, Mg^{2+} and Mn^{2+} content at multiple time points (Figure 4.7c). In particular, K^+ content in *ilk1/ILK1* was maintained at the same levels as untreated controls while progressive K^+ loss was observed in WT and *ilk1* seedlings treated with flg22. K^+ loss also occurs during osmotic and Na stress (Osakabe *et al.*, 2013). Indeed both salt stress and flg22 induced a net reduction in K^+ content in WT, though this reduction was not observed in the *ilk1/ILK1* lines (Figure 4.7d). Thus, flg22 has a significant effect on ion homeostasis which is partially mediated by *ILK1*.

ILK1 interacts with the high affinity K^+ transporter, HAK5

HAK5 is one of the most important transporters for K^+ acquisition and growth maintenance in limiting K^+ conditions including during salt stress (Pyo *et al.*, 2010; Rubio, Francisco & Rodríguez-Navarro, 2000; Nieves-Cordones *et al.*, 2010). Since phosphorylation is a regulatory mechanism controlling transport in the closely related barley HAK1 (Fulgenzi *et al.*, 2008) and given that we identified HAK5 as a potential ILK1 phosphorylation target (Figure 4.7a), we tested if ILK1 and HAK5 interact using two distinct approaches. The split-luciferase

complementation assay (SLCA) was carried out in protoplasts expressing luciferase-tagged ILK1 or CML9, along with the N-terminal and C-terminal cytosolic portions of HAK5, and showed that while ILK1 interacted with both fragments of HAK5, CML9 did not interact with either fragment (Figure 5.8a). Bimolecular fluorescence complementation (BiFC) in *Xenopus* oocytes was also employed in order to probe the potential interactions in the absence of other plant proteins. HAK5, ILK1 and CML9 were fused to a complementary half of split YFP. The various cRNA were co-injected into oocytes and analyzed by confocal microscopy. Co-injection of cRNA encoding *ILK1* with either *HAK5* or *CML9*, each tagged with the complementary non-fluorescent fragments of YFP, resulted in a significant YFP signal, indicating a direct interaction of the protein products (Figure 4.8b). In contrast, in cells co-injected with *HAK5* and *CML9* cRNA as BiFC partners, no specific YFP signal was detected. To determine if the observed HAK5 – ILK1 interactions were dependent on the presence of CML9, cells were injected with HAK5 and CML9 cRNA encoding the complementarily YFP fragments, and unlabeled ILK1. The observed lack of YFP signal (Figure 4.9a), suggests that *in vivo*, ILK1 interacts directly with HAK5 through the cytosolic regions of HAK5.

ILK1 and *HAK5* contribute to stress-induced K^+ fluxes and membrane depolarization

HAK5 is one of two transport proteins which mediate K^+ uptake in the high affinity range in *Arabidopsis* (Nieves-Cordones *et al.*, 2010). To determine if *ILK1* is involved in modulating high affinity K^+ transport, *ilk1* lines were grown under extremely limiting K^+. Both *ilk1* and *ilk1/K222A* mutants demonstrated a similar stunted root growth phenotype to that shown for *hak5-3* (Nieves-Cordones *et al.*, 2010) grown under similar conditions (Figure 4.10a). The

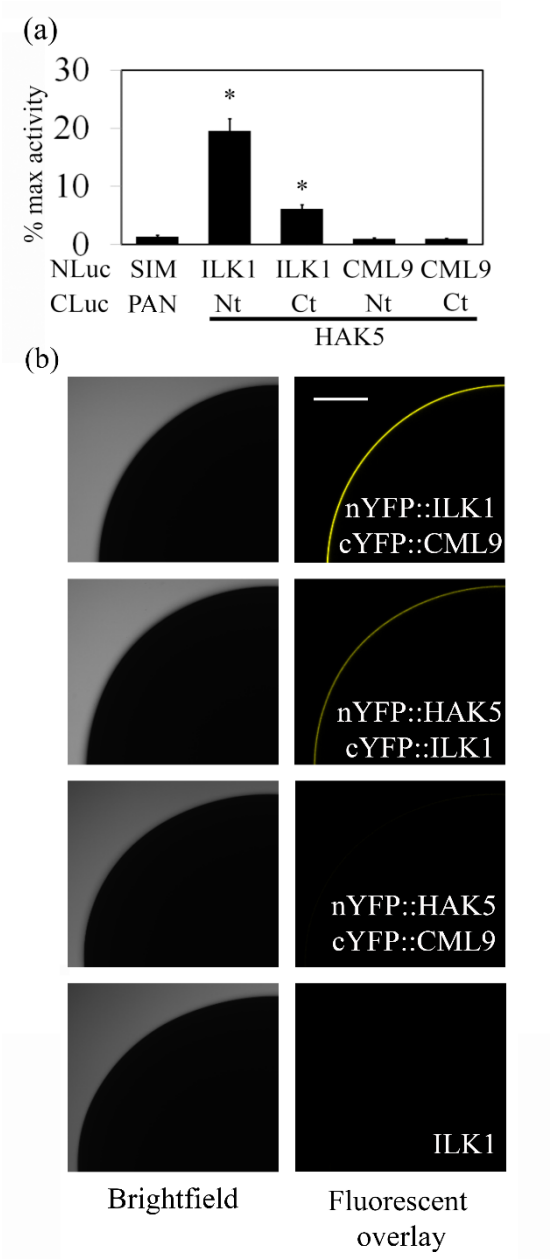

Figure 4.8 ILK1 interacts with the HAK5 K^+ uptake transporter.
(a) Luciferase activity in Arabidopsis protoplasts between bait (NLuc) and pray (CLuc) proteins were quantified relative to the positive control using the SLCA. The cytosolic N-terminal (Nt) and C-terminal (Ct) domains of HAK5 were used to test for interactions with ILK1 and CML9 and compared to the negative control pair (SIM-PAN).
(b) Images showing interaction of ILK1 with full-length HAK5 and CML9 by bimolecular fluorescence complementation in *Xenopus* oocytes. The image shows one quarter of the oocyte either fluorescing or under white light and was taken using scanning confocal microscopy. No interaction between nYFP::HAK5 and cYFP::CML9 was observed, and untagged ILK1 was transformed into cells as a negative control (n=6).

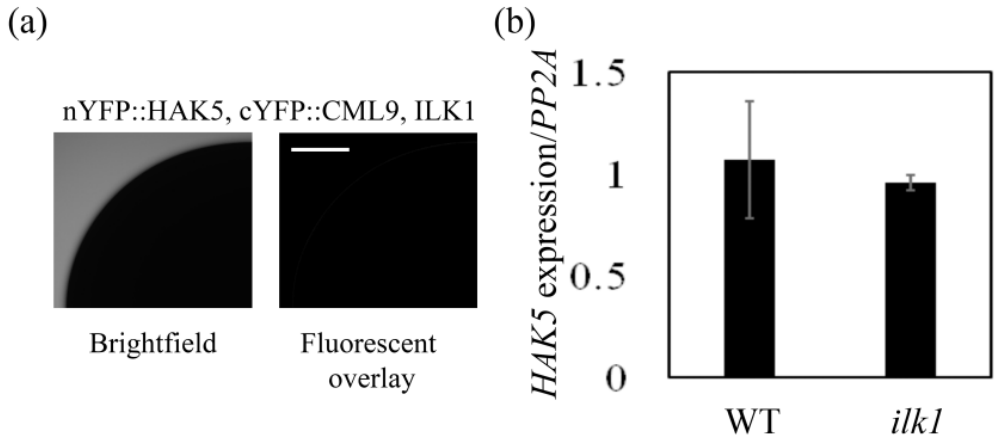

Figure 4.9 ILK1 does not promote HAK5 interaction with CML9 and *HAK5* expression is unaffected by *ILK1*.
(a) Interactions between N-terminal and C-terminal YFP-tagged proteins in *Xenopus* oocytes using the bimolecular fluorescence complementation assay. Pictures show one quarter of the oocyte co-expressing tagged CML9 and HAK5 along with untagged ILK1. The white bar indicates a scale of 200 µM.
(b) Expression of the *HAK5* gene in the *ilk1* T-DNA insert line relative to WT and normalized to *PP2A* expression (n=4).

Figure 4.10 *ILK1* and *HAK5* contribute to K^+ transport, flg22-induced plasma membrane depolarization and gene expression.
(a) Root growth under limiting K^+ conditions (10 µM) six days after germination.
(b) The K^+ concentration of media exposed to 100 mg of flg22-treated leaf tissue (n=5).
(c) Membrane depolarization time course in seconds following 10 nM flg22 application in *ilk1* and *hak5-3* (n=9-12)
(d) Membrane depolarization time course in seconds following 10 nM flg22 application in *ilk1/ILK1* and *ilk1/K222A* plants (n=5-7).
(e) Pre-treatment with the K^+ channel blocker, TEA (10 mM, 1h) slows flg22-induced membrane depolarization (n=8).
(f) Quantification of the number of seconds taken to reach the halfway point of membrane depolarization across lines and treatments.
(g) *FRK1* gene expression in two week old seedlings treated with 1 µM flg22, normalized to *PP2A* and to control conditions (n=5).
(h) Protein accumulation in the membrane fraction of *N. benthamiana* leaves of HAK5-GFP when co-expressed with GFP, CML-cMyc or ILK1-cMyc. Equal loading of total protein extract was verified by Ponceau stain.

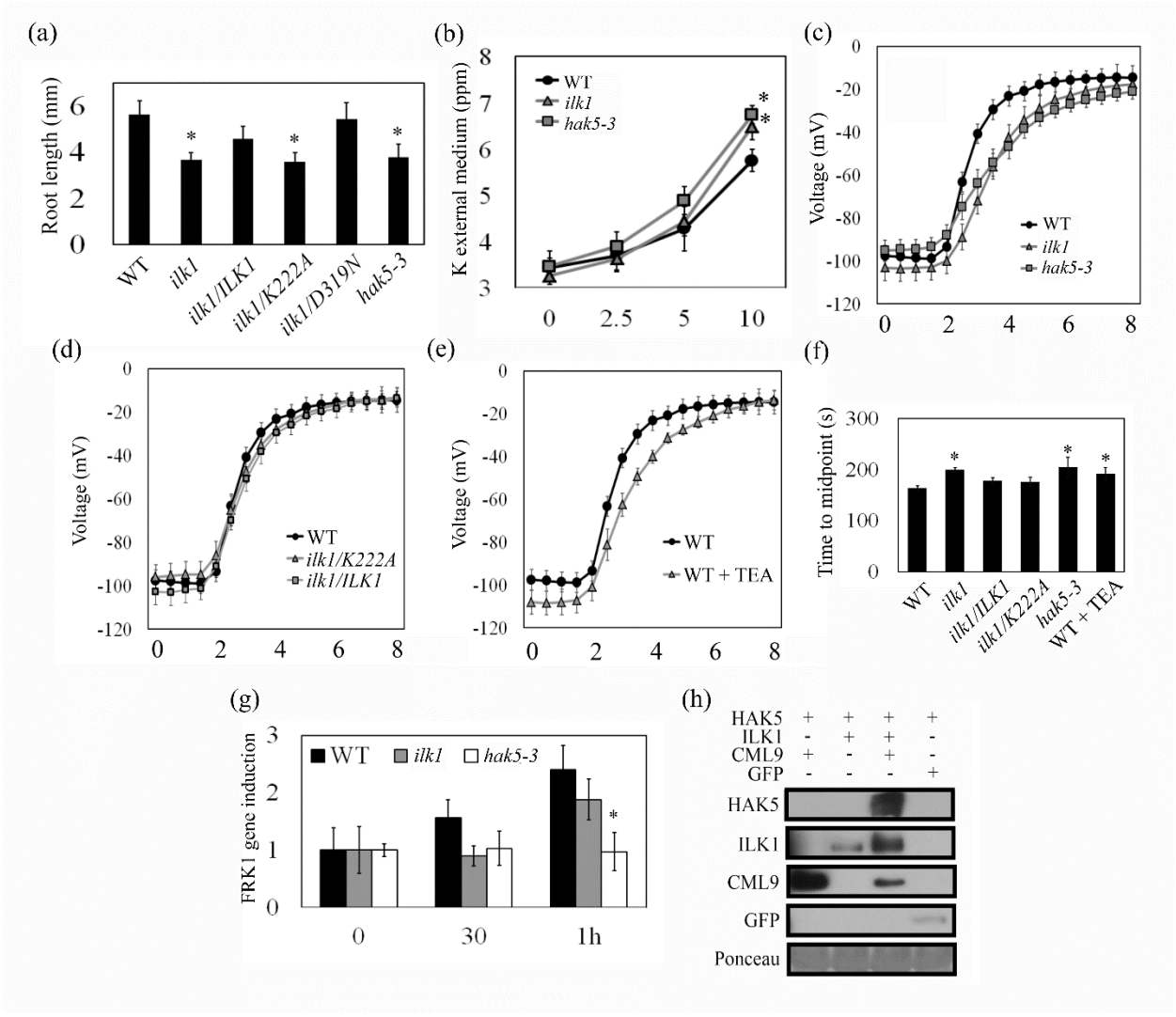
(a)
Root length (mm)
WT
ilk1
ilk1/ILK1
ilk1/K222A
ilk1/D319N
hak5-3
(b)
K external medium (ppm)
WT
ilk1
hak5-3
(c)
Voltage (mV)
WT
ilk1
hak5-3
(d)
Voltage (mV)
WT
ilk1/K222A
ilk1/ILK1
(e)
Voltage (mV)
WT
WT + TEA
(f)
Time to midpoint (s)
WT
ilk1
ilk1/ILK1
ilk1/K222A
hak5-3
WT + TEA
(g)
FRK1 gene induction
WT
ilk1
hak5-3
0
30
1h
(h)
HAK5
ILK1
CML9
GFP
Ponceau

phenotype could not be attributed to reduced *HAK5* expression, as no changes in *HAK5* mRNA accumulation were observed in the *ilk1* mutants (Figure 4.9b).

Our aforementioned ionomic study revealed that ILK1 overexpression enhanced K^+ accumulation during both flg22 and NaCl treatments in whole seedlings (Figure 4.7d). To determine how mature leaves respond to flg22, the epidermis of leaf disks of mature WT and *ilk1* plants was removed and leaf mesophyll cells were exposed to flg22 in a liquid medium. The net K^+ content in the external medium increased within 10 minutes of flg22 challenge in WT (Figure 4.10b). However, the K^+ concentration was higher in medium exposed to *ilk1* and *hak5-3* tissue indicating the leaves of these genotypes exhibited either reduced K^+ uptake or increased K^+ efflux relative to the WT. To determine if this K^+ transport contributes to the membrane depolarization, leaf disks were similarly exposed to flg22 and the trans-PM electrical potential was recorded in cells impaled with glass microelectrodes. The *ilk1* plants displayed delayed membrane depolarization (40 second delay) relative to WT (Figure 4.10c) but the amplitude of the depolarization was not altered. A similar delay was observed in the *hak5-3* plants but not in the *ilk1/ILK1* and *ilk1/K222A* plants (Figure 4.10d). Furthermore, a delay in the timing and not amplitude of the depolarization was observed in WT leaves treated with the K^+ channel-blocker, TEA (Figure 4.10e, f). In line with previous studies demonstrating a connection between gene induction and PM depolarization (Jabs *et al.*, 1997), *hak5-3* also displayed reduced flg22-induced *FRK1* induction after 1h (Figure 4.10g). Together, these results suggest that K^+ transport mediated by *ILK1* and *HAK5* is a component of the flg22-induced PM depolarization and downstream signaling responses.

ILK1 affects *HAK5* properties by acting at post-transcriptional level

The interaction between HAK5 and ILK1 may change the activation state of HAK5 or its transport properties. As the interaction between ILK1 and HAK5 was first shown by phosphorylation of HAK5 peptide YRPDSFIIEAGQT in the KiC assay, we tried to confirm this by incubating ILK1 with the cytosolic N-terminus of HAK5 in the presence of ATP. However, phosphorylation was not detected under the tested conditions (data not shown), though this could be due to improper folding or lack of other interacting proteins. Next, we explored the possibility that ILK1 modulates HAK5 by acting at a step in HAK5 synthesis, as previously shown for other K^+ transporters (Held *et al.*, 2011). Co-expression of both *ILK1* and *CML9* correlated with HAK5 protein accumulation in transgenic *N. benthamiana* leaves, while HAK5 could not be detected when expressed alone or in combination with either ILK1 or CML9 (Figure 4.10h). Thus, ILK1 modulates HAK5 at the post-transcriptional level by potentially affecting HAK5 stability or accumulation at the PM.

DISCUSSION

PAMP-triggered immunity (PTI) is dependent on an intact PAMP recognition and signal transduction system to fully induce immune responses. Bacterial flagellin can be perceived by diverse plant species and has been extensively studied as a model for PAMP perception (Felix *et al.*, 1999). In *Arabidopsis,* the flg22 peptide is bound by the FLS2 receptor which heterodimerizes with BAK1 to induce phosphorylation of BIK1 (Lu *et al.*, 2010). Both BIK1 and PBL1 promote transient cytosolic Ca^{2+} influx which is thought to contribute to immune signaling through activation of Ca^{2+}-binding proteins like CaMs and CDPKs (Ranf *et al.*, 2014). Ca^{2+} spiking activates ROS production by the *RbohD* NADPH oxidase (Torres *et al.*, 2002) and may

induce the transient ion fluxes which produce membrane depolarization (Jeworutzki *et al.*, 2010). Here, we demonstrated that *ILK1* and *HAK5*-mediated K^+ transport significantly altered the rate of membrane depolarization triggered by flg22 and that the dynamics of MAPK phosphorylation and gene induction were affected upon the same flg22 treatment. These responses seem to occur independently of CDPK-dependent gene induction and ROS production suggesting that ILK1-mediated pathways function genetically downstream of Ca^{2+} spiking. Uncoupling of flg22-induced ROS production and membrane depolarization has been demonstrated previously where both chemical inhibition of oxidases and mutants lacking *RbohD*/*RbohF* expression demonstrated unaltered depolarization (Jeworutzki *et al.*, 2010).

Our results suggest that ILK1-mediated PM depolarization occurs upstream of kinase signaling and contributes to its amplification, since a reduced depolarization rate within the first 5 minutes of flg22 treatment corresponded to a lack of progressive increase in MPK3 and MPK6 phosphorylation over 15 minutes and defense gene induction after 60 minutes. PM depolarization has been suggested to play a role in enhancing the duration or amplitude of immune responses based on studies of anion channels which are thought to contribute a majority of the ion flux required for membrane depolarization (Jeworutzki *et al.*, 2010). For example, blocking anion channels with chemical inhibitors influenced the duration and intensity of kinase activation and defense gene induction following application of the elicitor cryptogein in tobacco cells (Wendehenne *et al.*, 2002). A similar strategy in parsley cells demonstrated that blocking anion channels could reduce MAPK phosphorylation (Ligterink *et al.*, 1997), gene induction and phytoalexin accumulation (Jabs *et al.*, 1997) after induction with the Pep13 elicitor. PM depolarization also occurs in response to cold (Lewis *et al.*, 1997) and drought (Geiger *et al.*, 2009), suggesting that it is a common response during stress.

In our study, both *ilk1* and *hak5* exhibited a similar delay in flg22-induced membrane depolarization, flg22-induced K^+ accumulation and stunted growth phenotype in 10 µM K^+. Combined with physiological studies showing that *HAK5* is one of only two transporters facilitating K^+ uptake below 200 µM (Rodríguez-Navarro and Rubio, 2006), this suggests that *ILK1* is involved in the same physiological processes as *HAK5* and thus could be involved in K^+ uptake. K^+ uptake could contribute to flg22-induced membrane depolarization since uncompensated cation influx will depolarize the membrane potential. Moreover, *HAK5*'s effect may also be influenced by proton influx since it is predicted to be a H^+/K^+ co-transporter based on studies of the homologous *Neurospora crassa NcHAK1* (Rodriguez-Navarro *et al.*, 1986; Haro *et al.*, 1999). However, information regarding *HAK5*'s specificity and transport capacity is incomplete because of a lack of detectable transport in heterologous systems such as *Xenopus* oocytes (Rodríguez-Concepción *et al.*, 2000). In a recent report, the HAK5 ortholog from venus fly trap was characterized in oocytes as being a proton-driving high affinity transporter for K^+ (Scherzer *et al.*, 2015). However, this activity was only detectable when the Ca^{2+}-responsive CBL9-CIPK23 pair were co-expressed with the DmHAK5, and these proteins did not interact with AtHAK5 in yeast 2-hybrid assays previously suggesting different regulation of these transporters (Li *et al.*, 2006).

The role of *ILK1* and *HAK5*-mediated ion transport may change over time or across cell types. For example, *ILK1*'s role in regulating membrane depolarization and osmotic stress response is kinase-independent while its role in PTI and growth in low K^+ are kinase-dependent. We demonstrated that ILK1 and CML9 together promote accumulation of HAK5 protein and that CML9 represses ILK1 activity. This would suggest that HAK5 phosphorylation is not necessary for regulating membrane depolarization, in line with our observation that the kinase-

attenuated ILK1^{K222A} isoform rescued the *ilk1* depolarization delay. Indeed other kinases have been shown to facilitate trafficking of proteins to the PM in a kinase-independent manner. For example, CIPK6 and its Ca^{2+}-sensing interactor CBL4 facilitates AKT2 K^+ channel trafficking from the ER to the PM, and an intact CBL4-CIPK6-AKT2 complex is required for full transport activity (Held *et al.*, 2011). In line with *ILK1* serving a similar role, we observed ILK1-GFP at the PM and ER though it is not predicted to be membrane-bound. However, we also observed HAK5 accumulation in oocytes in the presence of ILK1 alone. This discrepancy may reflect the difference between techniques since the *in planta* assay relies upon *Agrobacteria*-mediated transformation while oocytes were directly injected with cRNA. It is also possible that other mechanisms regulating HAK5 protein transport and turnover are absent in oocytes, enhancing the accumulation of the protein. Thus, more study is warranted to determine the mechanisms underlying HAK5 accumulation in plant cells.

HAK5 may also be a phosphorylation target of ILK1, though phosphorylation of HAK5 domains was not observed here. This may be because of a lack of an intact HAK5 structure (ie full length protein) or because additional components may be necessary. ILK1 activity appears to be necessary for late PAMP responses and growth in low K^+ environments, as the ILK1^{K222A} expression did not rescue *ilk1* phenotypes. This suggests that ILK1 activity is either necessary to enhance K^+ uptake in these environments or required to activate other signaling processes. Interestingly, changes in K^+ supply induces defense gene expression including several genes involved in jasmonic acid production and defense compound production including glucosinolates (Armengaud *et al.*, 2004; Troufflard *et al.*, 2010). K^+ homeostasis also affects the transport of numerous other ions and molecules including sugars and osmolytes which are necessary for normal plant growth and stress responses (Osakabe *et al.*, 2013). Thus, it would be of interest to

determine ILK1's *in vivo* phosphorylation targets to clarify whether K^+ transport or additional ILK1-induced signaling pathways are contributing to the observed immune phenotypes.

The work presented here outlines a connection between K^+ nutrition, signaling and response to pathogens and osmotic stresses. Our data indicate that ion homeostasis is altered at both the cellular and whole-plant levels as early as 2-15 minutes after flg22 application and that *ILK1* contributes to these responses independently from Ca^{2+}-dependent signaling responses. We identified the first genetic components that contribute to membrane depolarization during the onset of the basal immunity and demonstrated that K^+ transport is an integral part of this process. These results provide novel genetic resources for probing stress signaling and suggest that the rate of membrane depolarization may modulate stress responses through a mechanism that remains to be discovered.

METHODS

Plant Material, Growth Conditions and Stress Treatments

Seeds of azygous control and transgenic plants were propagated as described previously (Lee *et al.*, 2011). Expression analysis, ion content and MAPK induction experiments were performed on two-week-old seedlings grown in liquid Murashige and Skoog (MS) media containing 3% sucrose. Germination assays were performed on 10 cm diameter petri dishes containing 25 mL of ½ MS media with 0.7% Phytoagar and sterile mannitol or NaCl at the indicated concentrations. Flg22-induced root growth inhibition was measured after 7 days on ½ MS media with 0.7% Phytoagar and 100 nM flg22. Unless otherwise indicated, all experiments were conducted three times and significance is indicated by an *, where $p \leq 0.05$. To generate *ilk1*, a segregating T-

DNA insertion line was obtained from The Arabidopsis Information Resource (SAIL-760-C05). Homozygous T3 *ilk1* insert and azygous lines were selected by PCR after backcrossing to Columbia plants and one round of selfing.

Constructs and *Arabidopsis* Transformation

The *ILK1* cDNA clone was obtained from ABRC and subcloned into the pDONRzeo Gateway. Following confirmation by sequencing, point mutations were made in the sequence using PCR and all constructs were cloned into pEARLEYGATE103 for localization ($P_{CaMV35S}$:*ILK1-GFP*), pEARLEYGATE102 for complementation ($P_{CaMV35S}$:*ILK1-CFP*), pYL436 for protein purification, pDuEx-Bait/pDuEx-Pray for SLCA and pNB1YNu/pNB1YCu for BiFC (Nour-Eldin *et al.*, 2006; Fujikawa and Kato, 2007). T1 seeds of *ILK1-CFP*, *K222A-CFP* and *D319N-CFP* lines were selected by PCR for the CFP gene and expression of *ILK1* was confirmed by qRTPCR.

Kinase Activity Assays

Recombinant C-terminal TAP-tagged ILK1 and ILK1 mutant proteins were purified from *N. benthamiana* leaves by immunoprecipitation as described in detail previously (Brauer *et al.*, 2014). Total protein content was quantified by Bradford assay and the presence of the cMyc-tagged protein was visualized by Western blot (Figure 4.3). To measure kinase activity, 650-700 ng of the protein preparation was incubated with kinase buffer to a final volume of 20 µL (5 mM Tris-HCl pH 7.5, 0.25 mM DTT, 1.25 µM $^{\gamma}P^{32}$-ATP, and 0.1 mg/mL substrate) and the amount of cofactor indicated in the figure legend. To verify consistent loading, a duplicate reaction was separated on a SDS-PAGE gel, transferred to a membrane and exposed to Ponceau staining.

Bacterial Infection Assays

The bacterial strains were grown overnight at 30^{o}C prior to being suspended in infiltration medium (10 mM $MgCl_2$) to 3x10^5 CFU/mL and infiltrated into plants using needleless syringes or flood-inoculation (Ishiga *et al.*, 2011). The plants were grown in high humidity for 2 d and tissue was harvested and quantified as described (Singh *et al.*, 2014).

MAPK Phosphorylation Assay

Protein was extracted from three two-week-old seedlings following exposure to 100 nM flg22 in 0.1 mM $MnCl_2$ as described (Brauer *et al.*, 2014) and quantified using the Bradford assay. Equal amounts of total protein was separated and probed with anti-p42/44 MAPK antibodies (1:1000, Cell Signaling Technology), anti-rabbit-HRP antibodies (1:2000, Sigma-Aldrich) and were stained with Ponceau following exposure.

RNA Extraction and qRT-PCR

RNA isolation and cDNA synthesis for expression analysis of two-week-old seedlings with and without stress treatments were performed as described previously (Moreau *et al.*, 2013). Three to five replicates containing 15-20 seedlings were harvested for each experiment. Quantitative RT-PCR was performed in 20 µL reactions using iTAQ SYBR Green (BioRad) and the *PP2A* gene for normalization.

Subcellular Localization of ILK1

N. benthamiana leaves were co-transformed with the $P_{CaMV35S}$*: ILK1-GFP* and $P_{CaMV35S}$*:HDEL-mCherry* or $P_{CaMV35S}$*:BDCaM53-mCherry* constructs according to Popescu et al. (2007). Red and green fluorescence was confirmed using a lambda scan and imaged using a confocal laser scanning microscope (SP5; Leica Microsystems). Co-localization of the GFP signal with mCherry signal was confirmed using Image-Pro 6.3 software. For localization in *Arabidopsis*, stably transformed lines expressing $P_{CaMV35S}$*:ILK1-GFP* were imaged using the same method. Membrane fractionation experiments were performed as described previously (Kjellbom and Larsson, 1984). Heterologous expression in *Xenopus* oocytes was performed as described previously, where YFP was visualized two to six days after injection (Ligaba *et al*. 2013).

Oxidative burst assay

Duplicate 6 mm leaf disks were collected from 9-12 plants per line and placed adaxial side up in deionized water overnight in a 96-well plate. The following day, the water was replaced with 100 µL of detection buffer (17 µL/mL luminol (Sigma-Aldrich), 20 µL/mL horseradish peroxidase (Sigma-Aldrich) containing 100 nM flg22. The plate was measured for luminescence for 45 min following buffer application in a Synergy 2 microplate reader (BioTek Instruments). The relative light units were calculated for each time point within an experiment.

Ion Content Measurement

Four replicate samples containing 25 two-week-old seedlings were exposed to 300 mM NaCl for 8h or 100 nM flg22 for the indicated time before rinsing and drying at 50^{o}C. The dried tissue was

homogenized and analyzed by inductively coupled plasma emission spectrometry as previously described (Maron *et al.*, 2008).

Electrophysiology

To determine membrane depolarization in leaf mesophyll cells from 5-10 week old rosette leaves, the epidermis was removed from the underside of the leaf and the leaf was affixed to 5 mm diameter circular glass slides using double-sided adhesive tape. The samples were incubated in a bath solution of 0.1 mM KCl, 1 mM $CaCl_2$ and 1mM MES/bis-Tris propane pH 6.0 for four hours prior to measuring flg22-induced membrane depolarization (10 nM) using the method described in Jeworutzki et al. (2010).

Split Luciferase Complementation Assays

The C-termini of proteins of interest were fused to either the N-terminal or C-terminal of *Renilla reniformis* luciferase and were coexpressed in Arabidopsis thaliana protoplasts. The cloning, protoplast preparation, and split-luciferase complementation assays were performed as described by Fujikawa and Kato (2007) using a Veritas microplate luminometer (Turner BioSystems). Expression vectors expressing a negative control protein pair, NLuc-SIM and CLuc-PAN, were constructed by inserting coding DNA sequences of SIAMES (AT5G04470) and PERIANTHIA (AT1G68640) in pDuExAn6 and pDuExDn6 (Kato and Jones, 2010), respectively.

Mass Spectrometry Analysis and Kinase Client Assay

Autophosphorylation of purified recombinant kinases (ILK1 and its D319N mutant) was detected using a LTQ Orbitrap XL ETD mass spectrometer (Thermo Fisher, San Jose, CA). The

kinase assay was conducted in kinase buffer (20 mM HEPES-KOH pH 7.4, 5 mM $MgCl_2$ or $MnCl_2$, 1 mM DTT, 2 mM ATP)(Ahsan *et al.*, 2013). The kinase client assay was performed with 5 mM $MnCl_2$ with purified ILK1 and a mixture of approximately 210 synthetic peptides (8 µM) per sample from a library of 2095 peptides which were designed based on the *in vivo* phosphoproteomic dataset available on the P^3DB website (http://www.p3db.org/). For mining KiC assay results, raw MS files were searched against a decoy database consisting of the random complement of the sequences comprising the peptide library, using SEQUEST (Proteome Discoverer, v. 1.0.3, Thermo Fisher). Identification data were evaluated using the XCorr function of SEQUEST, and phosphorylation-site localization was performed using phosphoRS (Proteome Discoverer, v. 1.0.3, Thermo Fisher). The XCorr values for each charge state were set to default, and no decoy hits were allowed. Peptide mass deviation was 10 ppm and a setting of one and two peptide/protein for KiC assay peptide and autophosphorylated kinase was used, respectively, to further filter the data. For final validation, each spectrum was inspected manually and accepted only when the phosphopeptide had the highest pRS site probability, pRS score, XCorr value and site-determining fragment ions allowed unambiguous localization of the phosphorylation site. Phosphopeptides with a pRS score ≥15 and/or a pRS site probability of ≥50% were accepted.

Functional Protein Microarray

Purified ILK1-V5 (9 µg) was used to probe both Arabidopsis protein chip 1 and 2 as described previously (Brauer *et al.*, 2014) except the probing buffer contained 12.5 mM Tris pH 7 and 1% BSA. Chips were probed in triplicate and compared to three control chips where signal of the Cy5-conjugated anti-V5 antibody was quantified using a Scan Array Express (Perkin Elmer).

REFERENCES

Adams, J. (2003) Activation loop phosphorylation and catalysis in protein kinases: is there functional evidence for the autoinhibitor model? *Biochemistry*, **42**, 601–607.

Ahsan, N., Huang, Y., Tovar-Mendez, A., Swatek, K.N., Zhang, J., Miernyk, J.A., Xu, D. and Thelen, J.J. (2013) A versatile mass spectrometry-based method to both identify kinase client-relationships and characterize signaling network topology. *J. Proteome Res.*, **12**, 937–948.

Armengaud, P., Breitling, R. and Amtmann, A. (2004) The potassium-dependent transcriptome of Arabidopsis reveals a prominent role of jasmonic acid in nutrient signaling. *Plant Physiol.*, **136**, 2556–2576.

Becker, D., Dreyer, I., HoTH, S., Reid, J.D., Busch, H., Lehnen, M., Palme, K. and Hedrich, R. (1996) Changes in voltage activation, Cs^+ sensitivity, and ion permeability in H5 mutants of the plant K^+ channel KAT1. *Proc. Natl. Acad. Sci.*, **93**, 8123–8128.

Bender, K.W. and Snedden, W. a. (2013) Calmodulin-related proteins step out from the shadow of their namesake. *Plant Physiol.*, **163**, 486–495.

Boller, T. and Felix, G. (2009) A renaissance of elicitors: perception of microbe-associated molecular patterns and danger signals by pattern-recognition receptors. *Annu. Rev. Plant Biol.*, **60**, 379–406.

Boudsocq, M., Willmann, M.R., McCormack, M., Lee, H., Shan, L., He, P., Bush, J., Cheng, S.-H. and Sheen, J. (2010) Differential innate immune signalling via Ca^{2+} sensor protein kinases. *Nature*, **464**, 418–422.

Brauer, E., Popescu, S. and Popescu, G. (2014) Experimental and analytical approaches to characterize plant kinases using protein microarrays. In G. Komis and J. Šamaj, eds. *Plant MAP Kinases SE - 17*. Methods in Molecular Biology. Springer New York, pp. 217–235.

Chinchilla, D., Frugier, F., Raices, M., Merchan, F., Giammaria, V., Gargantini, P., Gonzalez-Rizzo, S., Crespi, M. and Ulloa, R. (2008) A mutant ankyrin protein kinase from Medicago sativa affects Arabidopsis adventitious roots. *Funct. Plant Biol.*, **35**, 92–101.

Felix, G., Duran, J.D., Volko, S. and Boller, T. (1999) Plants have a sensitive perception system for the most conserved domain of bacterial flagellin. *Plant J.*, **18**, 265–276.

Felle, H.H., Kondorosi, É., Kondorosi, Á. and Schultze, M. (2000) How alfalfa root hairs discriminate between Nod factors and oligochitin elicitors. *Plant Physiol.*, **124**, 1373–1380.

Fujikawa, Y. and Kato, N. (2007) TECHNICAL ADVANCE: Split luciferase complementation assay to study protein–protein interactions in Arabidopsis protoplasts. *Plant J.*, **52**, 185–195.

Fulgenzi, F.R., Peralta, M.L., Mangano, S., Danna, C.H., Vallejo, A.J., Puigdomenech, P. and Santa-María, G.E. (2008) The ionic environment controls the contribution of the barley HvHAK1 transporter to potassium acquisition. *Plant Physiol.*, **147**, 252–262.

Geiger, D., Scherzer, S., Mumm, P., et al. (2009) Activity of guard cell anion channel SLAC1 is controlled by drought-stress signaling kinase-phosphatase pair. *Proc. Natl. Acad. Sci.*, **106**, 21425–21430.

Gómez-Gómez, L., Felix, G. and Boller, T. (1999) A single locus determines sensitivity to bacterial flagellin in Arabidopsis thaliana. *Plant J.*, **18**, 277–284.

Haro, R., Sainz, L., Rubio, F. and Rodríguez-Navarro, A. (1999) Cloning of two genes encoding potassium transporters in Neurospora crassa and expression of the corresponding cDNAs in Saccharomyces cerevisiae. *Mol. Microbiol.*, **31**, 511–520.

Held, K., Pascaud, F., Eckert, C., et al. (2011) Calcium-dependent modulation and plasma membrane targeting of the AKT2 potassium channel by the CBL4/CIPK6 calcium sensor/protein kinase complex. *Cell Res.*, **21**, 1116–1130.

Ishiga, Y., Ishiga, T., Uppalapati, S.R. and Mysore, K.S. (2011) Arabidopsis seedling flood-inoculation technique: a rapid and reliable assay for studying plant-bacterial interactions. *Plant Methods*, **7**, 32.

Jabs, T., Tschöpe, M., Colling, C., Hahlbrock, K. and Scheel, D. (1997) Elicitor-stimulated ion fluxes and O_2^- from the oxidative burst are essential components in triggering defense gene activation and phytoalexin synthesis in parsley. *Proc. Natl. Acad. Sci.*, **94**, 4800–4805.

Jeworutzki, E., Roelfsema, M.R.G., Anschütz, U., Krol, E., Elzenga, J.T.M., Felix, G., Boller, T., Hedrich, R. and Becker, D. (2010) Early signaling through the Arabidopsis pattern recognition receptors FLS2 and EFR involves Ca^{2+}-associated opening of plasma membrane anion channels. *Plant J.*, **62**, 367–378.

Kato, N. and Jones, J. (2010) The split luciferase complementation assay. In *Plant Developmental Biology*. Springer, pp. 359–376.

Kjellbom, P. and Larsson, C. (1984) Preparation and polypeptide composition of chlorophyll-free plasma membranes from leaves of light-grown spinach and barley. *Physiol. Plant.*, **62**, 501–509.

Kuchitsu, K., Yazaki, Y., Sakano, K. and Shibuya, N. (1997) Transient cytoplasmic pH change and ion fluxes through the plasma membrane in suspension-cultured rice cells triggered by N-acetylchitooligosaccharide elicitor. *Plant cell Physiol.*, **38**, 1012–1018.

Leba, L.-J., Cheval, C., Ortiz-Martín, I., Ranty, B., Beuzón, C.R., Galaud, J.-P. and Aldon, D. (2012) CML9, an Arabidopsis calmodulin-like protein, contributes to plant innate immunity through a flagellin-dependent signalling pathway. *Plant J.*, **71**, 976–989.

Lee, H.Y., Bowen, C.H., Popescu, G.V., Kang, H.-G., Kato, N., Ma, S., Dinesh-Kumar, S., Snyder, M. and Popescu, S.C. (2011) Arabidopsis RTNLB1 and RTNLB2 Reticulon-like proteins regulate intracellular trafficking and activity of the FLS2 immune receptor. *Plant Cell*, **23**, 3374–91.

Lewis, B.D., Karlin-Neumann, G., Davis, R.W. and Spalding, E.P. (1997) Ca^{2+}-activated anion channels and membrane depolarizations induced by blue light and cold in Arabidopsis seedlings. *Plant Physiol.*, **114**, 1327–1334.

Li, L., Kim, B.-G., Cheong, Y.H., Pandey, G.K. and Luan, S. (2006) A Ca^{2+} signaling pathway regulates a K^+ channel for low-K response in Arabidopsis. *Proc. Natl. Acad. Sci.*, **103**, 12625–12630.

Ligaba, A., Dreyer, I., Margaryan, A., Schneider, D.J., Kochian, L., Piñeros, M. (2013) Functional, structural and phylogenetic analysis of domains underlying the Al sensitivity of the aluminum-activated malate/anion transporter, taalmt1. *The Plant Journal* **76**(5), 766-780.

Ligterink, W., Kroj, T., Nieden, U. zur, Hirt, H. and Scheel, D. (1997) Receptor-mediated activation of a MAP kinase in pathogen defense of plants. *Science*, **276**, 2054–2057.

Lu, D., Wu, S., Gao, X., Zhang, Y., Shan, L. and He, P. (2010) A receptor-like cytoplasmic kinase, BIK1, associates with a flagellin receptor complex to initiate plant innate immunity. *Proc. Natl. Acad. Sci.*, **107**, 496–501.

Magnan, F., Ranty, B., Charpenteau, M., Sotta, B., Galaud, J.P. and Aldon, D. (2008) Mutations in AtCML9, a calmodulin-like protein from Arabidopsis thaliana, alter plant responses to abiotic stress and abscisic acid. *Plant J.*, **56**, 575–589.

Mähönen, A.P., Bonke, M., Kauppinen, L., Riikonen, M., Benfey, P.N. and Helariutta, Y. (2000) A novel two-component hybrid molecule regulates vascular morphogenesis of the Arabidopsis root. *Genes & development*, **14**, 2938-2943.

Maron, L.G., Kirst, M., Mao, C., Milner, M.J., Menossi, M. and Kochian, L. V (2008) Transcriptional profiling of aluminum toxicity and tolerance responses in maize roots. *New Phytol.*, **179**, 116–128.

Maydan, M., McDonald, P.C., Sanghera, J., et al. (2010) Integrin-linked kinase is a functional Mn2+-dependent protein kinase that regulates glycogen synthase kinase-3β (GSK-3β) phosphorylation. *PLoS One*, **5**, e12356.

Moreau, M., Westlake, T., Zampogna, G., Popescu, G., Tian, M., Noutsos, C. and Popescu, S. (2013) The Arabidopsis oligopeptidases TOP1 and TOP2 are salicylic acid targets that modulate SA-mediated signaling and the immune response. *Plant J.*, **76**, 603–614.

Nieves-Cordones, M., Alemán, F., Martínez, V. and Rubio, F. (2010) The Arabidopsis thaliana HAK5 K^+ transporter is required for plant growth and K^+ acquisition from low K^+ solutions under saline conditions. *Mol. Plant*, **3**, 326–333.

Nour-Eldin, H.H., Hansen, B.G., Nørholm, M.H.H., Jensen, J.K. and Halkier, B.A. (2006) Advancing uracil-excision based cloning towards an ideal technique for cloning PCR fragments. *Nucleic Acids Res.*, **34**, e122–e122.

Nürnberger, T., Nennstiel, D., Jabs, T., Sacks, W.R., Hahlbrock, K. and Scheel, D. (1994) High affinity binding of a fungal oligopeptide elicitor to parsley plasma membranes triggers multiple defense responses. *Cell*, **78**, 449–460.

Osakabe, Y., Arinaga, N., Umezawa, T., et al. (2013) Osmotic stress responses and plant growth controlled by potassium transporters in Arabidopsis. *Plant Cell Online*, **25**, 609–624.

Popescu, S.C., Popescu, G. V, Bachan, S., Zhang, Z., Seay, M., Gerstein, M., Snyder, M. and Dinesh-Kumar, S.P. (2007) Differential binding of calmodulin-related proteins to their targets revealed through high-density Arabidopsis protein microarrays. *Proc. Natl. Acad. Sci. U. S. A.*, **104**, 4730–4735.

Pyo, Y.J., Gierth, M., Schroeder, J.I. and Cho, M.H. (2010) High-affinity K^+ transport in Arabidopsis: AtHAK5 and AKT1 are vital for seedling establishment and postgermination growth under low-potassium conditions. *Plant Physiol.*, **153**, 863–875.

Rodríguez-Concepción, M., Toledo-Ortiz, G., Yalovsky, S., Caldelari, D. and Gruissem, W. (2000) Carboxyl-methylation of prenylated calmodulin CaM53 is required for efficient plasma membrane targeting of the protein. *Plant J.*, **24**, 775–784.

Rodriguez-Navarro, A., Blatt, M.R. and Slayman, C.L. (1986) A potassium-proton symport in Neurospora crassa. *J. Gen. Physiol.*, **87**, 649–674.

Rodríguez-Navarro, A. and Rubio, F. (2006) High-affinity potassium and sodium transport systems in plants. *J. Exp. Bot.*, **57**, 1149–1160.

Rubio, Francisco, Rodríguez-Navarro, A. (2000) Cloning of Arabidopsis and barley cDNAs encoding HAK potassium transporters in root and shoot cells. *Physiol. Plant.*, **109**, 34–43.

Scherzer, S., Böhm, J., Krol, E., et al. (2015) Calcium sensor kinase activates potassium uptake systems in gland cells of Venus flytraps. *Proc. Natl. Acad. Sci.*, 201507810.

Singh, D.K., Calviño, M., Brauer, E.K., et al. (2014) The tomato kinome and the tomato kinase library ORFeome: novel resources for the study of kinases and signal transduction in tomato and Solanaceae species. *Mol. Plant-Microbe Interact.*, **27**, 7–17.

Torres, M.A., Dangl, J.L. and Jones, J.D.G. (2002) Arabidopsis gp91phox homologues AtrbohD and AtrbohF are required for accumulation of reactive oxygen intermediates in the plant defense response. *Proc. Natl. Acad. Sci.*, **99**, 517–522.

Troufflard, S., Mullen, W., Larson, T.R., Graham, I.A., Crozier, A., Amtmann, A. and Armengaud, P. (2010) Potassium deficiency induces the biosynthesis of oxylipins and glucosinolates in Arabidopsis thaliana. *BMC Plant Biol.*, **10**, 172.

Wendehenne, D., Lamotte, O., Frachisse, J.-M., Barbier-Brygoo, H. and Pugin, A. (2002) Nitrate efflux is an essential component of the cryptogein signaling pathway leading to defense responses and hypersensitive cell death in tobacco. *Plant Cell Online*, **14**, 1937–1951.

CHAPTER 5

Conclusion and future directions

In this project, research on protein kinases in tomato, *N. benthamiana* and *Arabidopsis* were presented with a focus on immune signaling and cross-talk between stresses. The last 20 years has seen a rapid expansion of our understanding of this area from early studies of elicitors in parsley, tobacco, soybean, rice and tomato to the discovery of the MAPK cascade in plants and the molecular basis for PAMP perception (Seo *et al.*, 1995; Felix *et al.*, 1999; Boller and Felix, 2009). Arabidopsis in particular has been a useful model organism for mapping signaling transduction kinases including the MAPKs and CDPKs though the intrinsic functional redundancy of these pathways limits their study using genetic approaches (Ichimura *et al.*, 2002).

We now see a shift in focus to extend the lessons learned in Arabidopsis to other plant species such as rice and poplar which appear to have conserved kinase families, but divergent functional roles for individual members (Hamel *et al.*, 2006). This constitutes a significant challenge for the development of resistance in plants, since developing resistance may require knowledge of the signaling pathways in a particular species (Felix and Boller, 2003). Indeed, in chapter 3, we saw that FLS2 was not involved in basal immunity in *N. benthamiana*. While this result is in contrast to what is known about the importance of FLS2 in bacterial resistance in Arabidopsis, it is in agreement with other recent studies that in Solonaceous plants like tomato, where it seems that detection of flagellin does not correlate with bacterial resistance (Veluchamy *et al.*, 2014, Felix *et al.*, 1999). Nevertheless, a biotechology approach has been successfully used to confer bacterial resistance in *N. benthamiana* and tomato by expressing the *Arabidopsis*

EFR RLK, which detects the bacterial EF-Tu PAMP (Lacombe *et al.*, 2010). This implies that there is enough functional conservation of some signaling responses between these species to induce immunity, making this a promising strategy for developing resistance.

While protein kinase signaling networks are clearly complex, a number of themes have emerged from previous studies and the studies outlined here. The first is that like other organisms, plants have separated signal recognition and transmission/amplification steps between distinct kinase families, all of which contribute to immunity (Kültz, 2005). For example, we identified several novel RLKs and cytosolic kinases including RLCKs, MAPKs, CDPKs and Snf1-related protein kinases (SnRKs) involved in plant immunity and PCD responses in chapter 3. While PCD was regulated by both cytosolic and RLKs, over half of the kinases that contribute to basal immunity induced by the D29E effectorless strain were RLKs. In addition, the RLKs and RLCKs which contributed to immunity across bacterial strains were almost exclusively positive regulators. This finding is consistent with the idea that the most significant contribution of RLKs to immunity is through their role in activating signal transduction cascades (Macho and Zipfel, 2014). In contrast, cytosolic kinases perform diverse regulatory roles as both positive and negative regulators of stress response, to keep responses in check (Tena *et al.*, 2011).

The second theme which was highlighted in two studies presented here is that kinases function in response to multiple stresses. In other words, some stress response pathways seem to be activated by diverse stimuli. For example, in chapter 3, most of the kinases functioned in multiple signaling events including during basal immunity and PCD induced by different treatments. In chapter 4, we demonstrated a role for the *ILK1* in mediating salt, drought and PAMP signaling. These findings are consistent with the hypothesis that some molecular components are activated during diverse stress signaling responses and may constitute a

generalized stress response as discussed in chapter 1. However a generalized stress response does not account of all of the observed overlap in kinase signaling since many of the kinases in chapter 3 only demonstrated a role in basal immunity when responses were also perturbed with effectors. This would suggest that a hierarchy exists within the signaling network, where the signaling role of certain kinases only becomes important under conditions when other parts of the network are not functioning. This became important, particularly in our identification of susceptibility factors that inhibit immune responses in the presence of specific effectors. These kinases are particularly interesting both in terms of understanding the immune mechanisms which underlie this phenomenon but also in practical terms, since knocking out genes to produce resistance is an attractive method for developing crop resistance. In addition, while we saw that kinases may play a role in multiple stress response pathways, the relative importance and mechanisms underlying this role may change. Indeed, we identified kinases with both a positive and negative regulatory role in PCD, depending on the initial stimuli in chapter 3. It would be interesting to further explore the mechanism of some of these kinases, to develop our current limited understanding of the role of protein kinases in ETI.

Another important theme which arose during our research was that immune networks contain pathways which are both independent and interdependent of one another. For example, the fact that the presence of effectors alter the number of *KEI* lines showing an immune phenotype implies that effector-impacted signaling pathways influence other kinase-based pathways as outlined in chapter 3. In chapter 4, we observed that the ILK1 was involved in mediating MAPK but not CDPK-dependent gene induction consistent with previous studies which saw separation of these pathways (Boudsocq *et al.*, 2010). Partial pathway independence is thought to be an important aspect of biological networks, providing amplification of the stress

signal and perhaps some degree of signal specificity (Sato *et al.*, 2010). However, more data is needed to gain a complete picture of the cross-talk or independence of stress response pathways, which has also been investigated in yeast and mammals (Sachs *et al.*, 2005; Ross-Macdonald *et al.*, 1999).

Beyond these identified themes on the role of protein kinases in immunity, we have identified ILK1 and its interactor HAK5, as the first regulating molecular components regulating trans-plasma membrane electric potential during PAMP perception and connected this role with K^+ transport and MAPK signaling. However several questions remain unanswered in the wake of this study.

Does PAMP-induced alterations in the membrane potential function as a signal? Is this signal needed to regulate the downstream MAPK responses? Is HAK5 a phosphorylation target for ILK1 *in vivo*? Does HAK5 phosphorylation status alter its transport activity or protein stability? Are ILK1 and HAK5 modulating membrane depolarization in response to a wide range of stresses?

While some of these questions can be reasonably answered with more experimental work, the question of membrane potential as being a cellular signaling event has been asked previously and is difficult to test (Ward and Schroeder, 1997; Ashley *et al.*, 2006). Previous groups have proposed that plants use electrical signaling in a similar way as animal cells, where action potentials (rapid, transient changes in membrane potential) mediate muscle contraction and neuron communication (Brenner *et al.*, 2006; Volkov *et al.*, 2008). However the electrical pulses in plants are much slower than what is observed in animal cells and there is little genetic evidence in plants to support this notion. An alternative hypothesis would be that ion transport may activate signaling responses by producing localized changes in membrane fluidity thereby

activating mechanosensitive channels which have an effect signaling and development (Haswell *et al.,* 2008). However the precise molecular nature of membrane depolarization and the downstream effects of this process remains to be seen.

In conclusion, in an era where transcriptomics has become affordable for many research groups, it is important not to lose sight of the fact that gene expression is only one part of the stress response puzzle (Brauer *et al.*, 2014). Indeed we successfully identified a number of new immunity-associated protein kinases using unbiased proteomic screens (chapter 2) and defined roles for these kinases in signaling responses to bacterial pathogens (chapter 3). Our screens allowed us to identify the first kinase-transporter complex with a role in mediating PAMP-induced plasma membrane depolarization and demonstrated that this complex also contributes to MAPK signaling (chapter 4). Together, we have provided both mechanistic and network-level insights into how plants perform their never-ending dance with their bacterial pathogen partners.

REFERENCE

Ashley, M.K., Grant, M. and Grabov, A. (2006) Plant responses to potassium deficiencies: a role for potassium transport proteins. *J. Exp. Bot.*, **57**, 425–436.

Boller, T. and Felix, G. (2009) A renaissance of elicitors: perception of microbe-associated molecular patterns and danger signals by pattern-recognition receptors. *Annu. Rev. Plant Biol.*, **60**, 379–406.

Boudsocq, M., Willmann, M.R., McCormack, M., Lee, H., Shan, L., He, P., Bush, J., Cheng, S.-H. and Sheen, J. (2010) Differential innate immune signalling via Ca^{2+} sensor protein kinases. *Nature*, **464**, 418–422.

Brauer, E.K., Singh, D.K. and Popescu, S.C. (2014) Next-generation plant science: putting big data to work. *Genome Biol.*, **15**, 301.

Brenner, E.D., Stahlberg, R., Mancuso, S., Vivanco, J., Baluška, F. and Volkenburgh, E. Van (2006) Plant neurobiology: an integrated view of plant signaling. *Trends Plant Sci.*, **11**, 413–419.

Felix, G. and Boller, T. (2003) The highly conserved RNA-binding motif RNP-1 of bacterial cold shock proteins is recognized as an elicitor signal in tobacco. *J. Biol. Chem.*, **278**, 6201–6208.

Felix, G., Duran, J.D., Volko, S. and Boller, T. (1999) Plants have a sensitive perception system for the most conserved domain of bacterial flagellin. *Plant J.*, **18**, 265–276.

Hamel, L.-P., Nicole, M.-C., Sritubtim, S., et al. (2006) Ancient signals: comparative genomics of plant MAPK and MAPKK gene families. *Trends Plant Sci.*, **11**, 192–198.

Haswell, E.S., Peyronnet, R., Barbier-Brygoo, H., Meyerowitz, E.M. and Frachisse, J.-M. (2008) Two MscS homologs provide mechanosensitive channel activities in the Arabidopsis root. *Curr. Biol.*, **18**, 730–734.

Ichimura, K., Shinozaki, K., Tena, G., et al. (2002) Mitogen-activated protein kinase cascades in plants: a new nomenclature. *Trends Plant Sci.*, **7**, 301–308.

Kültz, D. (2005) Molecular and evolutionary basis of the cellular stress response. *Annu. Rev. Physiol.*, **67**, 225–257.

Lacombe, S., Rougon-Cardoso, A., Sherwood, E., et al. (2010) Interfamily transfer of a plant pattern-recognition receptor confers broad-spectrum bacterial resistance. *Nat Biotech*, **28**, 365–369.

Macho, A.P. and Zipfel, C. (2014) Plant PRRs and the activation of innate immune signaling. *Mol. Cell*, **54**, 263–272.

Ross-Macdonald, P., Coelho, P.S.R., Roemer, T., et al. (1999) Large-scale analysis of the yeast genome by transposon tagging and gene disruption. *Nature*, **402**, 413–418.

Sachs, K., Perez, O., Pe'er, D., Lauffenburger, D.A. and Nolan, G.P. (2005) Causal protein-signaling networks derived from multiparameter single-cell data. *Science (80)*, **308**, 523–529.

Sato, M., Tsuda, K., Wang, L., Coller, J., Watanabe, Y., Glazebrook, J. and Katagiri, F. (2010) Network modeling reveals prevalent negative regulatory relationships between signaling sectors in Arabidopsis immune signaling. *PLoS Pathog.*, **6**, e1001011.

Seo, S., Okamoto, M., Seto, H., Ishizuka, K., Sano, H. and Ohashi, Y. (1995) Tobacco MAP kinase: a possible mediator in wound signal transduction pathways. *Science (80)*, **270**, 1988–1992.

Tena, G., Boudsocq, M. and Sheen, J. (2011) Protein kinase signaling networks in plant innate immunity. *Curr. Opin. Plant Biol.*, **14**, 519–529.

Veluchamy, S., Hind, S.R., Dunham, D.M., Martin, G.B. and Panthee, D.R. (2014) Natural Variation for Responsiveness to flg22, flgII-28, and csp22 and *Pseudomonas syringae* pv. *tomato* in heirloom tomatoes. *PLoS One*, **9**, e106119.

Volkov, A.G., Carrell, H., Adesina, T., Markin, V.S. and Jovanov, E. (2008) Plant electrical memory. *Plant Signal. Behav.*, **3**, 490–492.

Ward, J.M. and Schroeder, J.I. (1997) Roles of ion channels in initiation of signal transduction in higher plants. In *Signal Transduction in Plants*. Springer, pp. 1–22.